2013

UNIQUE RELATIONSHIP BETWEEN SMALL STRAIN SHEAR MODULUS AND EFFECTIVE STRESSES AT FAILURE

Yaurel Guadalupe-Torres
University of Rhode Island, yaurel_gt@yahoo.com

UNIQUE RELATIONSHIP BETWEEN SMALL STRAIN SHEAR MODULUS AND EFFECTIVE STRESSES AT FAILURE

BY

YAUREL GUADALUPE-TORRES

A DISSERTATION SUBMITTED IN PARTIAL FULLFILLMENT OF THE REQUIREMENTS FOR THE DEGREE OF

DOCTOR OF PHILOSOPHY

IN

CIVIL AND ENVIRONMENTAL ENGINEERING

UNIVERSITY OF RHODE ISLAND

2013

DOCTOR OF PHILOSOPHY DISSERTATION

OF

YAUREL GUADALUPE TORRES

APPROVED:

Dissertation Committee:

Major Professor CHRISTOPHER D. P. BAXTER

AARON S. BRADSHAW

GOPU POTTY

NASSER H. ZAWIA

DEAN OF THE GRADUATE SCHOOL

UNIVERSITY OF RHODE ISLAND

2013

ABSTRACT

This dissertation is comprised of three manuscripts developed from different topics of geotechnical and earthquake engineering. The first topic investigates a link between small and large strain behavior of dilatant soils. The second topic deals with the use of a reduced density in the calculation of small strain shear modulus from shear wave velocity due to the occurrence of relative motion between the water and soil-skeleton as a shear wave passes through the soil. The third and final topic investigates ground motion selection and scaling procedures from various methods found in the literature for seismic hazard analyses in the northeastern United States.

Current geotechnical practice relies on empirical relationships with in situ tests to determine the effective stress strength parameters for dense cohesionless soils. Although these methods work reasonably well in practice, they cannot account for in situ effects related to time, fabric, and cementation. These factors are especially important for brittle or sensitive soils, such as loess and cemented sands. To develop methods that can predict strength in these types of soils, a better understanding of the link between small and large strain behavior is needed. The objective of the first manuscript and Appendices A and B is to evaluate the hypothesis of a unique relationship between the small strain shear modulus (G_0) and the effective stresses at failure (σ'_{1f}) for dilatant soils (i.e., G_0/σ'_{1f} = constant). This is accomplished by a laboratory testing program consisting of isotropically consolidated triaxial compression tests with shear wave velocity measurements throughout the test. The soils tested in this study include a quartz sand, calcareous sand, non-plastic silt, reconstituted high plasticity clay, and undisturbed

sensitive clay, and the results are compared to previous studies by the authors on weakly cemented sands. The results from these tests showed that the ratio G_0/σ'_{1f} was approximately 200 ± 20 for the quartz sand and non-plastic silt, 130 ± 6 for the clays, and 128 for the calcareous sand and was independent of void ratio, degree of cementation, and confining stress. If true for other soils, this finding could have important implications for evaluating staged construction on sensitive soils and estimating the strength of dilative soils in situ.

Small strain shear modulus (G_0) is an important dynamic soil property used in different aspect of geotechnical and earthquake engineering such as seismic site response analysis, liquefaction potential, soil-structure interaction, foundation vibrations, etc. Typically, G_0 is obtained in-situ or in the laboratory by measuring the shear wave velocity of the soil and knowing the bulk density of the soil ($G_0 = \rho v_s^2$). However, in a saturated media, and depending on the grain size (and thus, porosity and hydraulic conductivity) and frequency of the shear wave, this equation may be inaccurate and can lead to an overestimation of the small strain shear modulus. In some cases when the shear wave travels through the soil, a relative movement between the water and soil-skeleton occurs and a reduction of the density must be determined. The objective of the second manuscript is to investigate the concept of an "effective" (reduced) density required to obtain the correct small strain shear modulus. This was accomplished by measuring the shear wave velocity of three different materials of different sizes including 6-mm glass beads, coarse grained sand, and fine-to-medium grained sand, under dry and saturated conditions at different confining stresses. The results showed that using the total density overestimates G_0 by up to 20% in coarse materials (i.e., 6-mm glass beads

and coarse sand) and therefore the effective density must be used. Results for the fine-to-medium grained sand were inconclusive.

An important aspect of a seismic site response analysis is the choice of appropriate ground motions and the methods for scaling ground motion records. In the case of northeastern United States (NEUS), available recorded ground motions are limited and earthquakes sources are not well defined. Additionally, ground motions from this region contain a distinctive high frequency content not present in ground motions from regions with more seismic activity. This makes the use of ground motions from high seismicity areas not suitable for seismic response analyses in the NEUS. These limitations make the selection and scaling of ground motions a challenge in this region. The objective of this study is to evaluate and compare different methods of selection and scaling of recorded ground motions for a site specific seismic response analysis to determine which methods are most appropriate for the northeastern United States. Five different criteria were defined to critically evaluate and compare the selected methods. These criteria were defined to evaluate (1) the ability of the method to produce a median response spectrum at bedrock that matches the UHS and its variability, (2).the ability of the method to characterize a response spectrum over a period range versus a single period, (3) the ability of the method to account for a range of magnitude and site-to-source distance earthquakes that are consistent with the UHS, (4) the Set-up time and run time required to obtain the response spectrum at bedrock, and (5) how the site response analysis result is affected by the method. Overall, the method proposed by Kottke and Rathje (2008) performed very well in most of the criteria compared to the other evaluated methods.

ACKONWLEDGEMENTS

First of all, I thank God for putting in my way each and every one of the people who have made this dream a reality and a pleasant and amazing experience. Without them this achievement would not have been possible.

I want to express my gratitude to my advisor, Dr. Christopher Baxter for leading this project and for accepting me as his student even before we met. I thank him for trusting me with this work, and for his guidance and support within and outside the academia. I also extend my gratitude to the rest of my committee Dr. Aaron Bradshaw, Dr. Gopu Potty, Dr. Martin Sadd, and Dr. Tong Qiu for their suggestions, comments and their help throughout this long process. I especially want to thank Dr. Qiu for accepting being part of my committee in such short notice. I also thank Dr. William Kovacs for being part of this process. I am very grateful to Dr. Ravi Sharma who taught me, among other things, how to use the laboratory equipment and programing in Matlab. I'm also thankful for professors Dr. Russell Green, Dr. Adrián Rodríguez-Marek, and Dr. Melissa Landon Maynard for their support and contribution to this study.

I also want to acknowledge Gail Paolino, for being the best secretary ever and keeping me updated with all my paperwork and Fred Pease for crafting many of the equipment needed for the laboratory tests. I thank my officemates and friends Brian Baffer, Amir Banari, Jeff Costa, Sean Davis, Mike Dobling, Myriam El Bettah, Rich Genovesi, Joe Giampa, Stefanie Haffke, Anna Hernberg, Christian Janßen, Tania Lado, Andrés Núñez, Tayebeh S. Tajalli Bakhsh, Oliver Taylor and others for making this process easier and enjoyable. I am also grateful for my parents and brothers for their love, support and for believing in me.

This study would not have been possible without the contribution and funding of the National Science Foundation (NSF, Grant # 1031135), the University of Rhode Island Transportation Center, (URITC), the Rhode Island Department of Transportation (RIDOT) and the New England University Transportation Center (NEUTC). Their support is greatly acknowledged.

Finally, I am mostly grateful for my confidant, best friend and wife, Alesandra Morales for her love, caring, friendship, tolerance, and patience. I thank her for being my support, for being with me during this challenging process and for being the engine of my dreams. Without her this journey would have never been started.

PREFACE

This dissertation is organized in manuscript format and is comprised of three main manuscripts focusing on three different topics. The first two manuscripts focus on laboratory studies of small strain shear modulus and soil behavior. The third manuscript studies aspects of earthquake engineering regarding the selection and scaling of ground motions for the Northeastern Unites States.

The first manuscript evaluates the hypothesis of a unique relationship between small and large strain behavior of dilatant cohesionless soils at failure. Specifically, this study investigates the relationship between the small strain shear modulus (G_0) and the effective stresses at failure (σ'_{1f}) for dilatant soils. It is hypothesized that a unique relationship independent of confining stresses, void ratio, and degree of cementation exists between these two parameters. To evaluate this hypothesis, a laboratory testing program was performed involving isotropically consolidated drained triaxial compression tests under different confining stresses. Samples were prepared at different void ratios and the shear wave velocity was measured throughout the tests. Tested materials include weakly cemented sands, non-plastic silts, and quartz sand.

The second manuscript investigates the effects of grain size in saturated samples for the estimation of the small strain shear modulus. Passage of a shear wave through a porous media may cause relative movement between the water and the mass particle depending on the hydraulic conductivity and the frequency of the shear wave. To account for this relative movement, the total density must be adjusted when calculating the small strain shear modulus from shear wave velocity. To evaluate this phenomenon, three different materials including glass beads, coarse-grained sand and fine-to-medium

grained sand, were subjected to different consolidation stresses with shear wave velocity measurements.

The third manuscript describes, compares and discusses different methods for the selection and scaling procedures of recorded ground motions for the probabilistic seismic hazard analysis (PSHA) for the Northeastern United States. This is accomplished by conducting a literature review of existing methods, and the selection of six methods to be compared. Site response analyses were performed at two bridge sites in NEUS with different soil profiles, and the methods were evaluated based on five defined criteria.

Appendices A and B present additional laboratory tests related to the research conducted in Manuscript 1. In this study, the relationship between the small strain shear modulus and the effective stresses at failure was evaluated for two cohesive soils (Appendix A) and a cohesionless soil (Appendix B). The first is a reconstituted high plasticity clay from the Gulf of Mexico, the second is an undisturbed sensitive clay from Maine called Presumpscot clay, and the third is a calcareous sand from Cabo Rojo, PR.

Appendix C presents figures comparing shear wave velocity with void ratio and mean effective stresses, and a summary of the results obtained in Manuscript 1 and Appendices A and B.

Appendix D presents a preliminary study that attempts to establish a relationship between shear wave velocity (v_s) with the effective stress friction angle (ϕ') of cohesionless soils. The v_s-ϕ' relationship is derived from isotropic consolidated drained triaxial laboratory tests on non-plastic silts and calcareous sands with shear wave velocity measurements using bender elements. This correlation is then compared with published equations developed for cone penetration tests (CPT) to estimate effective friction angle.

TABLE OF CONTENTS

LIST OF TABLES

LIST OF FIGURES

CHAPTER 1

"Linking Small and Large Strain Behavior of Soils using Shear Wave Velocity Measurements in the Laboratory"

by

Yaurel Guadalupe-Torres[1], Christopher D.P. Baxter[2], M.S. Ravi Sharma[3]

is accepted for publication in the Transportation Research Record: Journal of the Transportation Research Board

[1] PhD. Candidate, Department of Civil and Environmental Engineering, University of Rhode Island, Narragansett, RI 02882. Phone: 787-467-3226, E-mail: yaurel_gt@yahoo.com

[2] Professor, Department of Ocean/Civil and Environmental Engineering, University of Rhode Island, Narragansett, RI 02882. Phone: 401-874-6575, E-mail: baxter@oce.uri.edu

[3] Ocean and Coastal Consultants Inc. a COWI Company, 35 Corporate Drive, Trumbull, CT 06611. Phone: 203-400-6527, E-mail: msravisharma@yahoo.com

Linking Small and Large Strain Behavior of Soils using Shear Wave Velocity Measurements in the Laboratory

Abstract

Current geotechnical practice relies on empirical relationships with in situ tests to determine the effective stress strength parameters for dense cohesionless soils. Although these methods work reasonably well in practice, they cannot account for in situ effects related to time, fabric, and cementation. These factors are especially important for brittle or sensitive soils, such as loess and cemented sands. To develop methods that can predict strength in these types of soils, a better understanding of the link between small and large strain behavior is needed.

The objective of this paper is to evaluate the hypothesis that there is a unique relationship between the small strain shear modulus (G_0) and the effective stresses at failure (σ'_{1f}) for dilatant soils. To accomplish this objective, isotropically consolidated drained triaxial compression tests were performed with shear wave velocity measured throughout the tests. The soils tested in this study include a quartz sand and non-plastic silt, and the results are compared to previous studies by the authors on weakly cemented sands.

It was found that the ratio G_0/σ'_{1f} was approximately 200 ± 20 for the three different soils tested, and was independent of density, degree of cementation, and confining stress. If true for other soils, this finding could have important implications for evaluating staged construction on sensitive soils and estimating the strength of dilative soils in situ.

Introduction

This paper focuses on linking small and large strain behavior of soils during triaxial compression tests. It is hypothesized from previous work by the authors (1, 2) that there is a unique relationship between the elastic shear modulus (i.e. stiffness) and effective stresses at failure for dilatant soils. This work involved 22 isotropically consolidated, drained triaxial compression tests on samples of weakly cemented sand at various densities, levels of cementations, and confining stresses. The work presented in this paper seeks to extend the results of the previous studies by evaluating this hypothesis for samples of quartz sand and non-plastic silt.

The practical importance of this study is that it may lead to an in situ method of assessing the strength of dilative or sensitive soils. Current geotechnical practice relies on empirical relationships developed from the Standard Penetration Test (SPT) and the Cone Penetration Test (CPT). The SPT consists of counting the blows required to penetrate a split-spoon sampler 0.3 m (1 ft) with a 63.5 kg (140 lb) hammer. The SPT blow count (N) is first corrected for the effects of hammer energy and effective stress and then correlated to soil properties such as internal friction angle (ϕ'), undrained shear strength (S_u), and unit weight (γ). The CPT consists of pushing an instrumented cone continuously through the soil while measuring the resistance at the tip and along the sleeve and the pore water pressure at some point on the cone. These data are used to classify the soil and estimate soil properties.

For both the SPT and CPT, correlations to soil properties have been developed from field studies, large calibration chamber tests, and laboratory tests on reconstituted soils. Although these correlations work reasonably well for dense, cohesionless soils,

they cannot capture the in situ effects related to time, fabric, and cementation. This is particularly true for brittle soils, such as loess and cemented sands. An improved method of estimating strength parameters in these types of soils that takes into account the in situ fabric would be of value to geotechnical engineering practice.

Shear wave velocity is a property that is strongly influenced by the fabric and state of the soil. The measurement of shear wave velocity in situ is increasingly being used in geotechnical engineering practice, especially in seismic response analyses and liquefaction potential assessment (3, 4, 5). Shear wave velocity can be measured both in the field and in the laboratory. Field methods include the cross-hole test, down-hole test (often in conjunction with CPT), Spectral Analysis of Surface Waves (SASW), Multi-channel Analysis of Surface Waves (MASW), and others (6). In the laboratory, small strain properties are most often measured using a resonant column to measure the small strain shear modulus or bender elements to measure shear wave velocity (7).

The small strain shear modulus is a dynamic soil property that depends on several parameters including effective stresses, void ratio, stress history, grain characteristics, and degree of saturation, among others (8), with the two most significant being effective stress (σ') and void ratio (e). The relationship between the small strain shear modulus and shear wave velocity can be obtained from the theory of elasticity by the following equation:

$$G_0 = \rho v_s^2 \tag{1.1}$$

where G_0 is the small strain shear modulus, v_s is the shear wave velocity, and ρ is the corresponding bulk density of the soil at the time of v_s measurement.

The objective of this paper is to evaluate the hypothesis that there is a unique relationship between the small strain shear modulus (G_0) and the effective stresses at failure for different dilatant soils. To accomplish this objective, isotropically consolidated drained triaxial compression tests were performed with shear wave velocity measured throughout the tests. The soils tested in this study include a medium quartz sand, and non-plastic silt. Samples were tested at different combinations of density and effective stress. The results of these tests are compared to previous work on weakly cemented sands by the authors.

Laboratory Testing Program

Properties of Soil Tested

Grain size distributions of the three soils presented in this paper are shown in Figure 1.1. The soils used in this study are a silty sand artificially cemented with Ordinary Portland Cement (OPC), a quartz sand, and non-plastic silt. Hoffman (9) summarizes the properties of the cemented sand. The specific gravity (G_s) of the silty sand used for the mixture and the Ordinary Portland Cement are 2.66 and 3.15, respectively. As a result, the final G_s of the cemented sand samples varied depending on the specified cement content. The sand samples have a G_s = 2.66, e_{max} = 0.835 and e_{min} = 0.460 as determined by ASTM D4253 and ASTM D4254 (10, 11). The silt used for this research is a blended material from three different sites in Providence, Rhode Island, and has a G_s = 2.75, e_{max} = 1.17, and e_{min} = 0.488.

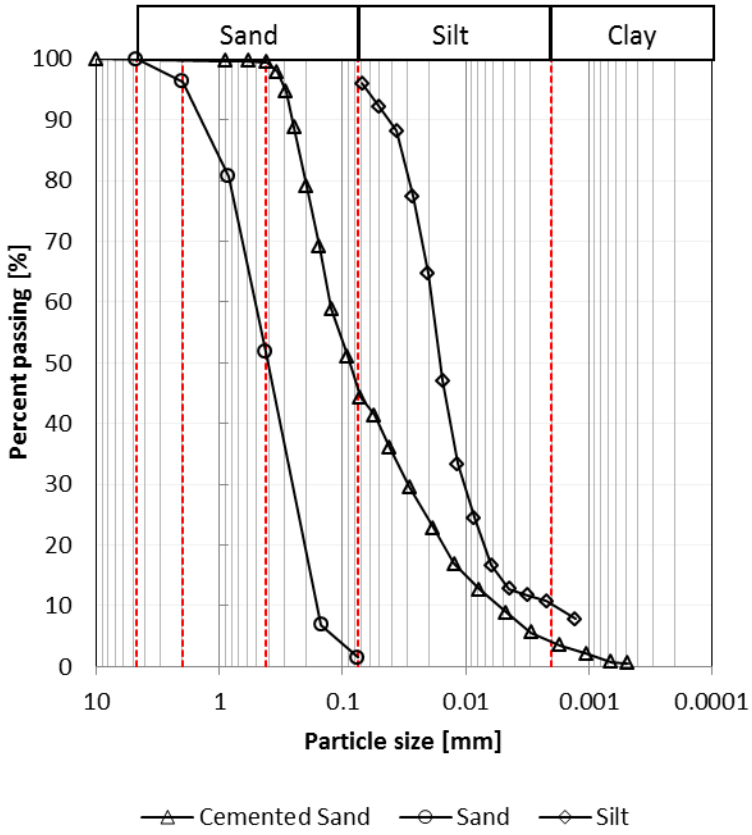

Figure 1.1 - Grain size distribution of the soils used in this study

Sample preparation techniques varied depending on the soil type. The weakly cemented sand samples were prepared and cured following the procedure suggested by Hoffman (9) with different OPC contents of 0, 1, 2.5, and 5% by weight. These samples were compacted using a modified moist tamping method developed by Bradshaw and Baxter (12) and Taylor (13). In this approach, samples are compacted in layers that are tamped to a specific energy. The layers are prepared at a specific molding water content, which greatly influences the resulting fabric of the specimen. A 3 kg compaction hammer was used, and the drop height and number of blows varied depending on the desired density. Uncemented samples were tested immediately after their preparation. Cemented samples were stored and weighed periodically until a constant weight was achieved due to drying (about 14 days) then tested (14).

The silt samples were also prepared using the modified moist tamping method. Sand samples were prepared by air pluviation and subsequent tapping (on the sides of the mold) on the triaxial cell to achieve the desired void ratio.

Test Method and Equipment

The isotropically consolidated drained (CID) triaxial tests were performed using an automated stress path apparatus. This equipment consists of a computer controlled load frame and two flow pumps to control the cell and sample pressures. The flow pumps allowed for automatic back pressure saturation of the samples and measurement of volume changes during consolidation and shear.

Table 1.1- Testing matrix for the laboratory testing program

Soil Type	Test Type	D_R (%) or Density (g/cc)	OPC Cement (%)	Confining Stress (kPa)
Weakly cemented sand	CID	1.8, 2.1, 2.25	0, 1, 2.5, 5.0	50, 100, 300
Quartz sand	CID	80, 60, 40	N/A	50, 100, 200
Non-plastic silt	CID	80, 60	N/A	50, 100, 200

The weakly cemented sands were saturated to a Skempton's B-value of at least 0.90, and sheared at a rate of 0.005%/minute to ensure drained conditions. The sand and silt samples were saturated to B-values of at least 0.95, and consolidated for a period no less than 60 minutes. They were sheared at a rate of 0.01%/minute. Table 1 shows the testing matrix for this study including the weakly cemented sands tested by Sharma et al. (1). Shear wave velocity measurements were taken both during consolidation and shear phases.

Shear Wave Velocity Measurement

Shear wave velocity measurements have become more common in research laboratories over the past decade. Such measurements have been used to observe changes in compressibility during consolidation (15), liquefaction potential (5), development of aging effects (16), and the effects of cementation (17, 18, 19, 20). Details of using bender elements, including prevention of electromagnetic coupling, directivity, resonant frequency, detection of first arrival, and near field effects are studied by Lee and Santamarina (21). A summary of best practices, including generation of input signals, interpretation of received signals and signal processing is presented by Yamashita et al. (22).

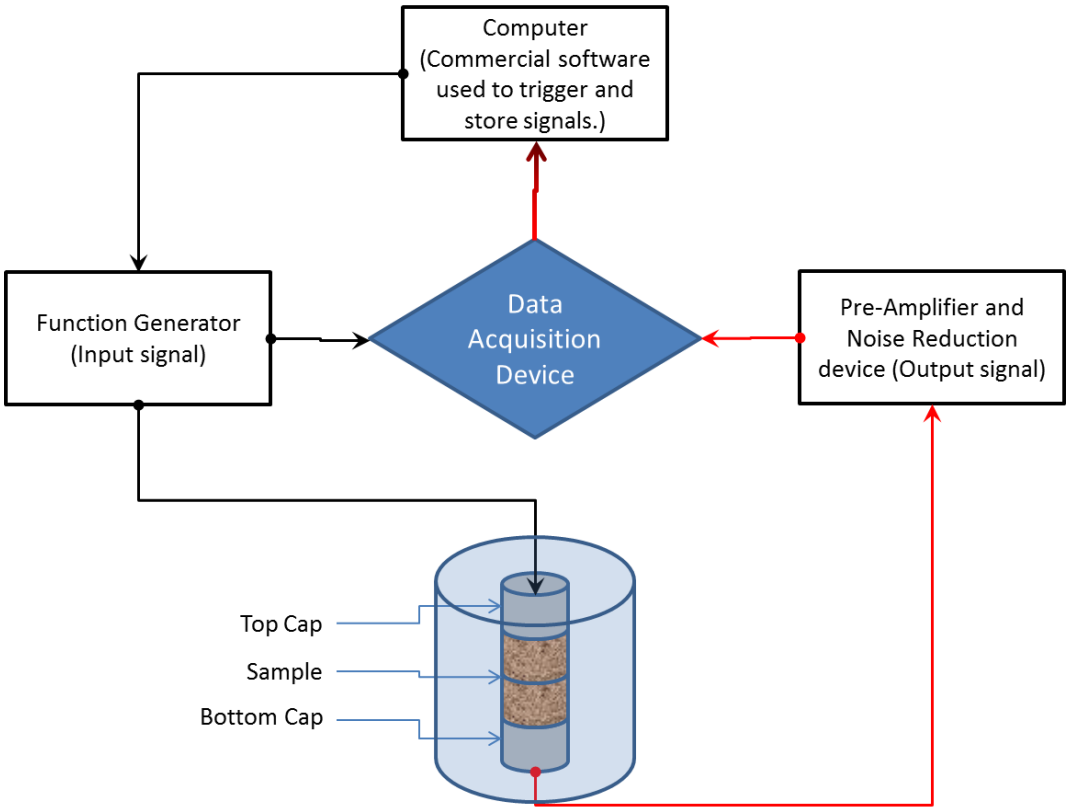

Figure 1.2 - Shear wave velocity measurement system

The equipment used to measure shear wave velocity in this study consisted of a pair of transducers installed in each sample end cap (one transmitter and one receiver), a function generator, a noise-reduction and pre-amplifier device, and a data acquisition card interfaced with a desktop computer. Figure 1.2 shows a schematic of the equipment setup. A commercial programming language software was used to trigger the input signal and store both the input and received signal. A single sinusoidal wave was used as the input signal with a voltage of 20 V peak to peak. The frequency of the input signal varied from 5 to 12 kHz depending on sample size and soil type. The burst period was set to 0.1 s, and the sampling frequency to 1 MHz (23).

Two types of shear wave transducers were used in this study: bender elements and torsional transducers. Bender elements have been widely accepted in the geotechnical community to measure shear waves and were first used in soil laboratory testing by Shirley (24). These piezoceramic elements are installed in each end cap leaving a small protrusion (about 0.6 cm) that is embedded into the sample. Each bender element consists of two-layered piezoelectric plates bonded together. One transducer is used as the transmitter and the other as the receiver. When the transmitter element is excited with a voltage it deforms in a bending motion due to the polarization of the plates. This produces a vibration that travels through the medium. At the other end, the receiver transducer detects the vibration, and produces a voltage. The torsional transducers consist of discs painted in sections with silver electrodes in a specific pattern (14). The sections are polarized by applying some voltage. Similarly, when the transmitter receives a voltage it produces a vibration which is detected by the receiver. Torsional transducers have the benefit that they do not penetrate into the sample, which is particularly useful for

rock and cemented samples. Wang et al. (25) and Hanchar (26) showed that torsional transducers produce comparable results to bender elements.

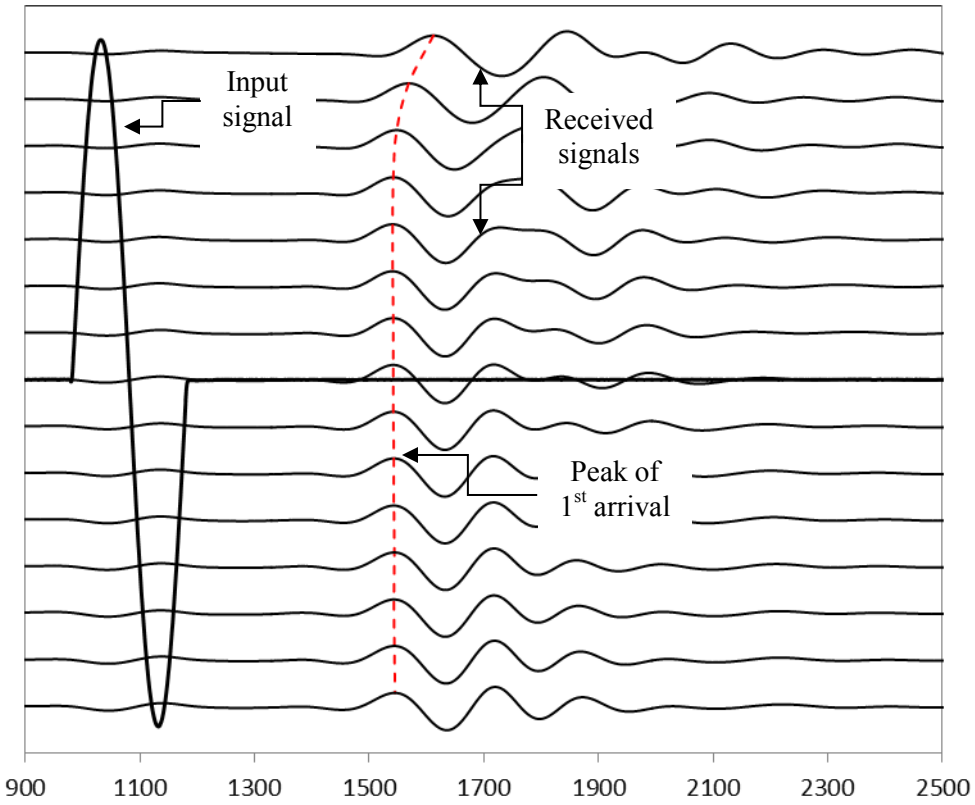

Figure 1.3 - Determination of the arrival time

As part of the data processing, an analog bandpass filter was applied to the received signal with a range of 100 Hz to 30 kHz. This analog filter was necessary to reduce the noise level. Additionally, the voltage of the received signal was amplified between 200 to 2000 times so it could be detected by the data acquisition card. Once the data was recorded and stored, an additional digital bandpass filter was applied. This digital filter was necessary to make possible an automated system to determine the arrival time of the shear wave. For this purpose the arrival time was defined as the difference between the peak of the transmitted and first received signal. Figure 1.3 shows an

example of a triggered signal and the first peak of arrival for multiple signals. The first arrival is typically measured from the initial slope of the transmitted and received signals (21), however it has been shown that using the peak-to-peak time difference results in an error of ~ 3% (14, 22). Using the peak-to-peak time difference makes it significantly easier to automate this process. Time delay caused by the whole system is measured and taken into account. Specific details of the measurement used in this study can be found in previous work performed by Sharma (23).

As the sample is sheared, the distance between the peaks shortens. The shear wave velocity v_s, at any time is calculated by:

$$v_s = \frac{L_{tt}}{\Delta t} \tag{1.2}$$

where L_{tt} is the length of the sample (if torsional transducers are used) or the tip-to-tip distance between the bender elements, and Δt is the time difference between the peak of the input signal and the first peak of arrival of the output signal.

Results

Stress-Strain Behavior of Weakly Cemented Sand

Figure 1.4 shows typical stress strain relationships for a weakly cemented sand. The variation of volumetric strain, shear wave velocity, and small strain shear modulus with axial strain is also shown. A discussion on the effect of cementation on the stress-strain behavior of weakly cemented sand is beyond the scope of this paper, and is presented in detail by Sharma et al. (2) and Baxter and Sharma (27). The focus of these figures is to

compare the small strain shear modulus with the other parameters shown. Six of the

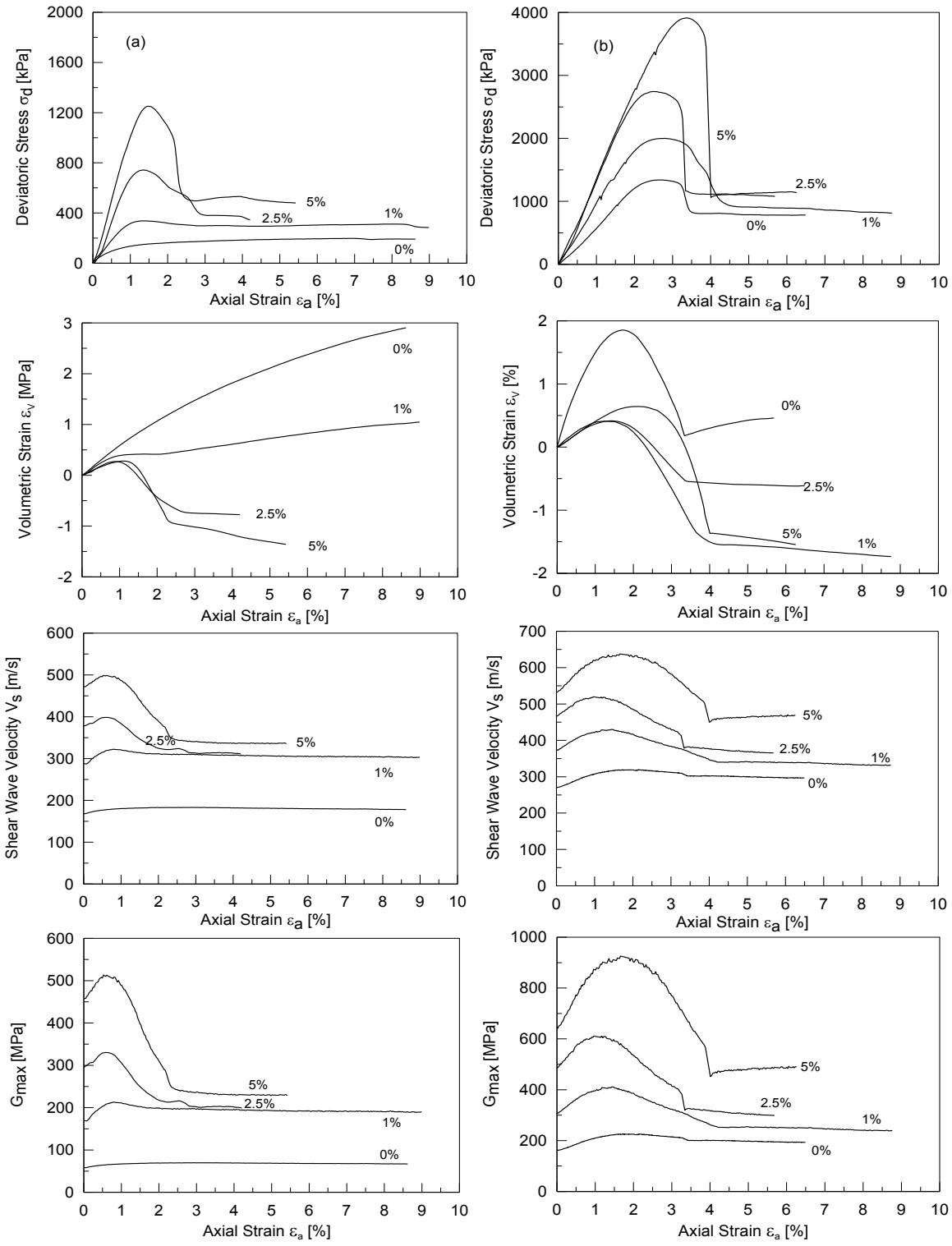

Figure 1.4 - Typical results of CID triaxial tests for weakly cemented sand. (a) Results for ρ_b = 1.8 g/cc, σ'_3 = 100 kPa. (b) Results for ρ_b = 2.1 g/cc, σ'_3 = 300 kPa. The percentages are the percent OPC by weight. (2)

eight samples (all dilative) exhibited a clear peak in the small strain shear modulus during shear. In contrast, two of the samples (contractive) do not show any peak in the shear modulus. It is evident that the presence of cementation increases the shear strength as well as the tendency to dilate and the initial shear modulus. The authors believe that the occurrence of this characteristic peak is fundamental for the development of a relationship between G_0 and σ'_{1f}.

Constant G_0/σ'_{1f} for Weakly Cemented Sand

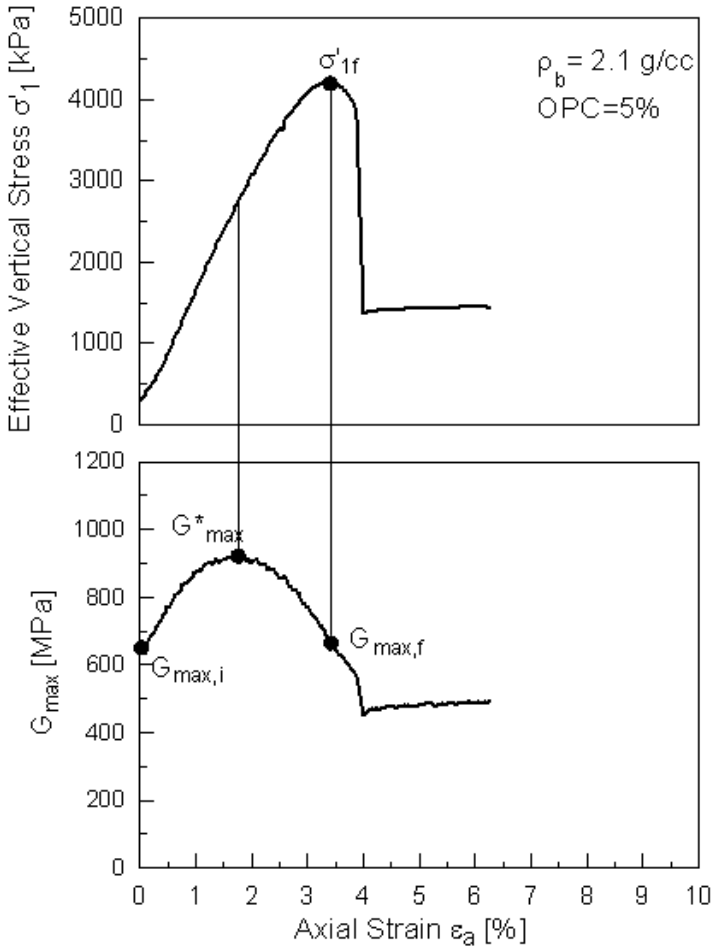

Figure 1.5 - Typical small strain shear modulus behavior for weakly cemented sand (2)

For each of the dilative samples tested, the variation of small strain shear modulus with strain followed a distinctive trend. At the beginning of shear, the small strain shear

modulus starts at G_0 ($G_{max,i}$), which is the initial shear modulus measured at the end of consolidation. During shearing, the small strain shear modulus increases up to a maximum point (G^*) and then decreases. The maximum peak G^* occurs at some point before the strength is fully mobilized (σ'_{1f}). Figure 1.5 shows this behavior, which was observed in all dilative tests. This increase in the small strain shear modulus follows a similar trend with the volumetric change; i.e. the maximum peak G^* occurs near the maximum point of contraction during the shear phase.

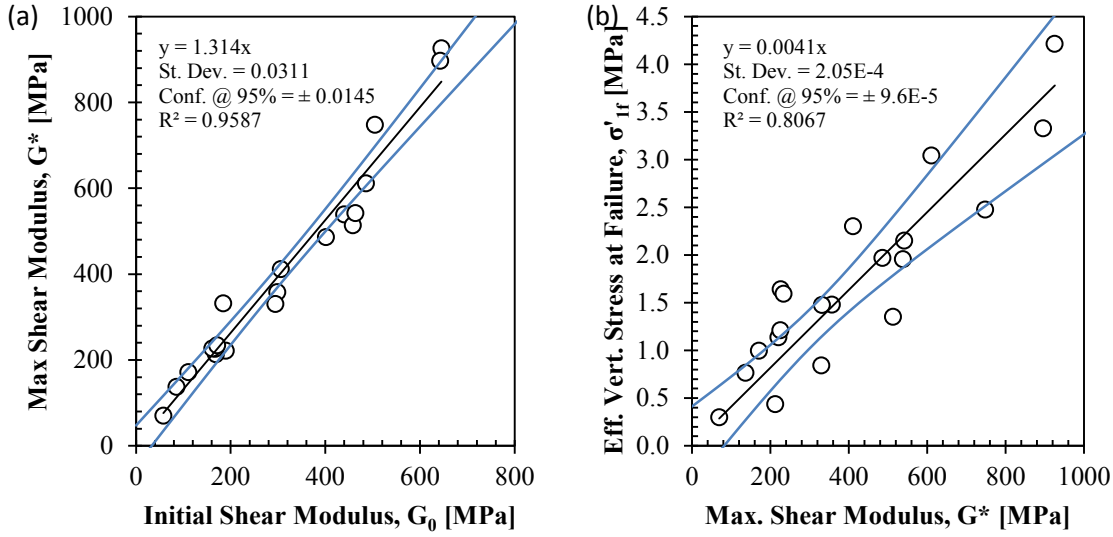

Figure 1.6 - Relationship of (a) G^*/G_0 and (b) σ'_{1f}/G^* for weakly cemented sand

A total of twenty-two samples of weakly cemented sand were tested. Plots of G^* vs G_0 and σ'_{1f} vs G^* are shown in Figure 1.6a and 6b along with the 95% confidence intervals. Figure 1.6a shows that during shear, the small strain shear modulus increased approximately 31% from G_0 to G^*. When comparing G^* and σ'_{1f} the data looks more scattered, however a relationship can be established between the two variables. A direct relationship between G_0 and σ'_{1f} is shown in Figure 1.7. Based on this figure the slope of the fitted curve is 0.00533, which gives a relationship $G_0/\sigma'_{1f} = 188$. It is important to

note that this ratio appears to be independent of sample density, degree of cementation, and effective confining stress.

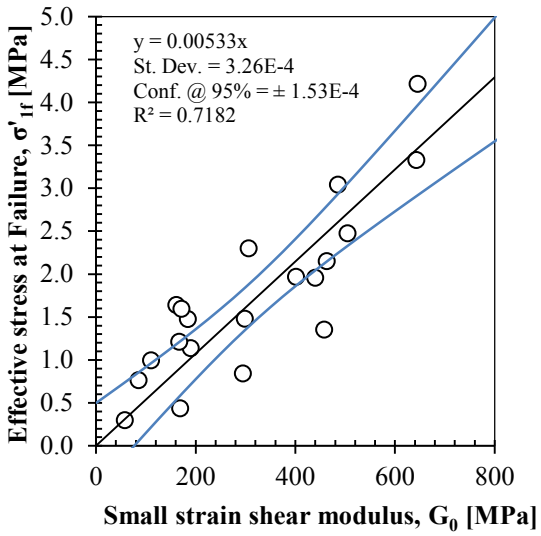

Figure 1.7 - G_0/σ'_{1f} for Weakly Cemented Sand

Stress-Strain Behavior of Quartz Sand

Figure 1.8 shows stress-strain relationships of samples of quartz sand, along with volumetric strain and small strain shear modulus behavior. As expected, for a given confining stress the sand exhibits higher tendency for dilation and higher values of small strain shear modulus as the relative density increases. Samples prepared at a relative density of 80% were clearly dilatant and exhibited similar behavior to the weakly cemented sands. The peak small strain shear modulus was less pronounced as the relative density decreased. However, Figure 1.8 clearly shows that the samples of quartz sand exhibited the same fundamental behavior as the weakly cemented sand; during shear the small strain shear modulus increased to a maximum value and then decreased despite the fact that deviator stress continued to increase until failure. With this soil, the peak value of the small strain shear modulus also occurs at approximately the peak value in the volumetric strain curve.

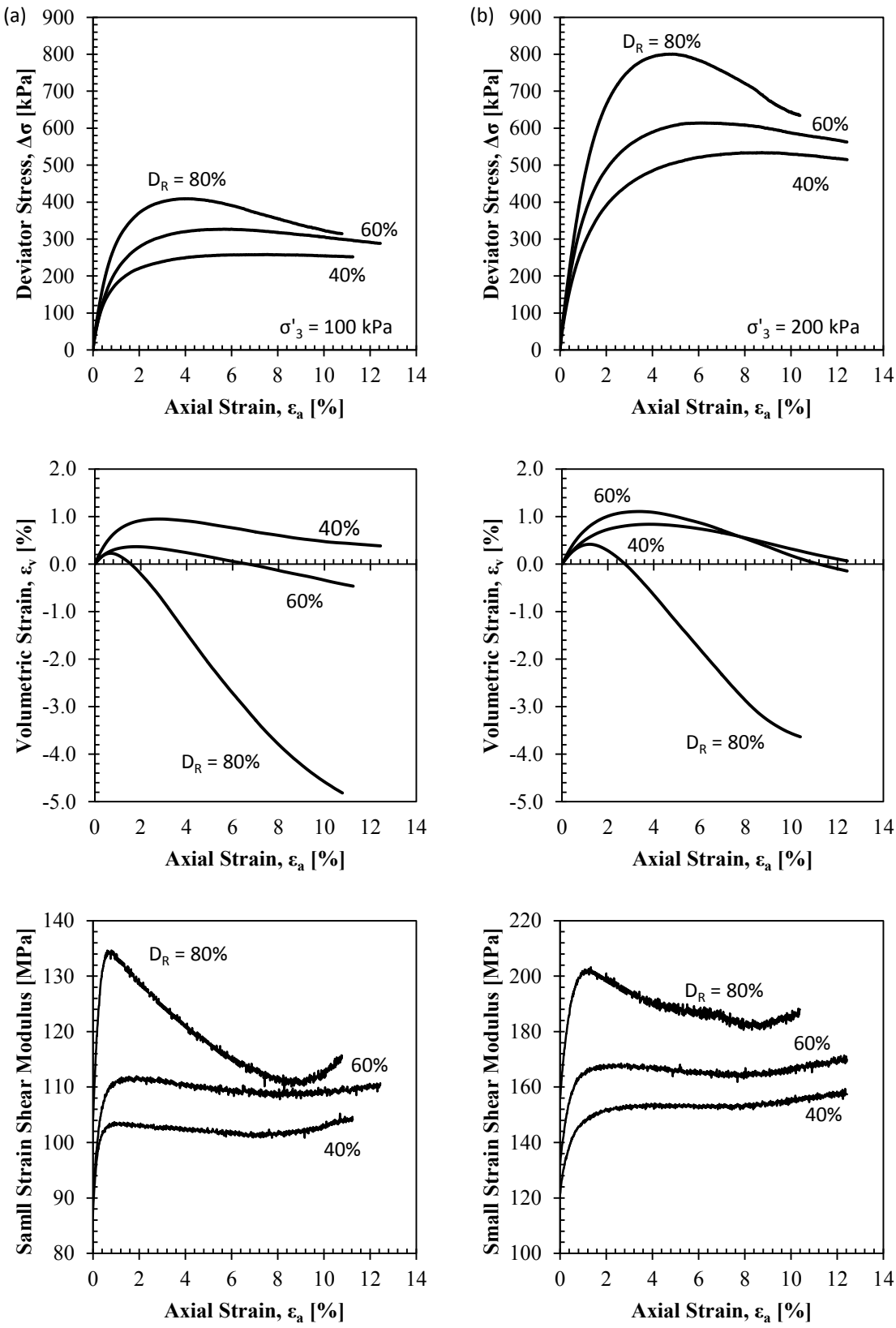

Figure 1.8 - Typical results of CID triaxial tests for quartz sand. (a) σ'_3 = 100 kPa, (b) σ'_3 = 200 kPa

A total of 15 tests were used to develop the G_0/σ'_{1f} relationship for the quartz sand. By direct relationship, the resulting ratio of G_0/σ'_{1f} = 180. The curves for a 95% confidence show that more than half of the data fits into this trend, as shown in Figure 1.9.

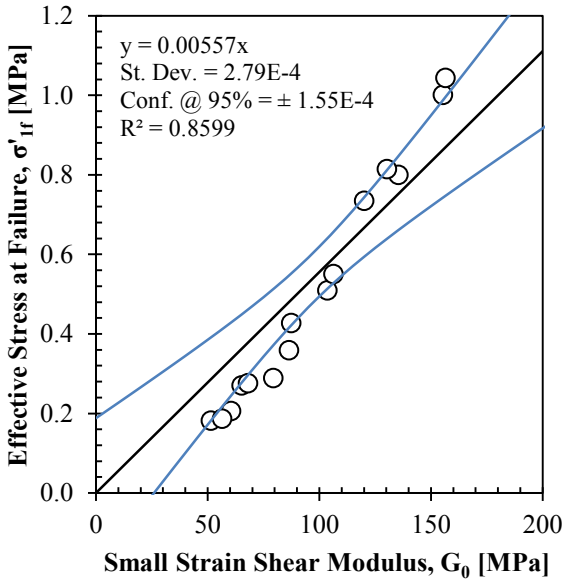

Figure 1.9 - G_0/σ'_{1f} ratio for quartz sand

Stress-Strain Behavior of Non-Plastic Silt

Typical results of tests performed on samples of non-plastic silt are shown in Figure 1.10. Comparable to the weakly cemented sand and the quartz sand, there is a clear relationship between G_0, and σ'_{1f}. One interesting difference with the silt data is that the small strain shear modulus from tests at different densities appears to converge at large values of strain, which may be analogous to a residual condition. Another difference observed from the non-plastic silt is the fact that the peak value of small strain shear modulus does not necessarily occur close to the peak value of the volumetric strain. Figure 1.11 shows the relationship between G_0 and σ'_{1f} of 14 tested samples along with the curves of 95% confidence. For the non-plastic silt, this relationship yields a G_0/σ'_{1f} ratio equal to 219.

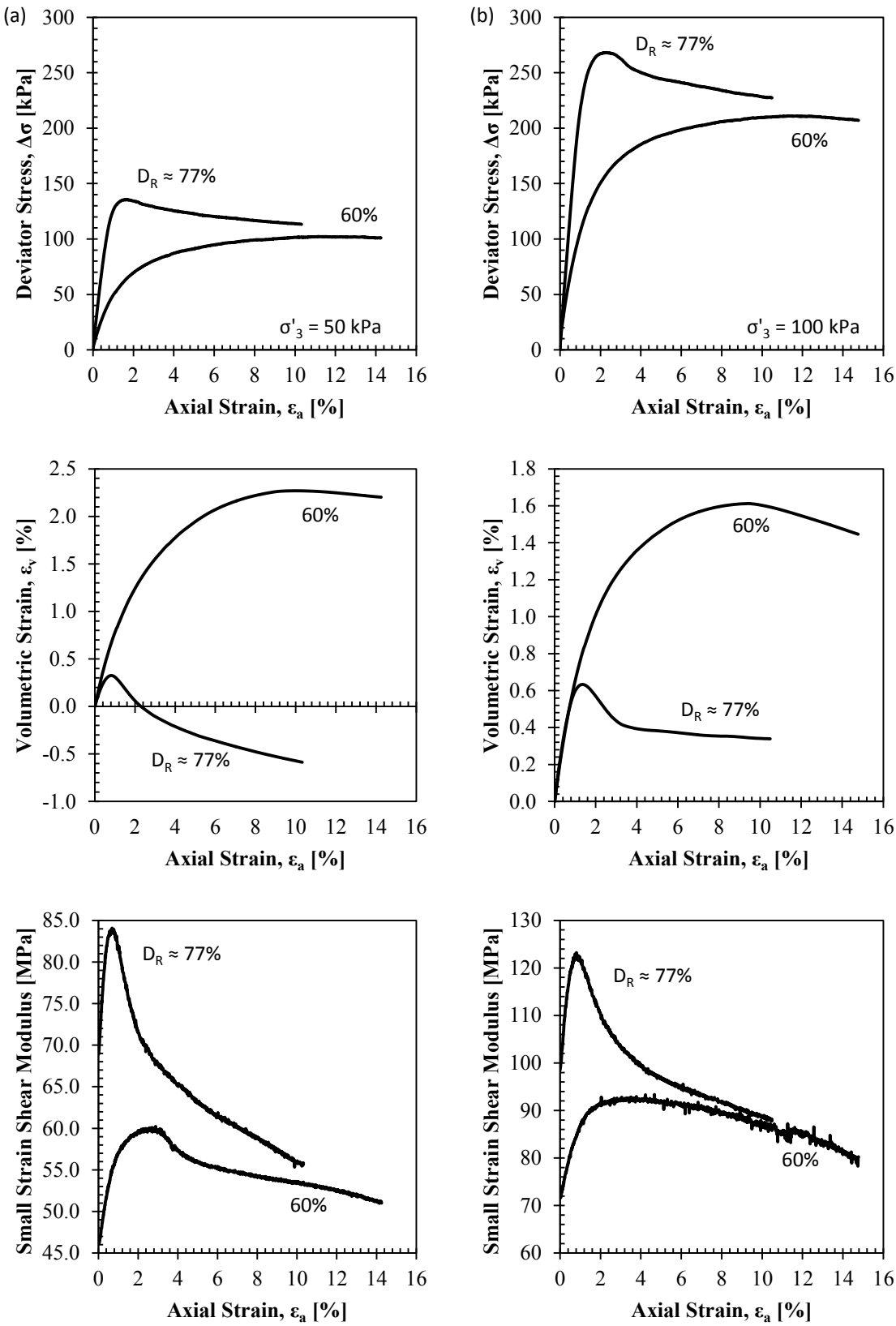

Figure 1.10 - Typical results for CID triaxial tests for non-plastic silt. (a) σ'_3 = 50 kPa, (b) σ'_3 = 100 kPa

This value is much higher than the results obtained from the cemented sand and quartz sand. It is possible that fines content may play a role in the G_0/σ'_{1f} ratio.

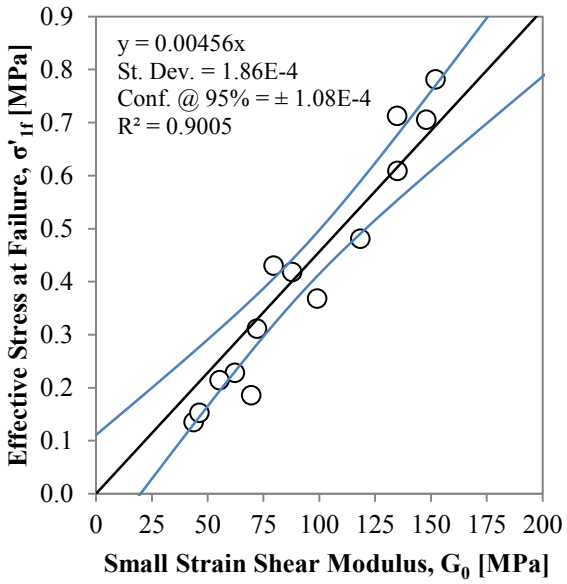

Figure 1.11 - G_0/σ'_{1f} for non-plastic silt

Discussion and Conclusions

This paper presents laboratory data to support the hypothesis that there is a unique relationship between small and large strain parameters for different soils. This unique relationship was first introduced by Sharma et al. (1, 2) in which they hypothesized a fundamental link between G_0 and σ'_{1f} for weakly cemented sands. The unique relationship is based on observations that the small strain shear modulus reaches a peak before full mobilization of the shear strength, and that the initial shear modulus and effective vertical stresses at failure are related by a constant ($G_0/\sigma'_{1f} = M$ = constant). This relationship may or may not be soil dependent, but for a given soil the relationship is independent of density, degree of cementation, and confining stress, as long as the samples develop a dilative response.

In order to test this hypothesis, two additional soils were tested as part of this study: a quartz sand and non-plastic silt. Samples were prepared at different densities and consolidation stresses, and isotropically consolidated-drained triaxial compressional tests were performed. It was found that all dilative samples of the tested soils followed this unique relationship. For all samples, the relationship G_0/σ'_{1f} was 200 ± 20. Even though the tested soils were different, the difference from the mean value (196) ranged from 8 to 12%. Also, an interesting trend was found in the silt samples in which the small strain shear modulus from tests at different densities converged at large values of strain. This behavior may be analogous to a residual condition. The results showed that the soil with the highest G_0/σ'_{1f} was the non-plastic silt (219), followed by the weakly cemented sand (188) and lastly the quartz sand (180). It is possible that there may be an influence of fines content on the G_0/σ'_{1f} ratio. However, more research is required to investigate this further.

The results of this study have several potential implications for geotechnical engineering practice. If this relationship is shown to be ubiquitous, it could be used for staged construction as a preventive warning for failure on sensitive soils by measuring v_s during construction and knowing the G_0/σ'_{1f} relationship of the soil. Another possible use is to estimate strength of soils in which sampling is difficult (e.g. loess, cemented sands). Additional studies suggest that this unique relationship may lead to the determination of soil strength parameters such as internal friction angle ϕ', and cohesion c' for dilative, brittle or sensitive soils.

Acknowledgements

This research was funded by grants from the National Science Foundation (No. CMMI 1031135), BP America, Inc., Rhode Island Department of Transportation (RIDOT), the New England University Transportation Center (NEUTC), and the University of Rhode Island Transportation Center (URITC). This support is gratefully acknowledged.

References

1. Sharma R., C. D. P. Baxter, and Y. Guadalupe. Unique Relationship between Small Strain Shear Modulus and Effective Stresses at Failure for Dilatant Soils, *NSF CMMI Research and Innovation Conference 2011*, 2011, Atlanta, Georgia, 8 pgs.

2. Sharma R., C. D. P. Baxter, and M. Jander. Relationship between shear wave velocity and stresses at failure for weakly cemented sand during triaxial compression. *Soils and Foundations*, Vol. 51, No. 4, 2011, pp. 761-771.

3. Andrus R. D. and K. H. Stokoe. Liquefaction Resistance of Soils from Shear-Wave Velocity. *Journal of Geotechnical and Geoenvironmental Engineering*, Vol. 126, No. 11, 2000, pp. 1015-1025.

4. Yunmin, C., K. Han, and C. Ren-peng. Correlation of Shear Wave Velocity with Liquefaction Resistance based on Laboratory Tests. *Soil Dynamics and Earthquake Engineering*, Vol. 25, 2005, pp. 461-469.

5. Baxter, C. D. P., A. S. Bradshaw, R. A. Green, and Jian-Hua Wang. Correlation between Cyclic Resistance and Shear-Wave Velocity for Providence Silts. *Journal of Geotechnical and Geoenvironmental Engineering*, Vol. 134, No. 1, 2008, pp. 37-46.

6. Kramer, S. L. *Geotechnical Earthquake Engineering*, Prentice Hall, Inc., New Jersey, 1996.

7. Dyvik, R and C. Madshus. Lab Measurements of G_{max} using Bender Elements. *Proceeding, ASCE Conference on Advances in the Art of Testing Soils Under Cyclic Conditions,* New York, 1985, pp. 186-196.

8. Richart, F. E., J. R. Hall, and R. D. Woods. *Vibrations of Soils and Foundations.* Prentice-Hall, Inc., New Jersey, 1970.

9. Hoffmann, W. Evaluation of real cohesion for a weakly cemented sand. *MS Thesis.* The University of Rhode Island, 2008.

10. ASTM D4253-00. Standard Test Methods for Maximum Index Density and Unit Weight of Soils Using a Vibratory Table. West Conshohocken, PA 19428-2959, US. 2000.

11. ASTM D4254-00. Standard Test Methods for Minimum Index Density and Unit Weight of Soils and Calculation of Relative Density. West Conshohocken, PA 19428-2959, US. 2000.

12. Bradshaw, A. S. and C. D. P. Baxter. Sample Preparation of Silts for Liquefaction Testing. *Geotechnical Testing Journal*, Vol. 30, No. 4, 2007, 9 pgs.

13. Taylor, O. D. S. Use of Energy-Based Liquefaction Approach to Predict Deformation in Silts due to Pile Driving. *PhD Dissertation*. The University of Rhode Island, 2011.

14. Jander, M. Small Strain Shear Modulus Degradation of Cemented Sand during Drained Shear. *MS Thesis*. University of Rhode Island, 2009.

15. Yun, T.S. and, J.C. Santamarina. Decementation, Softening, and Collapse: Changes in Small-Strain Shear Stiffness in k_0 Loading. *Journal of Geotechnical and Geoenvironmental Engineering*, Vol. 131, No. 3, 2005, pp.350-358.

16. Baxter, C.D.P. and J.K. Mitchell. Experimental Study on the Aging of Sands. *Journal of the Geotechnical and Geoenvironmental Engineering*, Vol. 130, No. 10, 2004, pp. 1051-1062.

17. Fam, M. and J.C. Santamarina, Study of Geoprocesses with Complementary Mechanical and Electromagnetic Wave Measurements in an Oedometer. *Geotechnical Testing Journal*, Vol. 18, No. 3, 1995, pp. 307-314.

18. Fam, M.A. and J.C. Santamarina. Study of Clay-Cement Slurries with Mechanical and Electromagnetic Waves. *Journal of Geotechnical Engineering*, Vol. 122, No. 5, 1996, pp. 365-373.

19. Fernandez, A.L. and J.C. Santamarina. Effect of cementation on the small-strain parameters of sands. *Canadian Geotechnical Journal*, Vol. 38, 2001, pp. 191-199.

20. Weil, M.H., J.T. DeJong, B.C. Martinez, B.M. Mortensen, and J.T. Waller. Seismic and Resistivity Measurements for Real-Time Monitoring of Microbially Induced Calcite Precipitation in Sand. *Geotechnical Testing Journal*, 2012, Vol. 35, No. 2, pp. 1-12, DOI: 10.1520/GTJ103365.

21. Lee, J-S., and J. C. Santamarina. Bender Elements: Performance and Signal Interpretation. *Journal of the Geotechnical and Geoenvironmental Engineering*, Vol. 131, No. 9, 2005, pp. 1063-1070.

22. Yashamita, S., T. Kawagushi, Y. Nakata, T. Mikami, T. Fujiwara, and S. Shibuya. Interpretation of International Parallel Tests on the Measurement of Gmax using Bender Elements. *Organized by TC-29 of International Society of Soil Mechanics Geotechnical Engineering,* 2007, 76 pgs.

23. Sharma, R. Strength Prediction of Weakly Cemented Sands from Geophysical Logs. *PhD Dissertation*. University of Rhode Island, 2010.

24. Shirley, D. J. An Improved Shear Wave Transducer. *Journal of Acoustical Society of America*, Vol. 63, No. 5, 1978, pp.1643-1645.

25. Wang, Jian-Hua, K. Moran, and C. D. P. Baxter. Correlation between Cyclic Resistance Ratios on Intact and Reconstituted Offshore Saturated Sands and Silts with the Same Shear Wave Velocity. *Journal of Geotechnical and Geoenvironmental Engineering*, Vol. 132, No. 12, 2006, pp. 1574-1580.

26. Hanchar, S. T. A Comparison of Bender Elements and Torsional Shear Wave Transducers. *MS Thesis*. University of Rhode Island, 2006.

27. Baxter, C.D.P. and R. Sharma. Shear Wave Velocity of Weakly Cemented Silty Sand During Drained and Undrained Triaxial Compression. *GeoCongress 2012*, 2012, ASCE, 12 pgs.

CHAPTER 2

"Evaluation of effective density to estimate the small strain shear modulus in saturated soils"

by

Yaurel Guadalupe-Torres[1], Tong Qiu[2], Christopher D.P. Baxter[3]

will be submitted to the Journal of Geotechnical and Geoenvironmental Engineering

[1] PhD. Candidate, Department of Civil and Environmental Engineering, University of Rhode Island, Narragansett, RI 02882. Phone: 787-467-3226, E-mail: yaurel_gt@yahoo.com

[2] Assistant Professor, Department of Civil and Environmental Engineering, Pennsylvania State University, University Park PA. Phone: 814-863-7305. E-mail: tqiu@engr.psu.edu.

[3] Professor, Department of Ocean/Civil and Environmental Engineering, University of Rhode Island, Narragansett, RI 02882. Phone: 401-874-6575, E-mail: baxter@oce.uri.edu

Evaluation of Effective Density to Estimate the Small Strain Shear Modulus in Saturated Soils

Abstract

Elastic theory is commonly used to define the small strain shear modulus (G_0) from bulk density (ρ) and shear wave velocity (v_s) by $G_0 = \rho v_s^2$. In saturated soils the saturated bulk density is used. However, this assumes that the soil skeleton and the water move together as a single phase as the shear wave passes. Recent work by Qiu and Fox (2008) has shown that, in some soils, this is not the case and in fact there is fluid motion relative to the soil skeleton. Using Biot's theory (Biot 1956a,b) and data from Hardin and Richart (1963), Qiu and Fox (2008) found that for some soils, a reduced density, termed effective density, should be used instead of the saturated density. The objective of this paper is to present experimental results in support of the effective density concept. A series of triaxial tests were performed on dry and saturated specimens and the small strain shear modulus was calculated from shear wave velocity measurements using bender elements. Three cohesionless materials with differing grain size distributions were tested: fine to medium sand, coarse sand, and 6 mm diameter glass beads. For the coarse sand and the gravel-sized glass beads, there was good agreement between the G_0 values for the saturated specimens using predicted values of effective density and values of G_0 from comparable dry specimens. These results suggest that use of an effective density may be appropriate when estimating the small strain shear modulus of coarse sands and gravels.

Introduction

Small strain shear modulus is an important soil property used in seismic site response analyses, machine vibration and settlement problems. Elastic theory is typically used to calculate the small strain shear modulus (G_0) of a soil from the bulk density (ρ) and the shear wave velocity (v_s) by $G_0 = \rho v_s^2$. This assumes that the soil skeleton and water in the pore space moves in phase with each other as the shear wave passes. In some cases, however, there is fluid motion relative to the soil skeleton and use of the saturated bulk density may be inappropriate for estimating G_0. Santamarina et al. (2001) attributed the relative motion between the fluid and the soil skeleton due to differential inertial effects caused by an increase in the shear wave frequency. In addition to high frequency, this effect becomes more significant when the porous media has large grain size, high porosity and high hydraulic conductivity. Qiu and Fox (2008) used Biot theory to develop an expression for a reduced density, termed effective density (ρ_{eff}), to account for these effects. The implication of not accounting for relative motion between the water and soil skeleton for certain saturated soils is that use of the saturated density may result in up to a 20% overestimation in estimates of G_0. This could affect the results of site response analyses in certain soils.

Background

Qiu and Fox (2008) defined the effective density as the density that controls shear wave velocity and accounts for the soil skeleton and the fraction of water that moves with the skeleton during shear wave propagation. It is expressed as

$$\rho_{eff} = \frac{G_o}{v_s} \tag{2.1}$$

Biot (1956a,b) proposed an analytical solution for the velocity of sinusoidal waves as a function of the specific gravity of solids, porosity, hydraulic conductivity, wave frequency, and an added mass term to account for soil tortuosity. He also defined a characteristic frequency (f_c) to differentiate between shear wave velocities at low and high frequencies. The characteristic frequency can be calculated as:

$$f_c = \frac{ng}{2\pi k} \tag{2.2}$$

where n = porosity, g = acceleration of gravity, and k = hydraulic conductivity. For frequencies $f < 0.15f_c$, the relative fluid motion is of Poiseuille type. This has some implications as noted by Qiu (2010): (1) the fluid velocity is in a single direction, (2) the shear stress at the pore walls is in the opposite direction and proportional to the average velocity and (3) the fluid motions are governed by Darcy's law. However, when the shear wave frequency, $f > 0.15f_c$, it is considered a high frequency velocity and the relative motion becomes more complex. In this case the motion can be in two directions, the shear strain is not proportional to the average velocity, and the flow becomes a non-Poiseuille type (Qiu, 2010).

Using Biot's solution, Qiu and Fox (2008) established the value of effective density bounded by two cases:

$$\rho_{eff} = \rho_{sat} \qquad \overline{f} \to 0 \tag{2.3}$$

$$\rho_{eff} = \rho_{sat}\left[1 - \frac{n}{\delta\left(G_s + n - G_s n\right)}\right] = \rho_d\left[1 - \frac{n\left(\delta - 1\right)}{\delta G_s\left(1 - n\right)}\right] \qquad \overline{f} \to \infty \tag{2.4}$$

where $\overline{f}$ = normalized frequency, G_s = specific gravity, ρ_{sat} = saturated density, and δ = structural factor representing the added mass caused by tortuosity of the pore space. The value of δ is difficult to determine for soils and Qiu and Fox (2008) used a relationship proposed by Sen et al. (1981):

$$\delta = n^{-\overline{\beta}} \tag{2.5}$$

where $\overline{\beta} = 0.5$. The normalized frequency, $\overline{f}$, is defined as

$$\overline{f} = \frac{f}{f_c} = \frac{2\pi f k}{ng} \tag{2.6}$$

where f = wave frequency. Equations 2.3, 2.4, and 2.6 show that the effective density is strongly influenced by hydraulic conductivity and frequency of the shear waves. High values of either k or f can lead to values of ρ_{eff} less than ρ_{sat}. For values of $\overline{f}$ between 0 and ∞, Qiu and Fox (2008) presented predictions of ρ_{eff} as shown in Figure 2.1.

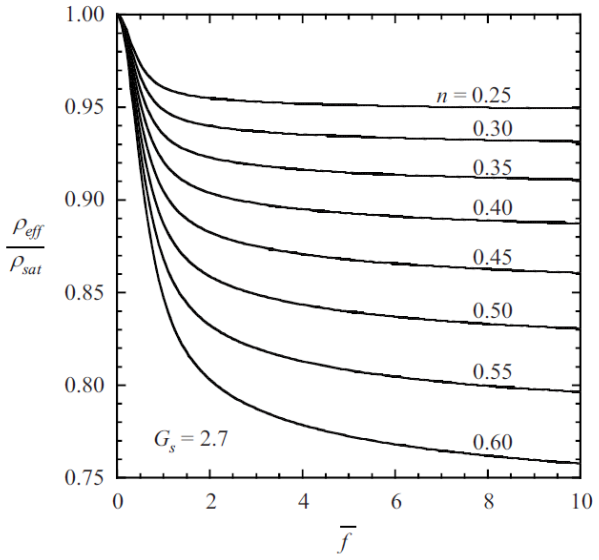

Figure 2.1 - Ratio of effective density to saturated density for water-saturated soil with G_s = 2.7 (from Qiu and Fox, 2008)

Qiu and Fox evaluated the effective density concept using published shear wave velocity data from Hardin and Richart (1963). Resonant column tests (RC) were performed on dry, saturated, and drained (i.e. moist) samples of two different sands at varying densities and effective confining stresses. The relationships between shear wave velocity and effective stress for dry and saturated samples of Ottawa sand are shown in Figure 2.2. The shear wave velocities for the dry sample are consistently larger than the shear wave velocities of the saturated sample.

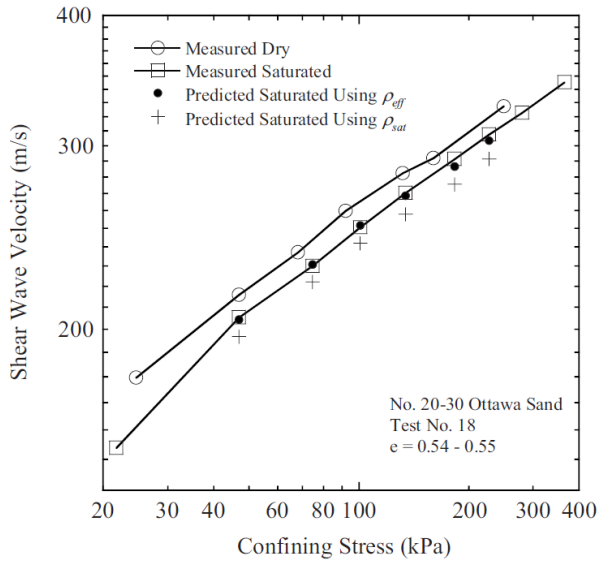

Figure 2.2 – Measured and predicted values of shear wave velocity for Ottawa sand (Qiu and Fox, 2008)

Assuming that the small strain shear modulus is equal for dry and saturated samples at comparable void ratios and effective stresses, Qiu and Fox (2008) compared measured and predicted shear wave velocities using measured values of saturated density and predicted values of effective density. For the estimation of normalized frequency (Eq. 2.6), the shear wave frequency from the experiments was used and the hydraulic conductivity was estimated using an empirical relationship (Chapuis 2004). The

agreement between the measured values of shear wave velocity and predicted values of effective density was excellent.

Youn et al. (2008) performed a similar study in which the small strain shear modulus of dry and saturated sands at different confining effective stresses was compared using different types of tests to generate and measure shear wave velocity: triaxial tests with bender elements (BE), resonant column (RC), and torsional shear (TS) tests. In their study they also used Biot's theory to correct the density of Silica sand and Toyoura sand under saturated conditions. Youn et al. (2008) considered two scenarios to determine the small strain shear modulus of saturated soils: low frequency and high frequency shear waves. Santamarina described the shear wave low frequency boundary as $f < 0.10 f_c$, as (Santamarina et al., 2001). They obtained the small strain shear modulus as follows:

$$G_{sk} = \left[(1-n)\rho_g + n\rho_f\right] v_{s0}^2 \tag{2.7}$$

where G_{sk} = small strain shear modulus of the soil-skeleton, ρ_g = density of the grains, ρ_f = density of the fluid, and v_{s0} = low-frequency limit of shear wave velocity. When the soil is fully saturated, Eq. 2.7 is equal to $G_0 = \rho_{sat} v_s^2$. Youn et al. used Eq. 2.7 for computing G_{sk} for the resonant column tests, as the resonant frequencies were below 100 Hz. However, when the frequency of the shear wave is much higher, the small strain shear modulus was obtained using the following equation:

$$G_{sk} = \left[(1-n)\rho_g + n(1-1/\alpha)\rho_f\right] v_{s\infty}^2 \tag{2.8}$$

where α = tortuosity factor, and $v_{s\infty}$ = high-frequency velocity. Santamarina et al. (2001) describes a high frequency shear wave when $f >> f_c$. Youn et al. used an input frequency of 11 kHz when using the bender elements, and used Eq. 2.8 to estimate the small strain shear modulus from those tests.

When the tortuosity factor tends to infinity ($\alpha = \infty$), as explained by Santamarina et al. (2001), the water is fully coupled with the soil skeleton and therefore its mass contributes to the total density of the soil. When the tortuosity factor $\alpha = 1$, the water is fully decoupled and it does not contribute its inertia during wave motion. As the permeability decreases (i.e. fine-grained material such as clays), the characteristic frequency increases and Biot's dispersion effects are less important. Biot's dispersion might also lose relevance with shear wave propagation at high frequencies, $f >> f_c$, as the propagation is likely to be mostly affected by grain scattering effects. A frequency increment will cause an increase in shear wave velocity as well due to abnormal dispersion. The viscous shear between the water and the pore walls increases with angular frequency, ω (where $\omega = 2\pi f$), and the inertial effects increase with the square of angular frequency ω^2. Santamarina et al. (2001) attribute the increment of shear wave velocity to the fact that the water tends to remain in place reducing the inertia or mass density of the soil.

Qiu and Fox (2008) also considered the frequency of the shear wave in estimating values of effective density, however the focus of their conclusions was on the practical implications of effective density on soils with high values of hydraulic conductivity (i.e. sands and gravels). The primary focus of the Youn et al (2008) was to highlight the effect of frequency on small strain modulus measurements considering that the shear wave velocities in practice are obtained using a variety of in situ (e.g. seismic cone penetration tests, analysis of surface waves) and laboratory (e.g. bender elements, resonant column) techniques that operate at different frequencies.

Experimental Program

Testing Procedure

A laboratory testing program was performed to evaluate the effective density concept proposed by Qiu and Fox (2008). The strategy was to measure the shear wave velocity as a function of effective stresses for samples under both dry and saturated conditions at the same void ratio. Values of small strain shear modulus were calculated for the dry samples using the dry density. Values of small strain shear modulus for the saturated samples were calculated using both the saturated density and the effective density predicted from theory.

Samples of three different materials, a fine to medium sand, coarse sand, and 6 mm diameter glass beads, were consolidated isotropically in a triaxial apparatus. Each sample was formed by air pluviation in layers followed by tapping the sides of the mold to achieve a desired dry density. Initially, each sample was subjected to two cycles of isotropic consolidation and unloading from 25 kPa to 400 kPa, and the shear wave velocity was measured at various stress levels. This cycling was done to minimize the changes in void ratio during the subsequent saturated testing phase.

After two cycles of loading, each sample was saturated and two more cycles of loading/unloading were applied while measuring shear wave velocity. Figure 2.3 shows the variation in volumetric strain with effective stress for the last two cycles of loading for each of the samples following saturation. Volume change was measured by the amount of water exiting or entering the saturated samples during loading/unloading, and it was assumed that the volume change behavior for the dry and saturated loading was the same.

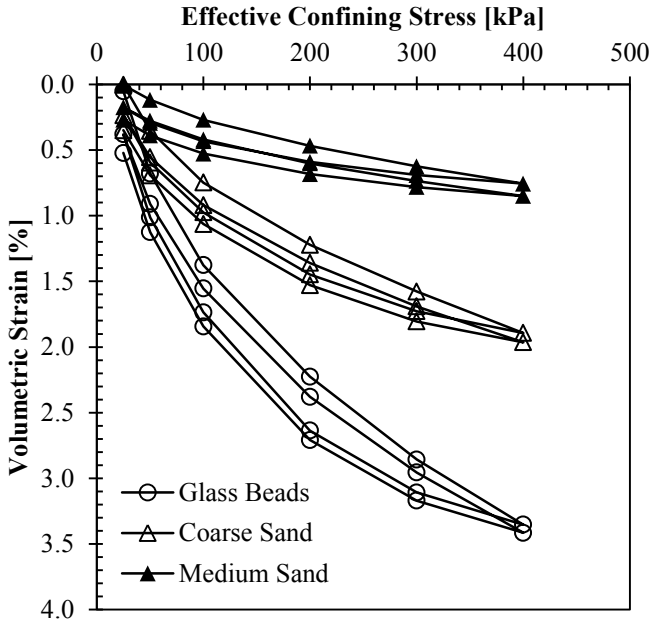

Figure 2.3 – Volumetric strain of saturated samples under cyclic stresses

Shear Wave Velocity Measurements

Shear wave velocity was measured using bender elements installed in the end caps of the triaxial apparatus (Figure 2.4). Shirley and Hampton (1978) first introduced bender elements to soil testing for measuring shear wave velocity, and Dyvik and Madshus (1985) found good agreement between shear wave velocities measured with bender elements and from resonant column tests. The bender elements are embedded in the end caps leaving a small protrusion of approximately 6 mm.

Bender elements consist of two piezo-ceramic sheets bonded together by a metal shim. The bender elements deform mechanically when a voltage is applied across the element and generate a voltage when deformed. They can be designed in parallel or in series. When wired in parallel they experience a higher deformation for a given input voltage, thus generating a stronger signal. Bender elements wired in parallel are typically

used as transmitters. When wired in series they produce a higher voltage for a given deformation and are most often used as receivers.

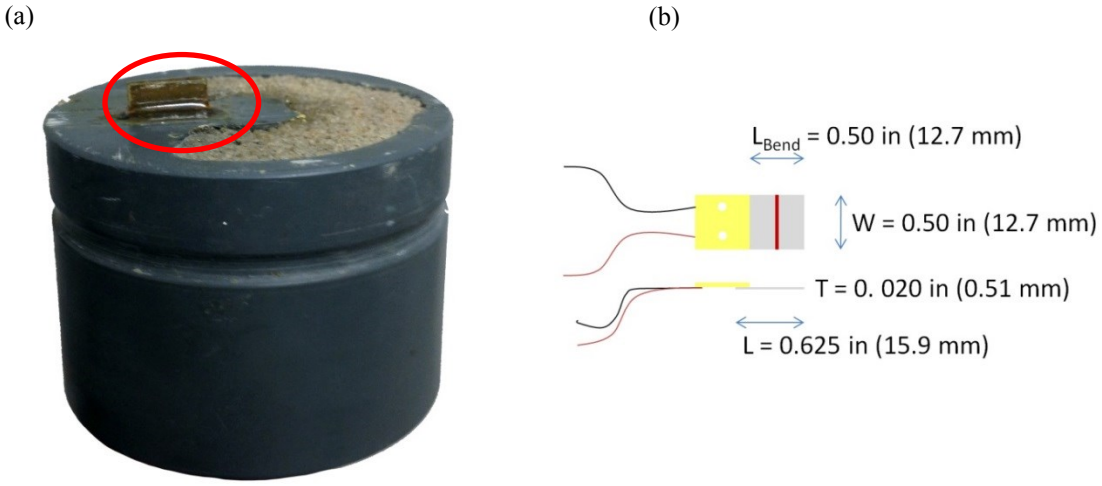

Figure 2.4 - (a) Bender elements installed in the triaxial end caps (b) bender element dimensions

A schematic of the shear wave velocity measurement system setup used in this study is shown in Figure 2.5. The transmitter is connected to a function generator that sends a single sinusoidal signal with ±10 volts amplitude (20 volts peak to peak) of variable frequency. The function generator is connected to a data acquisition card to store the input signal and to a desktop computer. The receiver is connected to a preamplifier which is also connected to the data acquisition card. The preamplifier amplifies the received signal and applies an analog band pass filter between 300 Hz and 30k Hz. A Matlab code was written to trigger the input signal, and to store both the input and received signals. The input frequency of the transmitted wave was varied until a value was found that yielded the clearest received signal, and for this study an input frequency of 3 kHz was used for all the tests.

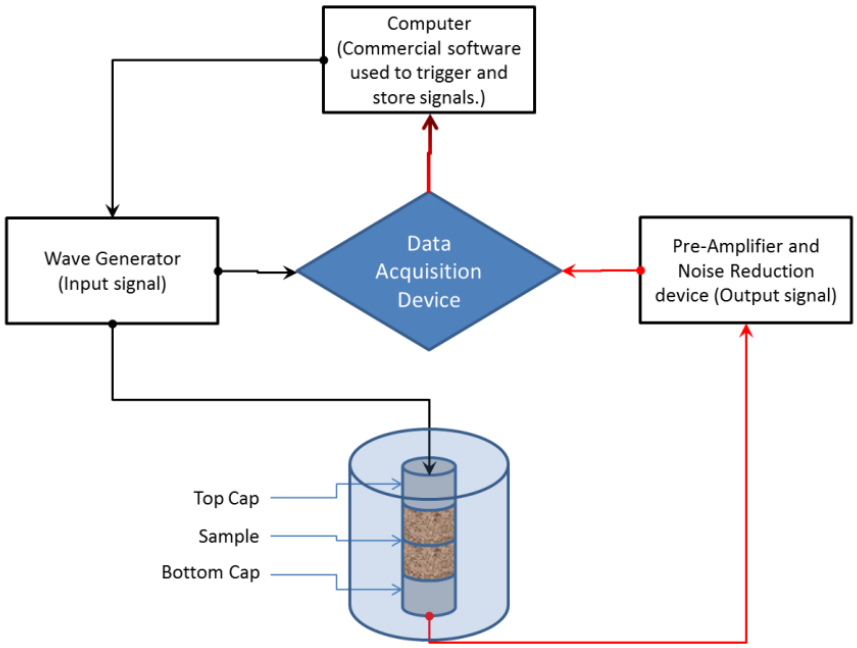

Figure 2.5 - System setup for measuring shear wave velocity

Properties of Materials Tested

Table 2.1 summarizes the properties of the materials tested. The grain size distribution was determined according to ASTM D422 for the fine to medium sand and the coarse sand. The glass beads had a uniform diameter of 6 mm. The Specific Gravity was determined according to ASTM D854. The glass beads and coarse sand are well rounded, and the fine to medium quartz sand is slightly angular.

Table 2.1 – Index properties of the materials tested in this study

Material	Specific Gravity	Grain Size [mm]	D_{10} [mm]
Glass beads	2.57	6.0	6.0*
Coarse sand	2.65	2.0 – 3.5	2.0*
Fine to medium sand	2.66	0.075 – 2.0	0.165

** Assumed for estimation of hydraulic conductivity using relationship proposed by Chapuis (2004)*

Results

Using the approach of Qiu and Fox (2008), predictions of effective density ratio (ρ_{eff}/ρ_{sat}) as a function of normalized frequency for the fine to medium sand, coarse sand and glass beads were made. These are shown in Figure 2.6. Each curve is based on specific values of Specific Gravity and porosity for each of the materials and these values are shown in Table 2.2. As shown in Equation 2.6, the normalized frequency is a function of the frequency of the shear wave, hydraulic conductivity, and porosity. The frequency was taken as the input frequency to the transmitting bender element (3 kHz) and the hydraulic conductivity was estimated using the grain size data in Table 2.1 and an empirical relationship proposed by Chapuis (2004). Based on these parameters, the calculated values of effective density ratio for the materials and environmental conditions during testing are 0.90 (6 mm glass beads), 0.891 (coarse sand), and 0.93 (fine to medium sand).

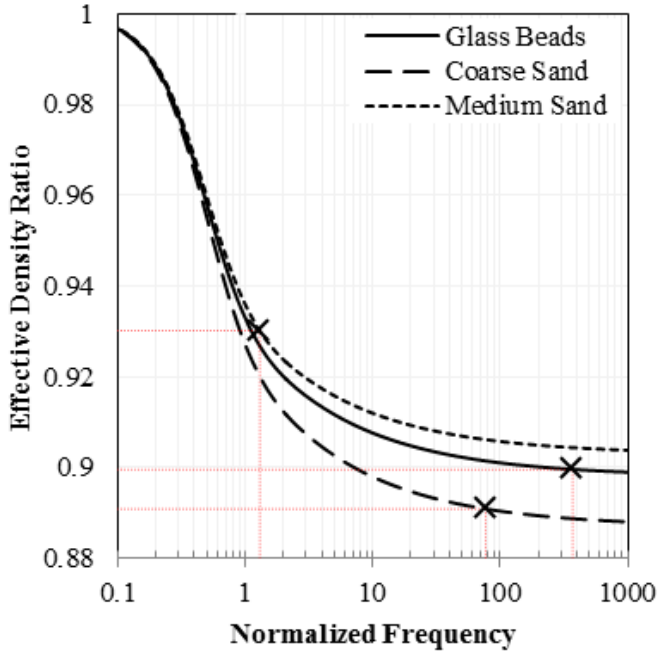

Figure 2.6 – Variation of effective density ratio with normalized frequency for the three materials used in this study. Values for the specific parameters of the laboratory testing program are marked by an "X"

Table 2.2 – Input parameters used to estimate values of effective density in this study. For parameters with a range of values (e.g. porosity), the values used are shown in parentheses

Material	Specific Gravity	Porosity, n *(used value)*	k_{ave} [m/s]	Frequency, f [kHz]	$\overline{f}$ *(used value)*	$\frac{\rho_{eff}}{\rho_{sat}}$
Glass beads	2.57	0.339 – 0.361 *(0.349)*	0.06722	3.0	350 – 400 *(370)*	0.900
Coarse sand	2.65	0.368 – 0.381 *(0.375)*	0.01504	3.0	75 – 81 *(77)*	0.891
Fine-to-medium sand	2.66	0.344 – 0.350 *(0.345)*	0.00024	3.0	*(1.3)*	0.930

Figure 2.7 shows the calculated values of small strain shear modulus for all the tests. The plots in the left column (a, c, e) show the variation of small strain shear modulus with effective stress for the last two cycles of loading/unloading. The shaded circles represent the small strain shear modulus calculated from the measured saturated density and its corresponding shear wave velocity. The open circles represent the small strain shear modulus obtained from the dry density and shear wave velocity is represented by the white circles. Lastly, the shaded triangles show the values of small strain shear modulus estimated from the measured shear wave velocity under saturated conditions and the effective density obtained from Figure 2.6. The plots in the right column of Figure 2.7 (b, d, f) show a 1:1 comparison of the small strain shear modulus using values of saturated and effective density with values of small strain shear modulus obtained with values of dry density.

The results show that, in all cases, the values of small strain shear modulus calculated using the saturated density were higher than the values of small strain shear modulus using the dry density. When using the effective density for the 6 mm glass beads (Figure 2.7a, b), the agreement with the dry small strain shear modulus was excellent. For the coarse sand (Figure 2.7c, d), the agreement was reasonable. The values

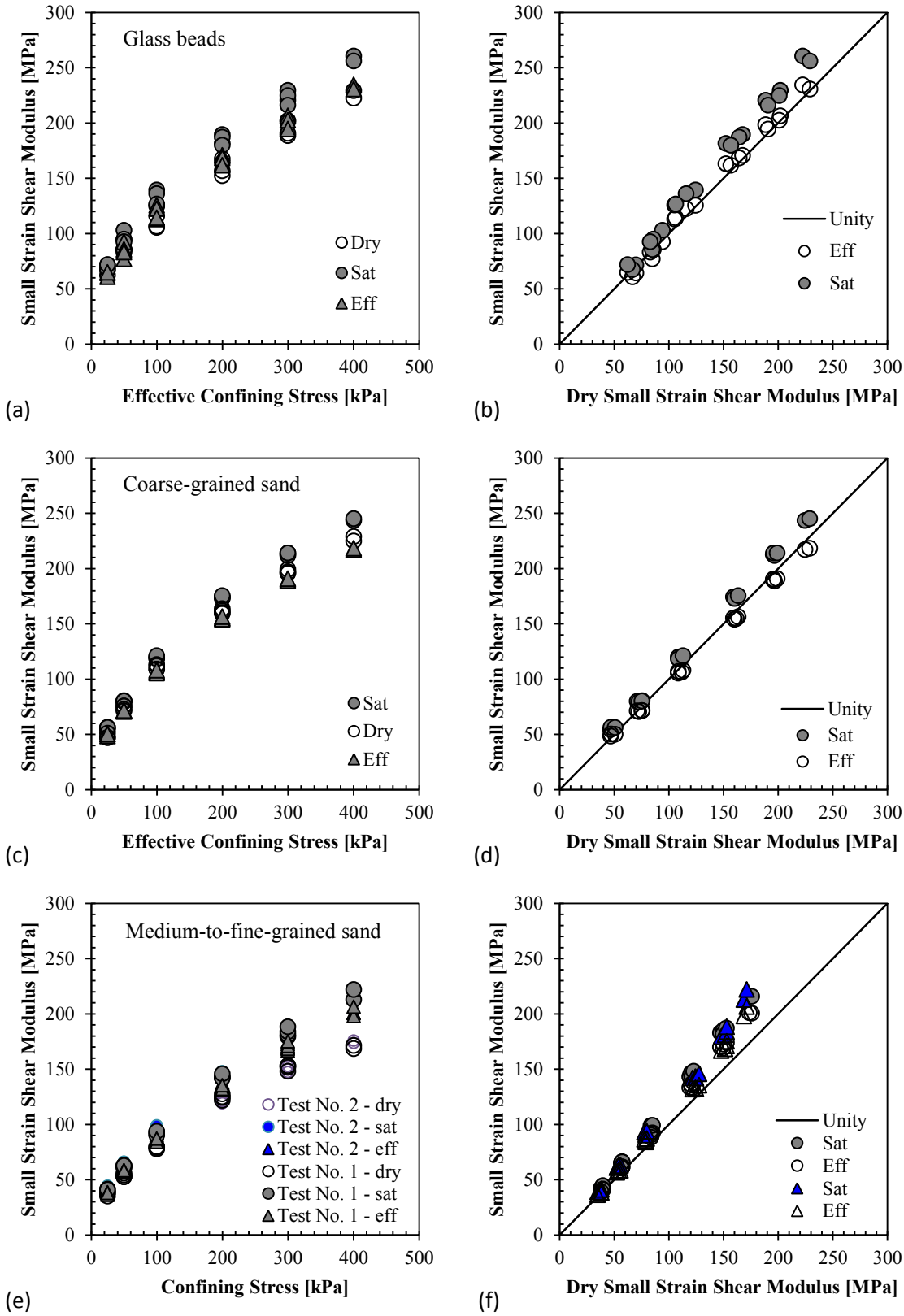

Figure 2.7 – Test results for (a, b) glass beads, (c, d) coarse-grained sands, and (e, f) medium-to-fine-grained sands

of small strain shear modulus using the effective density were slightly lower than the dry values of small strain shear modulus.

For the fine to medium sand the agreement was reasonable for effective stresses up to 200 kPa. Beyond 200 kPa, however, the values of small strain shear modulus using the effective density were significantly higher than the dry values of small strain shear modulus. This test was repeated on an identically prepared sample (Test 2 on Figure 2.7e, f) and the results were the same. The lack of agreement stems from the fact that the shear wave velocity-effective stress relationship for the fine to medium sand was practically identical for the dry and saturated conditions. This is contrary to the findings of Hardin and Richart (1963, see Figure 2.2) and others in the literature. It is unclear why the dry and saturated shear wave velocities were the same for these tests.

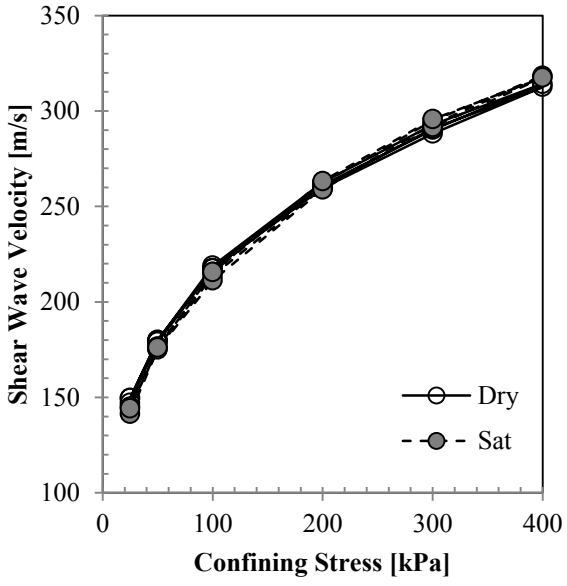

Figure 2.8 - Measured shear wave velocity for dry and saturated conditions on medium-to-fine sand

Conclusions

The objective of this study was to evaluate the effective density concept proposed by Qiu and Fox (2008), in which a reduced value of bulk density is used for certain soils to calculate the small strain shear modulus from values of shear wave velocity. The effective density is used to account for the fact that not all the water moves in phase with the soil skeleton as the shear wave passes. Using Biot theory, it can be shown that the effective density is a function of Specific Gravity, porosity, and hydraulic conductivity of the soil and the frequency of the shear wave velocity. In some soils, use of effective density can result in a 20% reduction in calculated values of small strain shear modulus compared to values calculated using values of saturated density.

In this study, three materials with different grain sizes were tested, including 6-mm glass beads, coarse sand, and fine to medium sand. An experimental program consisted of measuring the shear wave velocity using bender elements of samples at various effective stress levels under both dry and saturated conditions. Using the approach of Tong and Qiu (2008), estimated values of effective density ratio (ρ_{eff}/ρ_{sat}) for the materials tested ranged from 0.89 to 0.93. For the coarse sand and the gravel-sized glass beads, there was good agreement between the values of small strain shear modulus for the saturated specimens using predicted values of effective density and values of small strain shear modulus from comparable dry specimens. For the fine to medium sand the agreement was reasonable for effective stresses up to 200 kPa. Beyond 200 kPa, however, the values of small strain shear modulus using the effective density were significantly higher than the dry values of small strain shear modulus. The lack of agreement stems from the fact that the shear wave velocity-effective stress relationship

for the fine to medium sand was practically identical for the dry and saturated conditions. The implications of these findings are that use of an effective density may be appropriate when estimating the small strain shear modulus of coarse sands and gravels.

References

Biot, M. A. (1956a). Theory of Propagation of Elastic Waves in a Fluid-Saturated Porous Solid. I. Low-Frequency Range. *Journal of the Acoustical Society of America*, *28*(2), 168-178.

Biot, M. A. (1956b). Theory of Propagation of Elastic Waves in a Fluid-Saturated Porous Solid. II. Higher Frequency Range. *Journal of the Acoustical Society of America*, *28*(2), 179-191.

Chapuis, R. P. (2004). Predicting the saturated hydraulic conductivity of sand and gravel using effective diameter and void ratio. *Canadian Geotechnical Journal*, *41*, 787-795.

Dyvik, R., & Madshus, C. (1985). Lab Measurements of Gmax using Bender Elements. *Proceedings ASCE Annual Convention: Advances in the Art of Testing Soils under Cyclic Conditions*, 186-196.

Hardin, B. O., & Richart, F. E. (1963). Elastic Wave Velocities in Granular Soils. *Journal of the Soil Mechanics and Foundations Division, 89*(SM 1), 33-65.

Qiu, T., & Fox, P. J. (2008). Effective Soil Density for Propagation of Small Strain Shear Waves in Saturated Soil. *Journal of Geotechnical and Geoenvironmental Engineering, 134*(12), 1815-1819.

Santamarina, J. C., Klein, K. A., & Fam M. A. (2001) *Soils and Waves*. 1st Ed. John Wiley & Sons, Ltd, 217-248.

Sen, P. N., Scala, C., & Cohen, M. H. (1981). A self-similar model for sedimentary rocks with application to the dielectric constant of fused glass beads. *Geophysics, 46*(5), 781-798.

Shirley, D. J., & Hampton, L. D. (1978). Shear-wave measurements in laboratory sediments. *Journal of the Acoustical Society of America, 63*(2), 607-613.

Youn, J.-U., Choo, Y.-W., & Kim, D.-S. (2008). Measurement of small-strain shear modulus Gmax of dry and saturated sands by bender element, resonant column, and torsional shear tests. *Canadian Geotechnical Journal, 45*, 1426-1438.

CHAPTER 3

"Comparison of Ground Motion Selection Methods for Northeastern United States"

by

Yaurel Guadalupe-Torres[1] and Aaron S. Bradshaw[2]

will be submitted to the Journal of Earthquake Spectra

[1] PhD. Candidate, Department of Civil and Environmental Engineering, University of Rhode Island, Narragansett, RI 02882. Phone: 787-467-3226, E-mail: yaurel_gt@yahoo.com

[2] Assistant Professor, Department of Civil and Environmental Engineering, University of Rhode Island, Kingston, RI 02881. Phone: 401-874-2680, E-mail: bradshaw@egr.uri.edu

Comparison of Ground Motion Selection Methods for Northeastern United States

Abstract

This paper compares various methods for selection and scaling of ground motions for site response analyses in the Northeastern United States (NEUS). Unlike the Western US (WUS) the sources of earthquakes are not well defined and the available recorded ground motion database is limited in this region, particularly from larger events (i.e. $M > 5$) which are of engineering significance. Input ground motions are typically determined by either synthetically generating motions to match a target spectrum or by selecting/scaling a suite of recorded motions to match the target spectrum. Site response analyses were performed at two different bridge sites having different shear wave velocity profiles. A uniform hazard spectrum (UHS) was used as the target spectrum. Five evaluation criteria were used to compare six different methods for selecting/scaling ground motions in the northeastern United States. The criteria evaluate (1) the ability of the method to produce a median response spectrum at bedrock that matches the UHS and its variability, (2) the ability of the method to characterize a response spectrum over a period range versus a single period, (3) the ability of the method to account for a range of magnitude and site-to-source distance earthquakes that are consistent with the UHS, (4) the set-up time and run time required to obtain the response spectrum at bedrock, and (5) how the site response analysis result is affected by the method. Overall, the method proposed by Kottke and Rathje (2008) performed very well in most of the criteria compared to the other evaluated methods.

Introduction

When working on sites that can potentially develop resonance (i.e. soft soils) which can be poorly characterized by the generic demand curves found in the codes, or when designing critical structures such as, for example, dams, hospitals, and nuclear power plants, it is necessary to conduct a site specific seismic response analysis rather than using the conventional guidelines of available design codes and standards (ICC 2006, ASCE 7-05; FEMA-350, FEMA P695, etc.). These response analyses typically involve site response analysis using 1-D site response programs. They also require the input of ground motions at bedrock that are used to determine the response at ground surface where the structure is located. These ground motions can be generated artificially (synthetic motions) or can be obtained by real recordings.

In the Northeastern United States (NEUS), as opposed to the Western United States (WUS) the number of recorded ground motions with significant intensity to cause damage to structures is limited and the sources of earthquakes are not well defined (Bradshaw et al., 2007; Hines et al., 2011). The characteristic event in NEUS may be different depending on the return period of the site. For example low period events (i.e. $T \leq 0.5$ s) are characterized by low magnitudes earthquakes from short site-to-source distances. On the other hand, high period events (i.e. $T \geq 1.0$ s) are characterized by high magnitude earthquakes from long site-to-sources distances.

The earthquakes in NEUS, contrary to the WUS, have high frequency content which tends to exceed the level defined by the ASCE 7-05 (Hines et al, 2011). This is in part because in NEUS ground motions attenuate less rapidly with distance compared to the WUS (McGuire et al, 2001). Also, NEUS contains lower damping and shallower

crust thickness compared to WUS. Using ground motions from more active regions like the WUS will not contain the high frequency content that is characteristic in the NEUS and therefore is not advisable to use them (NIST, 2011). Another difference between NEUS and WUS is that earthquakes with low intensity ground motions in the NEUS produce greater soil amplification than the high intensity earthquakes common in the WUS. Hines et al (2011) pointed out that structural ductility also contributes to the differences between the regions in part because in NEUS, low ductility structures are very common and their design would be unacceptable in the WUS. All of these factors make motion selection and the quantification of hazard potential of the earthquake sources more difficult.

It is common practice in the NEUS to synthetically generate a single bedrock motion that matches a target spectrum. However, because the common practice is to use the UHS as the target spectrum, one of the problems with spectrally-matched synthetic ground motions is that they generally have high energy content and therefore do not represent real earthquakes. They also may be different from real earthquakes in terms of number of cycles, phase content, and duration (Hancock et al., 2006).

An alternative approach to using a single spectrally-matched synthetic record is to use databases of recorded ground motions that represent similar seismic setting of the site of interest (i.e. intraplate earthquake). An example of this database is the one developed by McGuire et al. (2001) for the Nuclear Regulatory Commission (NRC). To effectively use a ground motion database, various methods have been proposed for both the selection and the scaling of motions. However the problem is that there is no unified procedure to effectively select and scale these records for a site-specific seismic response analysis.

Therefore, an appropriate or suitable approach to be used in a site specific seismic response analysis in the NEUS is uncertain.

The objective of this study is to evaluate and compare different methods of selection and scaling of recorded ground motions for a site specific seismic response analysis to determine which methods are most appropriate for the northeastern United States. Five different criteria were defined to critically evaluate and compare the selected methods. These criteria were defined to evaluate (1) the ability of the method to produce a median response spectrum at bedrock that matches the UHS and its variability, (2).the ability of the method to characterize a response spectrum over a period range versus a single period, (3) the ability of the method to account for a range of magnitude and site-to-source distance earthquakes that are consistent with the UHS, (4) the Set-up time and run time required to obtain the response spectrum at bedrock, and (5) how the site response analysis result is affected by the method. The latter was accomplished by conducting site specific seismic response analyses at two bridge sites in Rhode Island using selected methods identified in the literature.

The organization of this paper is presented as follows. First, a literature review is given identifying some of the existing methods used to select and scale records for a seismic hazard analysis. This is followed by the description of the evaluation criteria and the site conditions of two different bridge projects in Northeastern US for the seismic evaluation. The next section describes in detail six selected methods, how they work and how they were implemented in this study. Finally, a summary of the results for the response spectra at bedrock and ground surface using each of the selected methods is presented with a comparison and discussion of their advantages and disadvantages.

Review of Existing Selection/Scaling Methods

For this study, a literature review was prepared identifying some of the methods used in the selection and scaling procedure for seismic site response analyses. Table 3.1 describes very briefly some of these methods. This is, by no means, an exhaustive list of existent methods, but a simple guide to show the variability of available procedures found in the literature. Methods selected in this study for comparison are described in detail in the following sections.

Several codes such as ASCE-4-98 (ASCE, 2000), ASCE-7-05 (ASCE, 2006), and ASSHTO (2012) have been created as guidelines for site response analysis. It is common practice in some codes to approach the selection of motions by considering the magnitude, site to source distance and rupture mechanism of the earthquakes as selection criteria. Usually a range of 3 to 7 motions are recommended by the codes for a site response analysis. Table 3.2 shows some of the requirements established by various codes in terms of selection and scaling of ground motions. However, there is no consensus on which of the procedures is most appropriate for the selection and scaling of records.

Recently, a report for the National Institute for Standards and Technology (NIST) was prepared with the objective of generating guidelines for the selection, generation and scaling of ground motions for use in seismic response analyses. As part of an extensive review of the state of practice regarding selection and scaling of ground motions, the report was focused in three main topics identified as (1) selection of ground motions based on conditional spectrum, (2) response-spectrum matching, and (3) near fault ground motions and fault-rupture directivity (NIST, 2011). Discussion on these topics is

beyond the scope of this study. The report suggests the spectral shape as the principal criterion for ground motion selection for a period range of interest for distant sites. Records with a geometric mean similar to the target spectrum minimize the need of scaling and modification (NIST, 2011). Secondary criteria include magnitude, site-to-source distance, dominant ε at period $\overline{T}$ (where $\overline{T}$ = average first mode period of the horizontal directions of the building), and site conditions. The parameter ε is a measure of the difference between the spectral acceleration of a record and the mean of the ground motion prediction equation at a given period. For near-fault sites, the two most important factors are the spectral shape and the presence of velocity pulse. The report also presents a summary of the rules specified in several US codes for the selection and scaling of records.

Synthetic motions are designed to fit the design spectra throughout the whole spectrum and do not require scaling. SIMQKE (Vanmarcke et al., 1976), for example, is a software program written in standard FORTRAN 77 developed to generate these motions. This program can generate simulated ground motions using recorded ground motions or without any real ground motions. An existing problem with synthetic ground motions is that they generally have high energy content that does not represent real earthquakes. They also differentiate from real earthquakes in terms of number of cycles, phase content, and duration (Hancock et al., 2006). For this reason recorded earthquake motions are preferred. However, to effectively use recorded motions, it is necessary to have a large database for the analysis.

Table 3.1 - Summary of ground motion selection/scaling methods from the literature

Reference	Ground Motion Selection/Scaling Method
Ambraseys, et al. (1996)	Selection based on magnitude range, source to site distance, closest distance to the projection of the fault rupture, and site conditions. Provides equation to estimate the target spectrum
Naeim et al. (2004)	Uses a generic algorithm to select and scale the motions to fit a target response spectrum over a specified period range. It measures the deviation of the target by the mean square of error between the square root of the sum of the squares of the average scaled spectrum and the target. The elements of the generic algorithm are: (i) population, (ii) fitness function, (iii) crossover, (iv) mutation, and (v) natural parent selection. Method suggests using a suite of 7 motions and 7 scaling factors
Watson-Lamprey and Abrahamson (2006)	Uses the Newark displacement model for selection of motions. In addition to magnitude, distance and site conditions, the peak ground velocity, root mean square of acceleration and duration are required. The motions can be scaled to the PGA, PGV, Arias intensity or to the spectral acceleration averaged over a period range.
Dhakal et al. (2006)	Selection based on geological characteristics, distance. The identification of critical ground motions is based on Incremental Dynamic Analysis (IDA). This procedure consists of a nonlinear analysis of a prototype structure subjected to a set of ground records scaled at several intensity levels until the structure collapses. This procedure compares the capacity of the structure and the demand form the earthquake in terms of maximum drift or displacement and intensity measure such as the PGA or the amplitude of the spectral acceleration.
Zhai and Xie (2007)	Pre-selection of records is based on site conditions and considers only one component of the record. Selection based on most unfavorable seismic design ground motion. Records are ranked by PGA, PGV, PGD, EPA, EPV, Duration, IV, and ID for two groups, and the top 10 records of each group are selected as the candidates. The method estimates the damage potential based on ground motions parameters and structural seismic damage criteria in terms of strength, deformation hysteretic energy and dual damage of Park and Ang (1985) damage index.
Beyer and Bommer (2007)	Provides a summary of selection/scaling from different codes Selection according to: 1. Earthquake scenario such as (i) Magnitude, (ii), Source-site distance, (iii) Site classification 2. Spectral matching and duration Different D_{rms} approaches Uses median rather than mean Two methods of scaling Scale the median pSa to the target spectrum Scale each record individually to the target spectrum

Table 3.1 - Summary of ground motion selection/scaling methods from the literature (cont'd)

Reference	Ground Motion Selection/Scaling Method
Bommer and Acevedo (2008)	Presents multiple methods for motion selection including: 1. Strong-motion parameters Average root-mean-square deviation, D_{rms} 2. Geophysical parameters (i) Earthquake magnitude (recommends a narrow window), (ii) Source-to-site distance, (iii) Site classification, (iv) Rupture mechanism (only if there is plenty number of records) Matching/Scaling selected records to the elastic response spectrum (i) Direct matching using D_{rms}, (ii) Scaling in amplitude, (iii) Using wavelets, (iv) Scale in time and amplitude Scaling is performed over a period range and it can be obtained from the average value of the group of records or can be obtained individually.
Kottke and Rathje (2008)	Pre-selection of records can be based on different scenarios including (i) magnitude, (ii) source to site distance, (iii) site conditions. Selection is based on automated algorithm that builds suites of n records by comparing the root-mean-square error (*RMSE*) and the σ_{ln} *RMSE* based on a best fit of the scaled records to the target spectrum. The suites are generated randomly by an iterative procedure. The suite with the lowest *RMSE* is considered the best set of records. In this procedure the scaling factors are obtained simultaneously. It considers only one component of the record.
Katsanos et al. (2010)	Presents a summary of different alternatives for ground motion selection found in the literature Selection based on: (i) magnitude and distance: (ii) additional criteria such as: soil profile, duration, seismic tectonic environment or other geophysical parameters, and acceleration to velocity ratio (iii) recording based on several methods of spectral matching including: Root-mean-square deviation, average spectrum deviation, Root-mean-square deviation using a scaling factor (iv) ground motion intensity measures
Catalán, et al. (2010)	Pre-selection is based on the European median attenuation prediction model of Ambraseys et al. (1996). This method group records based on ε, and using μ, $+1\sigma$, -1σ, $+2\sigma$, etc. for each period. Scale the records at four points, the fundamental period, T1, 1.1T1, 1.2T1, and the period of the second mode T2. Recommends a minimum of 30 records
Bradshaw and Green (2011)	This method generates 10 bins organized by magnitude and source to site distance. A number of motions are selected randomly for each bin. A contribution to hazard factor is applied to each bin based on the epsilon obtained from the deaggregation data in the USGS database. After the contribution to hazard is applied, the median pseudo spectral acceleration is obtained and compared to the target spectrum to calculate the scaling factor.
Hines et al. (2011)	Based on magnitude, frequency content, PGA with lower and upper boundary factors of 0.5 and 2.0, respectively Simulated motions are filtered based on ± 1 log normal std. dev. from the UHS 2002 on selected periods A ground motion would be considered acceptable for the suite if it matched at least one UHS point very closely and did not vary from any other UHS point by more than a factor of approximately 2.0

Table 3.1 - Summary of ground motion selection/scaling methods from the literature (cont'd)

Reference	Ground Motion Selection/Scaling Method
Kayhan et al. (2011)	Selects and scales real motions using a meta-heuristic harmonic search algorithm. Pre-selection of records based on magnitude, distance, and site conditions to form the original ground motion database. The algorithm is designed to build suites by selecting and scaling records following the criteria specified in the Eurocode 8. Datasets with seven ground motions are developed for each soil class.
Wang (2011)	Pre-selection can be based on range of magnitude, type of faulting, range of distances, etc. This method takes into account the median, the standard deviation and the correlation structure of the spectral distribution. Uses an algorithm to select and scale the records by comparing and obtaining the minimum weighted sum of squared errors (WSSE). Recommends a minimum of 3 motions to achieve statistically stable results.
Bradley (2012)	Uses and algorithm to select and scale the motions based on the generalized conditional intensity measure (GCIM) approach by incorporation a good-of-fit method. This approach creates a distribution set based on various intensity measures (PGA, PGV, etc.), and is considered the target to be used for the motion selection. This approach has been implemented in the open-source software OpenSHA.
Ay and Akkar (2012)	Uses the following criteria to limit the number of records in the database: $M_{target} - 0.25M \leqslant M_{target} \leqslant M_{target} + 0.25M$, $d_{target} - 25\ km < d_{target} < d_{target} + 25\ km$, If there are enough records, the motions can also be filtered by the type of faulting and site conditions imposed by the target spectrum. The scaling is performed using the spectral displacement (S_d) although the spectral acceleration can be used as well. The procedure scales each record to its individual target level based on the ground motion prediction equation (GMPE). For this, two parameters are defined called the logarithmic difference and the scaling origin.

Table 3.2 - General specifications from design codes and guidelines

Code or Guideline	Number of records	Period range of interest for scaling	Ground motion component	Other considerations
ASCE 7-05	3 or 7	$0.2*T_n$ to $1.5*T_n$	2D – horizontal records 3D – pair of horizontal records	Magnitude, fault distance, source mechanisms
ASCE 41-06	3	$0.2*T_n$ to $1.5*T_n$	Two horizontal components, one vertical if required	Magnitude, fault distance, source mechanism
AASHTO LRFD Bridge Design Specifications	3 or 7	$0.5*T_n$ to $2.0*T_n$	Three components (x, y, z) for nonlinear analysis	Tectonic setting, magnitude, fault type, source-to-site distance, local soil conditions
FEMA 65	3	Not specified	Pair of horizontal components	Magnitude, source-to-site distance, fault rupture mechanisms, transmission path properties, regional and geological conditions
FEMA 302	3	$0.5T_D$ to $1.25T_M$	Pair of horizontal components	Magnitude, fault distance, source mechanisms
FEMA 350	10 to 20	T_n	Not specified	Site conditions, hazard level
FEMA P695	Not specified, required a large number of records	T_n	Pair of horizontal components	Near-field, far-field set of records, magnitude, source type, source-to-site distance, site conditions,

In some cases it is desired to pre-select a group of motions before choosing a selection/scaling method. There is no specific procedure for this and the pre-selection can be based on magnitude of the earthquake, site to source distance, site conditions, duration, etc. However, the idea of the pre-selection is to have enough motions to start with, and is not advisable to apply too many filters from the start if the available data is limited. Bommer and Acevedo (2008), Beyer and Bommer (2007), and Katsanos et al. (2010) summarized several methods from the existing codes and procedures found in the literature used for the selection and scaling of motions.

One of the most common methods for selecting ground motions is to randomly select a number of records (i.e. one, three or seven) form a database using magnitude and

site-to-source distance from the deaggregation for a particular site, probability of exceedance and period. A basic individual scaling is applied to each ground motions to match the UHS at the particular period of interest (i.e. PGA, fundamental period of the site or of the structure). Alternatively, when more than one ground motion is used, the median acceleration spectrum can be obtained to scaling factor of the records.

Other methods utilize boundaries based on the target spectrum. Such is the case of the procedure proposed by Hines et al. (2011). The pre-selection of motions of this method is done by filtering the amplitude of motions from a database using a band of 0.5 to 2.0 times the peak ground acceleration (PGA) of the design spectrum. For the final selection of motions, a boundary condition is defined based on the design spectrum along the whole period range. This method does not scale the motions.

Catalán et al. (2010) also define a boundary around the target spectrum; however they do scale the records. The target spectrum is defined by an attenuation model presented by Ambraseys et al. (1996). The mean value μ and the standard deviation σ are obtained for a set of records. Sets of motions are grouped based on different intensity values defined as μ, $\mu \pm 1\sigma$, $\mu \pm 2\sigma$, and $\mu - 3\sigma$. The boundary condition in each group is defined by $\varepsilon = \pm 0.5$. The groups of motions are used to calculate the probability of collapse and select the appropriate set.

It is worth mentioning that the attenuation models developed by Ambraseys et al. (1996) were generated using earthquakes sources from Europe and adjacent areas. Their objective is to provide equations capable of predicting the absolute spectral acceleration for sites with similar geology of Europe and Middle-East. However, these attenuation equations may not be recommended for the NEUS. Alternatively, Frankel et al. (1996),

Toro et al. (1997), Somerville et al. (2001), among others, have developed attenuation relations for the central and eastern United States.

Dhakal et al. (2006) incorporate the incremental dynamic analysis (IDA) for the selection of ground motions. IDA subjects a prototype structure to seismic loads, forcing a dynamic instability. For this, the records are scaled at increasing intensities. For each increment the non-linear analysis is performed until the structure collapse. The non-linear analysis uses an engineering demand parameter (EDP) given from a critical response obtained by an intensity measure (IM) such as the PGA. Zhai and Xie (2007) also include structural parameters for the selection and scaling of the records. They characterize the damage potential based on various parameters and select the suite that produces the most unfavorable response. The parameters considered in the analysis are peak ground acceleration (PGA), peak ground velocity (PGV), peak ground displacement (PGD), effective peak acceleration (EPA), effective peak velocity (EPV), duration, maximum incremental velocity (IV), and maximum incremental displacement (ID). The records from the database are first grouped in four site conditions (*Vs*) and ranked based on these parameters. The first top 10 records are considered for the most unfavorable scenario. The database is ranked for a second time by considering the demanded yield strength of the structure and the hysteretic energy for three period range and the four site conditions.

Naeim et al. (2004), incorporate a generic algorithm for the section and scaling of records by matching a number of motions to the design spectrum along a period range of interest. The algorithm combines seven records and corresponding scaling factors and treat them as a single individual. The selection and scaling is repeated until the least mean

square of deviation is obtained. Kottke and Rathje (2008), also use an algorithm to select and scale the records. Their algorithm compiles random suites of ground motions and matches them to the design spectrum and fits the amplitude and the standard deviation of the target by incorporating individual scaling factors. The suite with the lowest root-mean-square-error and its minimum root-mean-square-error of the standard deviation is selected. In the randomization procedure for the selection of motions, they incorporated a factor to reduce considerably the number of trials required to obtain the selected suite of motions.

Wang (2011) uses an algorithm to select a suite of ground motion time histories that captures the median, the standard deviation and the correlation structure of the spectral distribution, given a specified earthquake magnitude, distance, site condition, etc. Then it selects and scales the records by spectral matching using the weighed sum of squared errors between the records and the target spectrum. Kayhan et al. (2011) uses the harmonic search algorithm to select and scale the records that are compatible with the design spectra obtained using the Eurocode 8 (CEN, 2004). The algorithm is based on natural musical performance processes and utilizes the harmony memory considering rate and the pitch adjusting rate as part of the procedure for the selection, scaling and spectral matching the records.

Bradley (2012) uses and algorithm to select and scale the motions based on the generalized conditional intensity measure (GCIM) approach by incorporation a goodness-of-fit method. The method can be applied to both recorded and synthetic motions. This approach creates a multivariate distribution set of ground motions intensity measures (PGA, PGV, etc.). The GCIM is created in two steps by first determining the probability

that a ground motion with an intensity measure was caused by a specific rupture. Then it determines the distribution of other ground motion intensity measures based on the observed ground motion from the specified rupture.

Watson-Lamprey and Abrahamson (2006) use the Newark displacement model, as a simple model of a yielding system, for the design event and selection of motions. They developed the model by conducting a regression analysis using the characteristics of the ground motion time series. In addition to magnitude, distance, and site conditions, the model also requires the peak ground velocity, root mean square of acceleration and duration of the ground motion. The motions can be scaled to the PGA, PGV, Arias intensity or to the spectral acceleration averaged over a period range. The group of records with the lowest root mean square of difference with the design event is selected. Bradshaw and Green (2011) use a contribution factor obtained from the deaggregation database generated by the USGS. The method determines the earthquake percent contribution to hazard using ε as the criteria and generates 10 bins organized by magnitude and source to site distance corresponding to the McGuire et al. database. This contribution factor is applied to each bin. A determined number of motions are selected randomly for each bin from the database. After the percent contribution to hazard is applied, the median pseudo spectral acceleration is obtained and compared to the target spectrum to calculate the scaling factor at a desired period.

Ay and Akkar (2012) pre-select the ground motions by filtering the database using a specified range for the magnitude and distance as their primary criteria. If there are enough records, the motions can also be filtered by the type of faulting and site conditions imposed by the target spectrum. A number of bins are created and the records

within each bin are scaled individually to their target intensity level. The scaling is performed using the spectral displacement (S_d) although the pseudo spectral acceleration or the peak ground motion values (PGA, PGV) can be used as well. Its implementation is based on the difference between the actual record and its estimation from a ground motion prediction equation. For this, two parameters are defined called the logarithmic difference and the scaling origin.

Methodology

Response analyses were performed at two study sites in the NEUS using six different selection/scaling methods. These methods were select to represent different aspects of the procedures involved in the selection/scaling of the records. For example, the differences shared within these methods include the number of records used, the usage of a single horizontal component or horizontal pair, synthetic and recorded ground motions, using scaled and unscaled records, scaling of the records to a particular period or period range, use of weighting factors, among other criteria.

Often, guidelines for ground motion selection are needed for the analyses of multiple structures or for multiple structural components, in which case ground motion selection methodology tied to a single structure is not desirable (Rodríguez-Marek, personal communication, 2013). Site response analyses involving structural parameters and structural analyses tend to be more expensive and therefore are unlikely to be adopted practitioners. For this reasons, evaluation criteria will not include any evaluation based on structural analyses. Details of the analyses are described in subsequent sections.

Evaluation Criteria

Five different criteria were defined to critically evaluate and compare the selected methods. The five criteria were defined as follows:

1. The ability of the method to produce a median response spectrum at bedrock that matches the UHS and its variability.

   The Uniform Hazard Spectrum (UHS) is commonly used for seismic hazard analyses and therefore is the target spectrum selected for this study. For each selected method, the median pSa response is calculated and compared to the UHS at bedrock. To evaluate the ability of the methods to capture variability, a standard deviation measure is also selected, and the standard deviation of ground motions selected with each method is obtained and compared to the selected UHS.

2. The ability of the method to characterize a response spectrum over a period range versus a single period.

   For some seismic hazard analyses, it is common to define a period range rather than a single period. This can be justified by different reasons, for example, (1) when a structure has multiple degrees of freedom, (2) when there are multiple structures on site, or (3) when a structure is expected to go into the nonlinear range and hence drift away from its linear predominant period. To account for these conditions, it is necessary to perform ground motion selection considering a frequency band. Some methods have the capacity of generate a response spectrum over a period range by running the method once. Other methods require multiple runs (i.e. one run for each period) to develop a response spectrum over a period range.

3. The ability of the method to account for a range of magnitude and site-to-source distance earthquakes that are consistent with the UHS.

A common practice in US is to use the modal values of magnitude and distance from the deaggregation developed by the USGS as a first step for pre-selection of ground motions from a database. This might be appropriate in WUS where the modal value is a good representation for most of the earthquake ground motions in that region. In NEUS, however, the contribution of ground motions comes from multiple sources with different magnitudes and distances, and the modal value does not necessarily represent the common earthquake. A method capable of factor in the contribution of all the earthquakes might be more suitable for this region.

4. Set-up time and run time required to obtain the response spectrum at bedrock.

   The engineering effort required to obtain a pSa response at bedrock varies from method to method. For some methods (i.e. a method that incorporates an algorithm), a program software is provided to accelerate the procedure for the suite selection. Many other methods do not have a computer software program to obtain the suite of ground motions, forcing the user to develop a procedure using a numerical analysis program. Other methods require hand pick selection of the final suite of ground motions.

5. How the site response analysis result is affected by the method.

   All the aforementioned selection criteria focus on the pSa response at bedrock. After the suite of motions is selected, it is desired to understand how each method affects the results at the ground surface. For this, a site response analysis is performed with the suite of motions assembled from each method to evaluate and compare the effects of motion selection/scaling procedure at the ground surface. This is achieved by computing the median pSa response spectrum and the plus one standard deviation for each method.

Study Sites

The study sites are located in the state of Rhode Island as shown on the map in Figure 3.1 and include the Washington River Bridge site in Providence and the Sakonnet River Bridge site in Portsmouth. These sites were selected because extensive site investigation data including in situ shear wave velocity were available and represent two different site classes. The soil conditions at the Washington bridge site are shown in Figure 3.2. The bedrock in this site has a shear wave velocity of approximately 2000 m/s. The Washington Bridge site is classified as Site Class D based on the calculated V_{s30} (220 m/s) defined by the following equation (ASCE 7-05; AASHTO, 2012):

$$V_{s,30} = \frac{\sum d_i}{\sum \frac{d_i}{V_{s,i}}} = \frac{30}{\sum \frac{d_i}{V_{s,i}}} \tag{3.1}$$

where d_i = thickness of the ith layer (in meters). The fundamental period (T_s) of the site was also estimated to be 0.69 seconds based on the following equation:

$$T_s = \frac{4H}{V_s} \tag{3.2}$$

where H = soil thickness, and V_s= weighted shear wave velocity above bedrock.

The profile of Sakonnet River Bridge site is shown in Figure 3.3. The bedrock has a shear wave velocity of approximately 920 m/s. This site is classified as Site Class E based on a $V_{s,30}$ of 161 m/s. The fundamental period was estimated to be 0.87 s.

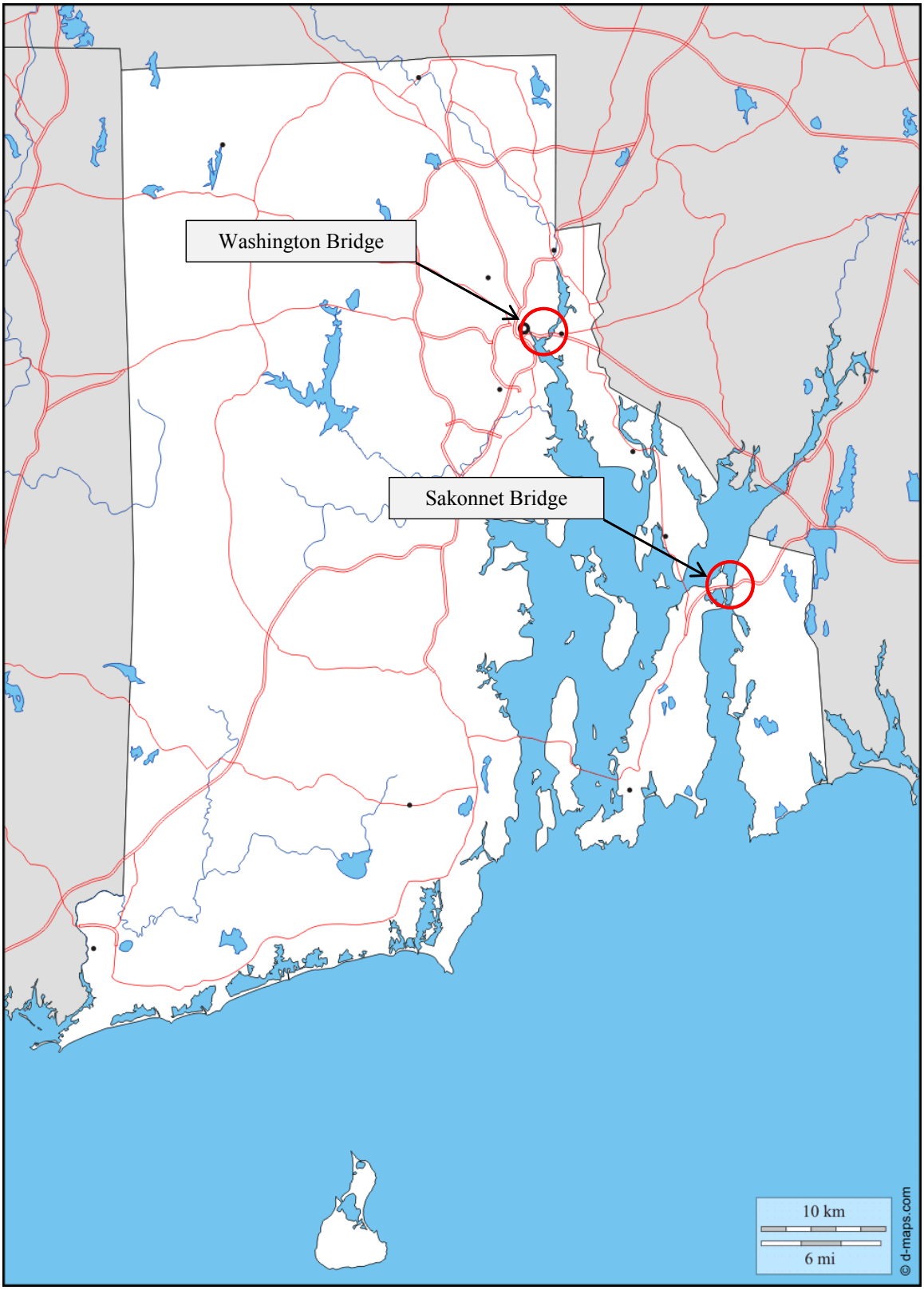

Figure 3.1 – Map of Rhode Island with the selected sites for this study, Sakonnet River Bridge and Washington bridge (source http://d-maps.com/carte.php?num_car=7630&lang=en)

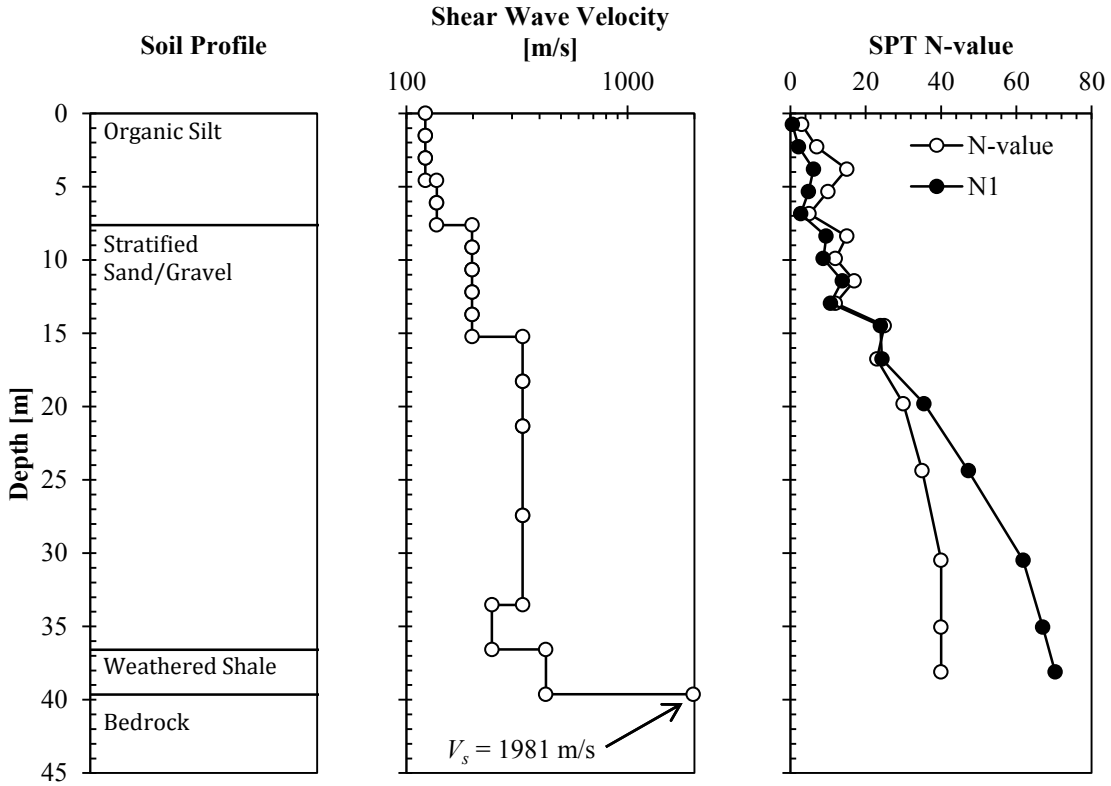

Figure 3.2 - Soil profile with shear wave velocity and SPT N-values for Washington Bridge site

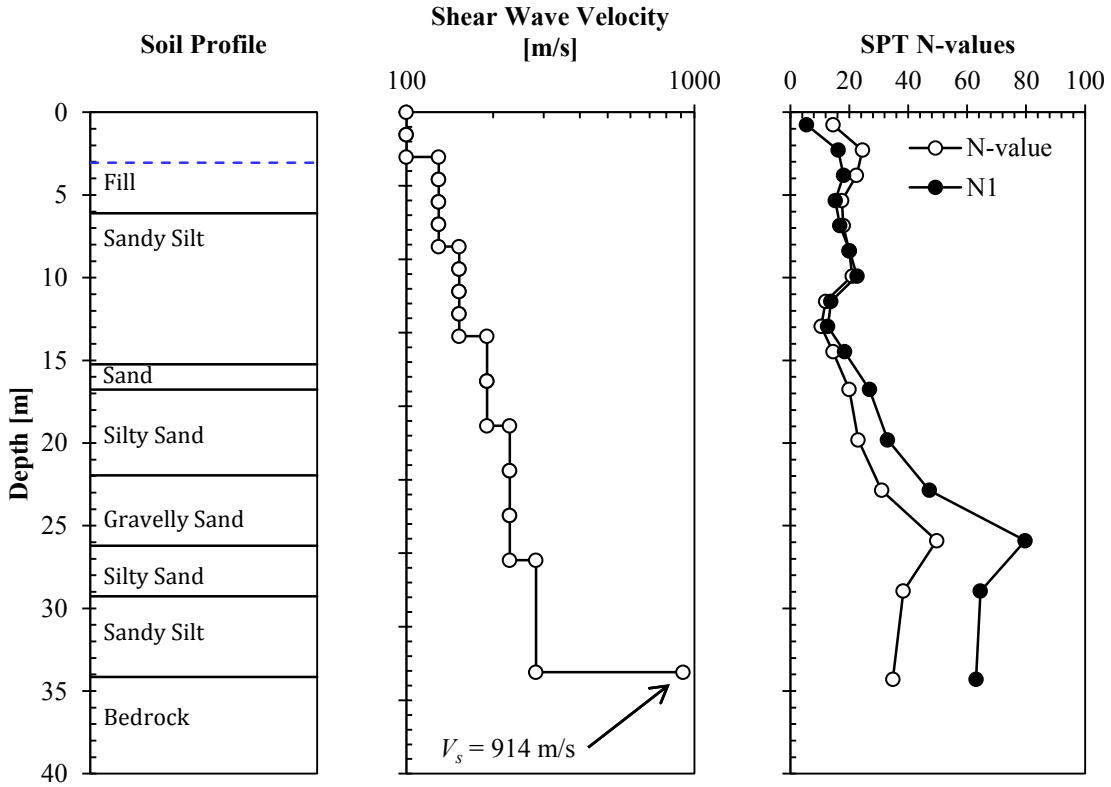

Figure 3.3 - Soil profile with shear wave velocity and SPT N-values for Sakonnet River Bridge site

Site Response Model

A 1-D site response analysis was performed using the program Strata (Rathje and Kottke, 2013) that is based on the equivalent linear method. The soil column was modeled as 16 layers including bedrock using thinner layers in the upper part of the soil profile. Soil damping and shear modulus degradation curves were developed using Ishibashi and Zhang (1993). Due to the stress dependency of the shear modulus, a different curve was developed for every layer. Response spectra were calculated at both the bedrock and ground surface levels.

Target Spectrum

Two target spectra for bedrock were used in this study. The first was a uniform hazard spectrum (UHS) determined from a probabilistic seismic hazard analysis (PSHA) performed by the USGS. The second was a UHS developed from a site-specific PSHA performed by a local seismology expert. The USGS UHS at bedrock was obtained using the web-based java tool based on the geographical location of the study sites. The design spectrum was defined at periods T = 0.0, 0.1, 0.2, 0.3, 0.5, 1.0, and 2.0 s. Two probabilities of exceedance were selected, 2% and 10% in 50 years, that is events with return periods of 2500-yr and 500-yr, respectively (see Figure 3.4).

The site-specific UHS was only available for the Sakonnet River Bridge project, and it is shown in Figure 3.5. The UHS at bedrock was developed from a site-specific PSHA from a local seismology expert but specific details on the analysis were not available.

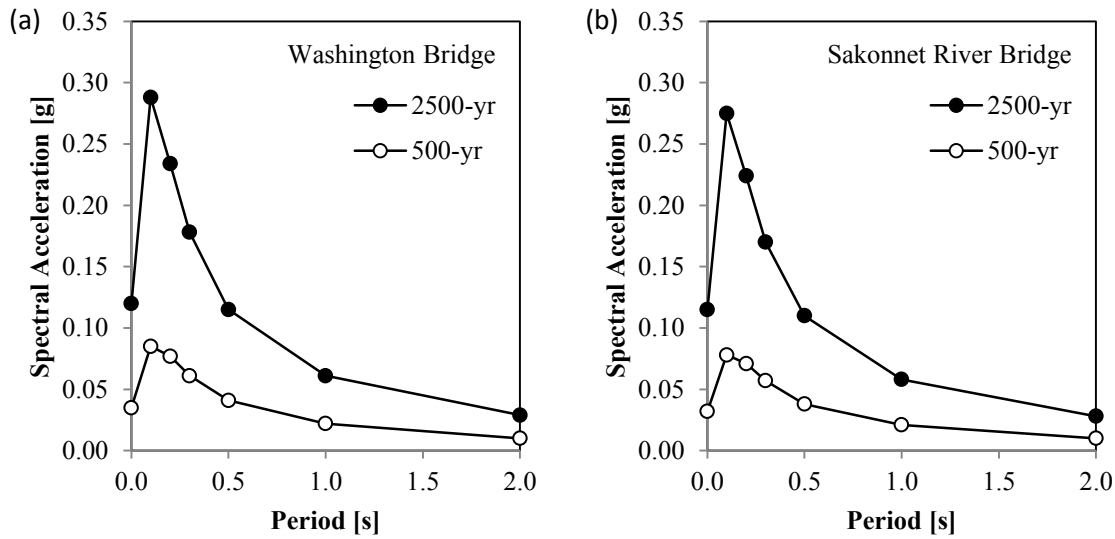

Figure 3.4 - USGS-based uniform hazard spectrum for (a) Washington bridge and (b) Sakonnet River bridge

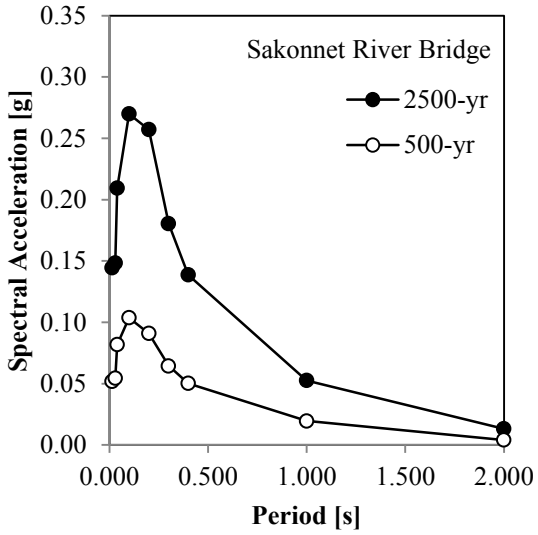

Figure 3.5 - Site-specific uniform hazard spectrum for Sakonnet River Bridge

Ground Motion Database

The McGuire et al. (2001) database was used as the source for input ground motions. This database has a total of 151 records comprised of triaxial recordings, and is organized in bins grouped primarily by magnitude and site-to-source distance. The motions contained in this database were recorded from earthquakes with magnitudes from 4.5 to 7.6 and site-to-source distances between 0 and 200 km. Figure 3.6 shows the

distribution of the records with respect to magnitude and source to site distance. It is important to clarify that the McGuire et al. records are not entirely from the Northeastern US. This database contains ground motions recorded mostly from Western US and other places, and were adjusted using theoretical transfer functions to simulate the tectonic environment (i.e., intra-plate motions) common in NEUS (Hines et al., 2011).

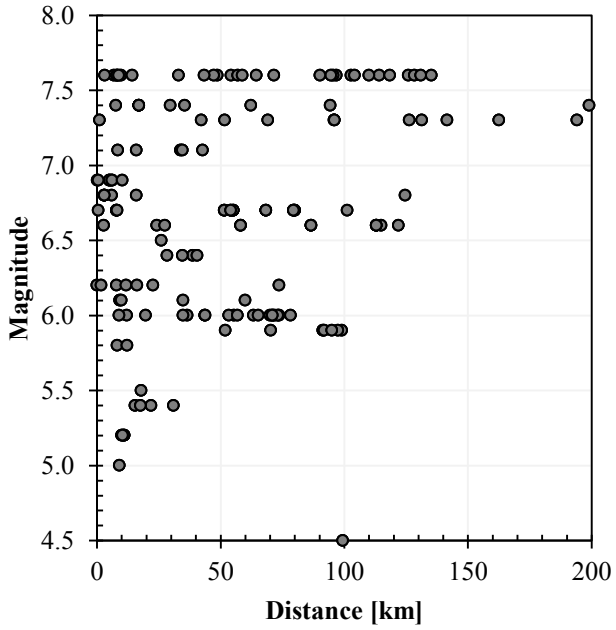

Figure 3.6 - Distribution of the McGuire et al (2001) database used in this study with respect to magnitude and source to site distance

Ground Motion Selection and Scaling

Method 1: Basic "Individual" scaling

Method 1 selects a suite consisting of 7 pairs of records and scales each record individually to a specified period of the UHS for bedrock to obtain 14 different scaling factors. The number of records and the usage of both horizontal components are consistent with the general guidelines of some of the building codes and standards used for seismic hazard analyses for the selection of ground motions (i.e., ASCE 7-05). The

records were scaled at a particular period of interest as it is done in common practice (i.e., anchoring the acceleration response at the PGA). A maximum scaling factor was limited to 4.0, and if at least one of the horizontal components of the ground motion pair exceeded this limit the pair was discarded and a new pair was selected. The specific procedure is outlined below:

1. For the required period, define an upper and lower boundary for the magnitude (M) and distance (R) based on the modal values from the deaggregation figures provided by the USGS. This was performed using a similar approach proposed by Ay and Akkar (2012), in which the range for magnitude was defined as $0.75M < M < 1.25M$, and the distance range as ±20 km from R.

2. Filter the ground motion database using the upper and lower bounds established in Step 1 to obtain the batch of pre-selected records.

3. From the acceleration time histories of pre-selected records compute the pseudo spectral accelerations and determine the scaling factor for each record at the specified period using the design spectrum. ATH-to-PSA computation was performed using Matlab applying the central limit method.

4. Eliminate pair of records for which at least one of the components has a scaling factor of $SF \geq 4.0$. If the number of available records is limited, engineering judgment must be used to allow SF slightly above 4.0.

5. Randomly select seven pairs from the remaining records. Using Excel, the records filenames were sorted in alphabetical order then the function rand() was used to arrange the records randomly. The top seven records (and their correspondent horizontal component) were selected as the final suite of records for the site specific seismic response analysis.

6. Repeat Steps 1 through 5 for periods having different modal values of magnitude and distance.

7. Repeat Steps 1 through 6 for different design events (i.e. 2500-yr and 500-yr).

Following the above procedure, two different batches of pre-selected ground motions were obtained due to the differences in the modal values of magnitude and distance at lower and higher periods. For the probability of exceedance of 2% in 50 years (2500-yr event), the low period ($T \leq 0.5$ s) modal values were $M = 4.9$ and $R = 14.6$ km, while the high periods ($T \geq 1.0$ s) are $M = 7.0$ and $R = 405$ km. For the probability of exceedance of 10% in 50 years (500-yr event), the modal values of the low period range were $M = 4.9$ and $R = 36$ km, and for the high period range $M = 7.1$ and $R = 530$ km.

Because the minimum magnitude in McGuire et al. database is $M = 5.0$, the modal value used for the selection was slightly increased to allow a higher number of records. McGuire et al. records are limited to a maximum distance of 200 km and therefore it was necessary to relax the distance restriction for the high period range. For the low period range ($0.0 \leq T \leq 0.5$ s), a group with 44 records was used for the 500-yr event and another group with 34 records for the 2500-yr event. For the high period range ($T \geq 1.0$ s) only one group was created with 44 records. Since both sites have similar deaggregation figures, these groups were used in both.

Method 2: Basic "Median" scaling

Method 2 determines the median spectral acceleration of a suite consisting of 7 pairs of records and scales it to the UHS to obtain a single scaling factor that is applied to all records. The median spectral acceleration was calculated assuming that the spectral acceleration is log-normally distributed. The following steps summarize the procedure used for Method 2.

1. Follow Step 1 and Step 2 as described in Method 1.

2. Randomly select seven pairs from the remaining records. Using Excel, the records filenames were sorted in alphabetical order then the function rand() was used to arrange the records randomly. The top seven records (and their correspondent horizontal component) were selected as the final suite of records for the site specific seismic response analysis.

3. From the acceleration time histories compute the pseudo spectral acceleration and calculate the median pSa using a log-normal distribution. This was performed using Matlab.

4. Determine the scaling factor between the median pSa and the design spectrum at the specified period.

5. Repeat Steps 1 through 5 for periods with different modal values of magnitude and distance.

6. Repeat Steps 1 through 6 for different design events (i.e. 2500-yr and 500-yr).

Method 3: Bradshaw and Green (2011)

Method 3 is based on the method proposed by Bradshaw and Green (2011). The major feature is that scaling factors are developed based on a weighting scheme that is linked to the contribution of the various sources to the seismic hazard at the site. The percent contribution to the hazard is obtained from the deaggregation matrices that can be readily obtained from USGS. The following steps were performed for Method 3:

1. Create a number of bins organized by magnitude and distance similar to Table 3.5. For this study, 10 bins were generated using the same category defined in the McGuire et al. (2001) database.

Table 3.3 - Contribution to hazard from seismic deaggregation for the 2500 year rock motions (Washington site)

M	*R* (km)	Contribution to Hazard, C(T) (%)	
		***T* = 0.2 s**	***T* = 1.0 s**
4.5 to 6	0 to 50	35.8	8.4
4.5 to 6	> 50	9.3	4.8
6 to 7	0 to 10	0.0	0.0
6 to 7	10 to 50	11.5	9.2
6 to 7	50 to 100	9.8	8.5
6 to 7	> 100	15.0	29.8
>7	0 to 10	0.0	0.0
>7	10 to 50	3.3	3.2
>7	50 to 100	4.5	4.5
>7	> 100	10.7	31.7

2. Compute the contribution to hazard for every bin at a particular period. The data for this can be obtained from the USGS deaggregation matrix using the magnitude, the distance, and the epsilon value. The data must be organized, separated and arranged by magnitude and distance following the same criteria used to define the bins. The sum of epsilon in each group is the contribution to hazard percent of that particular bin.

3. Randomly select a number of records per bin. For this study 5 records per bin were selected. If possible avoid using too many records in the same bin from the same source to reduce bias. The random selection was done using Excel by arranging the data and using rand() function.

4. Convert the acceleration time histories to pseudo spectral acceleration and calculate the median pSa per bin.

5. Multiply the median pSa of each bin by its percent contribution to hazard percent and sum the products to obtain the overall pSa for the specified period:

$$SA_{avg}(T) = \sum_{i=1}^{10} C_i(T) \cdot SA_{mediani}(T) \tag{3.3}$$

where C_i = percent contribution to hazard (in decimals) for the *i*th *M*-*R* bin, and $SA_{median\ i}$ = median pseudo spectral acceleration for the *i*th *M*-*R* bin.

6. Calculate the scaling factor for each specified period of the UHS defined as the ratio of the SA_{UHS} to the SA_{avg}.
7. Repeat Steps 1 through 7 for different design events (i.e. 2500-yr and 500-yr)

The analysis used a total of 50 records for each specified period.

Method 4: Kottke and Rathje (2008)

Method 4 is based on the method proposed by Kottke and Rathje (2008). The criteria for the record selection for the suites is based on an algorithm randomly selects a pre-defined number of motions to build the suites, then scales each motion individually to match the target spectrum based on the lowest calculated root mean squared error. The algorithm was implemented using the software program SigmaSpectra that is integrated with Strata (Kottke and Rathje 2013). This program requires the user to input the target spectrum and the standard deviation, the motion catalog, the number of motions per suite, and the number of seed motions. The following steps were used for Method 4:

1. Follow Steps 1 and 2 as described previously in Method 1
2. Repeat Step 1 for periods with different modal values of magnitude and distance.
3. Combine all the pre-selected records into a single batch.
4. Run SigmaSpectra
    a. Define the design (target) spectrum and the standard deviation. If the design spectrum comes from a PSHA, the standard deviation is zero.

b. Define the number of motions per suite. Seven records seem to provide stable statistical results.

c. Define n_{seed} and suites to save. Typically 2 gives acceptable results.

d. Load the batch of records from Step 3 and compute. To reduce bias in the selection algorithm, it is recommended to check the box for "One component per recording station".

5. Verify that none of the records of the suite with the lowest RMSE has a scaling factor SF $\geq$ 4.0. If this is the case, disable the record and execute the calculation again. Repeat the procedure until there are no records with SF $\geq$ 4.0. Select the suite of motions with the lowest *RMSE* and $\sigma_{ln}RMSE$.

6. Repeat Steps 1 through 5 for different design events (i.e. 2500-yr and 500-yr).

In this study the predefined database was the same used in Method 1 combining the low and high period ranges. Therefore, 88 and 78 records were selected for the 500-yr and 2500-yr events, respectively. These two databases were used to compile suites of recorded ground motions comprise of seven records.

Method 5: Hines et al. (2011)

Method 5 is based on the method proposed by Hines et al. (2001). It involves the selection of a representative suite of ground motions within upper and lower bounds of the UHS and does not perform any amplitude scaling of the selected records. Method 5 was performed using the following steps.

1. Filter the recorded ground motion database using a magnitude based on the modal value of the deaggregation matrix. For this study the range used was the same proposed by Hines et al. (2011), that is $5 \leq M \leq 7.5$.

2. Identify the PGA of the design spectrum and define the lower and upper amplitude boundaries as 0.5*PGA and 2.0*PGA, respectively.

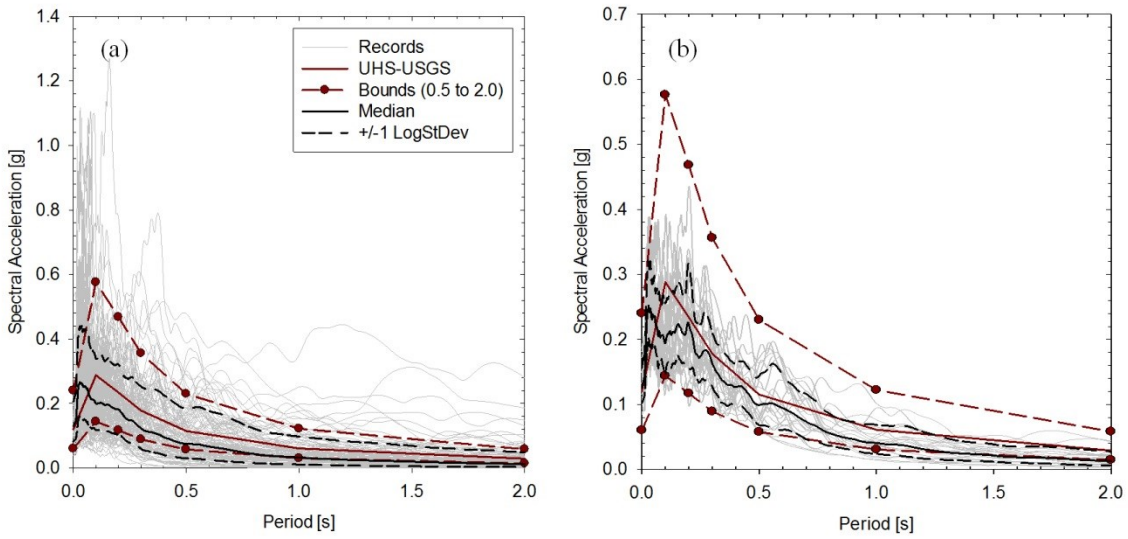

Figure 3.7 – Defined boundaries for motion selection of Washington Bridge site for the 2500-yr event

3. Select pairs of records if at least one of the horizontal components falls within the boundaries.

4. Define the lower and upper boundaries for the whole design spectrum same as Step 1 for every defined period.

5. From the acceleration time histories compute the pseudo spectral accelerations and plot the pre-selected ground motions from Step 3 with the design spectrum.

6. Manually and graphically, discard the records that exceed the defined boundaries as shown in Figure 3.7b. When few records are available, engineering judgment must be used to keep some of the records that exceed these criteria.

7. Repeat Steps 1 through 6 for different design events (i.e. 2500-yr and 500-yr).

Method 6: Single Spectrally-Matched Synthetic Motion

Method 6 refers to a single synthetic motion spectrally-matched to a target spectrum. Several software programs have been developed over the past years to generate

synthetic motions such as SIMQKE (Vanmarcke et al., 1976), RASCAL (Silva and Lee, 1987), and SMSIM (Boore, 2005). Typically these programs implement a stochastic method to generate the synthetic motions. For this study, the synthetic motion was provided by a professional seismologist for the Sakonnet river bridge for both 500 and 2500-yr return period events. However, no details were given on how the synthetic motions were generated.

Results and Discussion

The median pseudo spectral acceleration (pSa) response and its variability are shown in Figures 3.8 through 3.11 for both sites at bedrock for the 500-year and 2500-year design events. The bedrock uniform hazard spectrum (UHS) is shown for comparison. The variability of the methods was compared using standard deviation in log space (σ_{ln}). This was compared to aleatoric standard deviation of the UHS defined by the equation proposed by Toro et al. (1997). For this equation, the modal values of magnitude and source-to-site distance from the USGS deaggregation figures were used.

The evaluation and discussion of Method 6 is limited to the Sakonnet River Bridge site with a single record being generated and therefore there is not enough data to develop the standard deviation. Also, the record was generated using a site-specific UHS (SS-UHS) and not the UHS from USGS. These results are shown in Figure 3.12. Method 4 is included in these figures for comparison purposes. The results and discussion will follow the evaluation criteria defined previously.

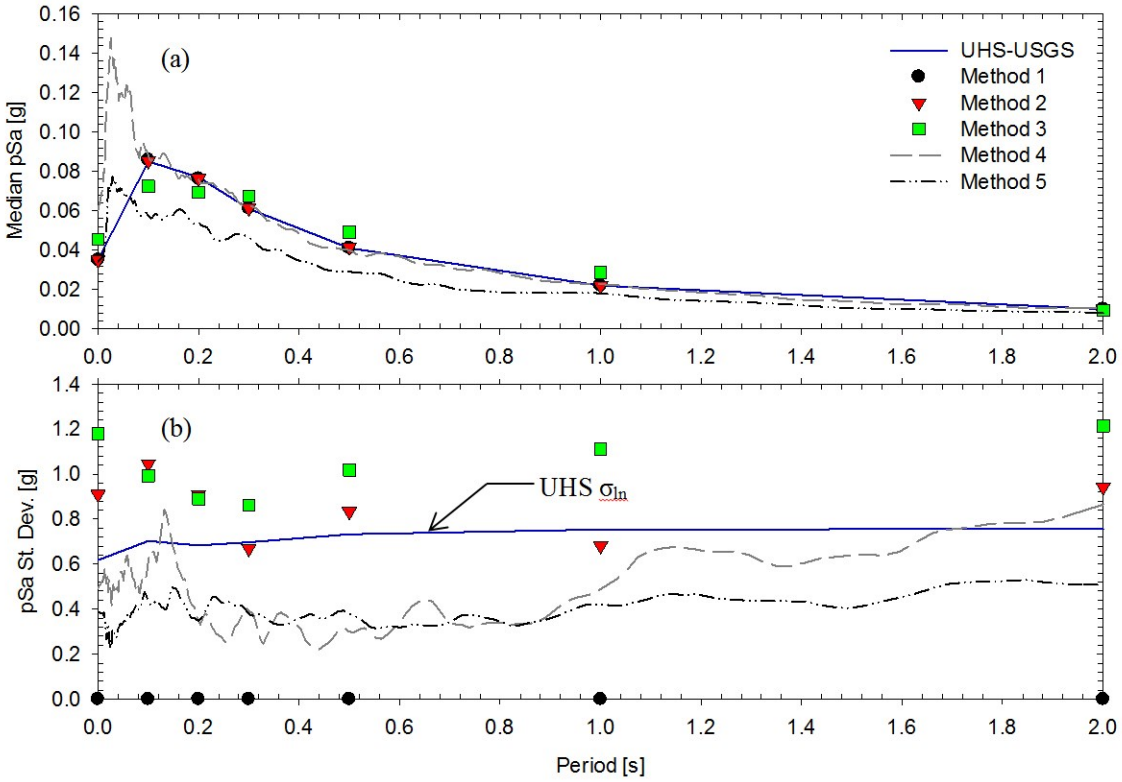

Figure 3.8 – (a) Median pSa response and (b) StDev at bedrock for Washington Bridge, 500-yr event

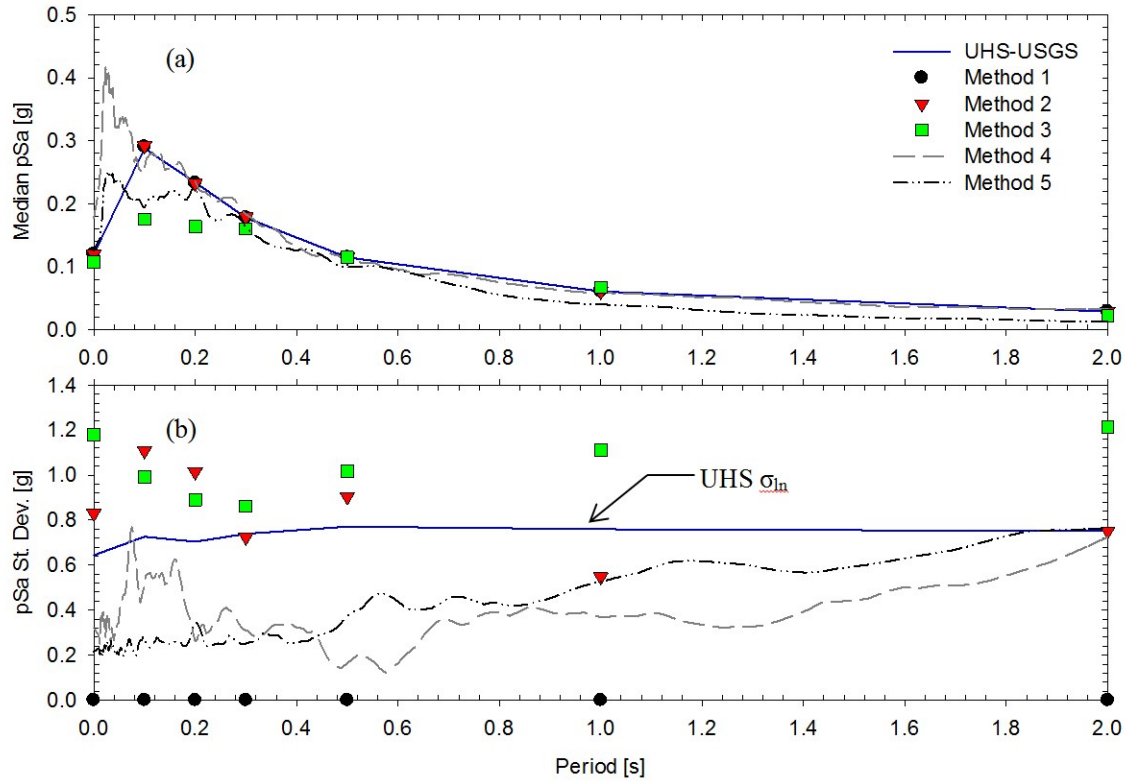

Figure 3.9 – (a) Median pSa response and (b) StDev at bedrock for Washington Bridge, 2500-yr event

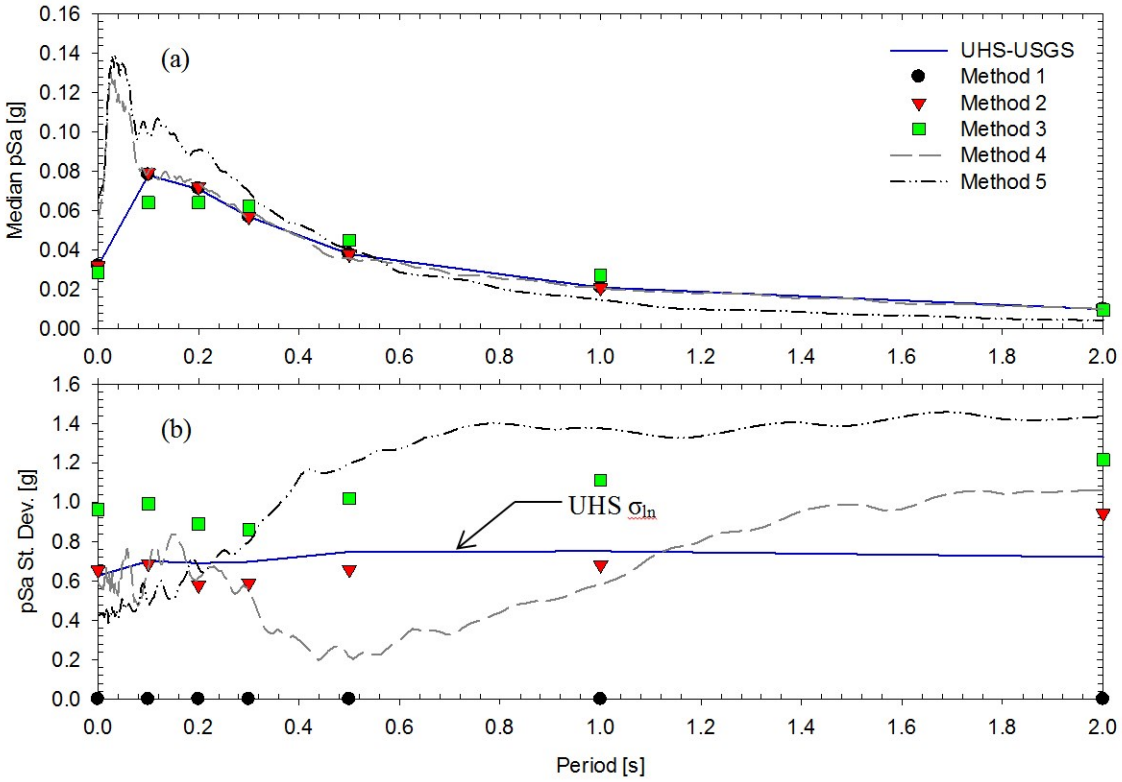

Figure 3.10 – (a) Median pSa response and (b) StDev at bedrock for Sakonnet River Bridge, 500-yr event

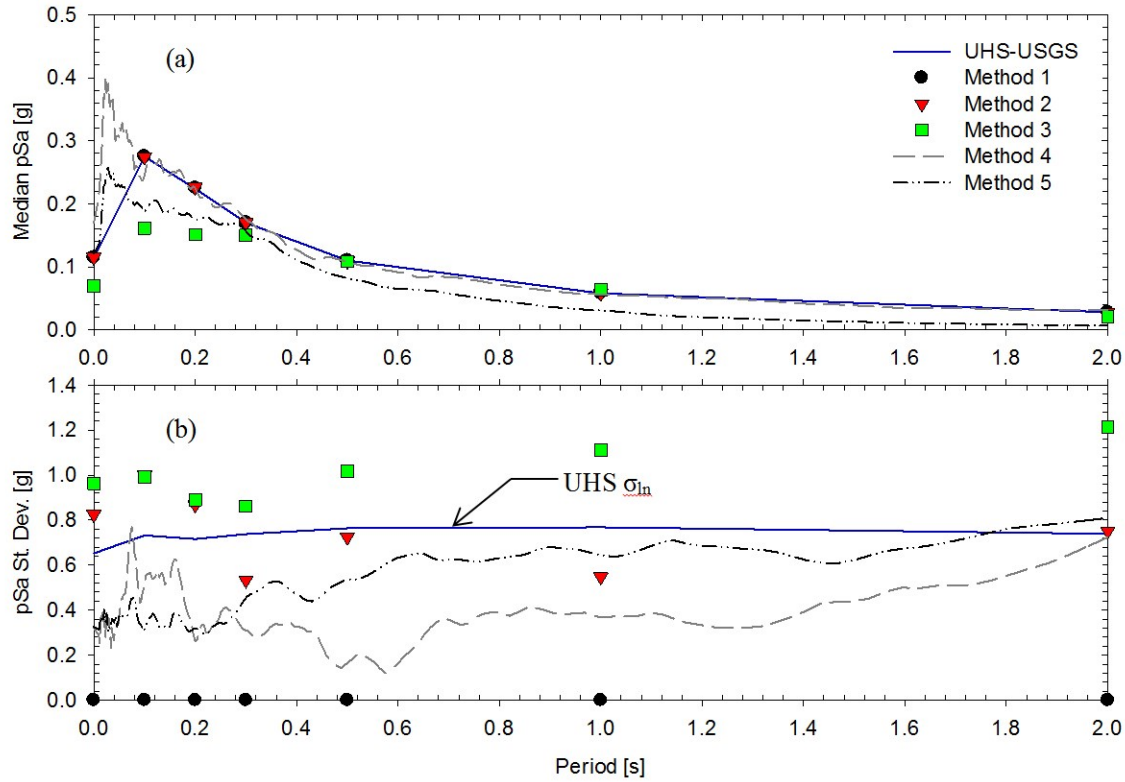

Figure 3.11 – (a) Median pSa response and (b) StDev at bedrock for Sakonnet River Bridge, 2500-yr event

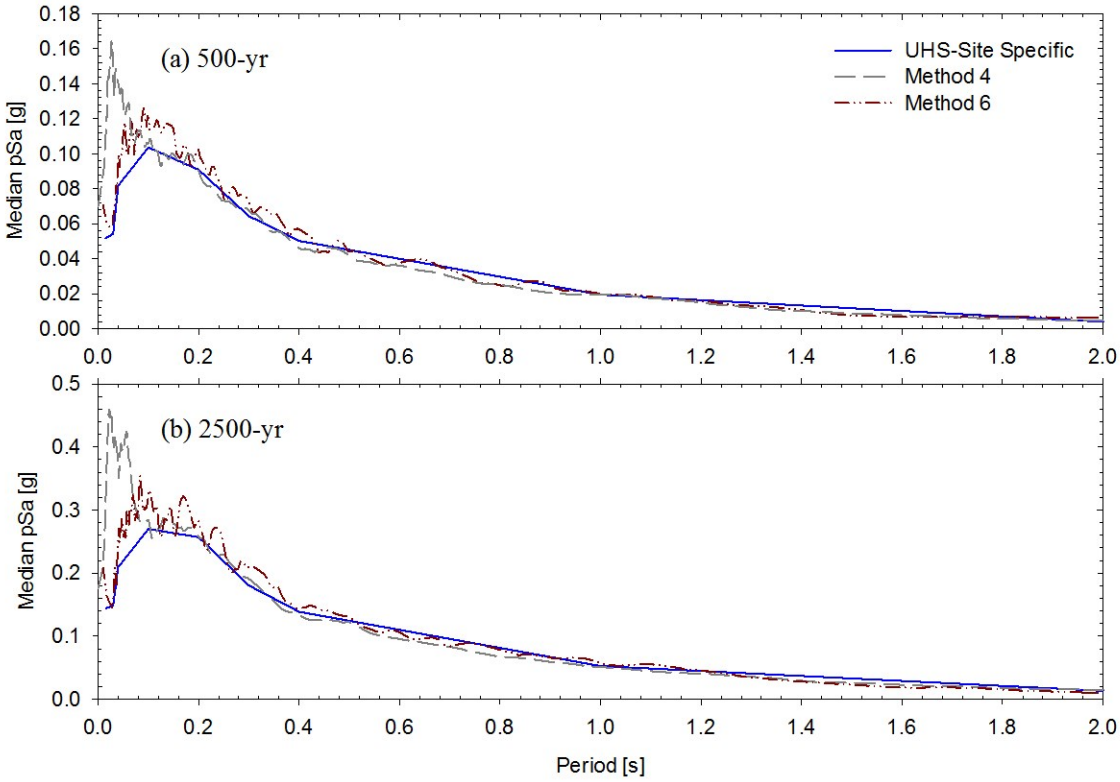

Figure 3.12 - Response spectra at bedrock for Sakonnet Bridge with SS-UHS, for (a) 500 and (b) 2500-yr event

1. The ability of the method to produce a median response spectrum at bedrock that matches the UHS and its variability.

All the selected methods are capable of obtaining the median pseudo response spectrum. The results obtained from Method 1 at bedrock (individual basic scaling) and Method 2 (median basic scaling) matches perfectly the UHS as shown in Figures 3.8a through 3.11a. This is expected given that the procedures in both methods scale the records or the median of the records to match the UHS.

Since Method 1 scales each record individually to match the UHS at a specified period there is no variability in the motions. Method 2 scales the median of a group of records and therefore includes some variability and the standard deviation compares very well with the UHS standard deviation. The difference of the standard deviation of

Method 2 was within 21% of the UHS standard deviation on average. Although there is no trend with period, it seems that the variability from Method 2 is higher at lower periods ($T \leq 0.3$ s) compared to the UHS variability. The method appears to preserve some of the natural variability in the ground motions by scaling the median of a group of records.

The median response spectrum of Method 3 (Bradshaw and Green, 2011) at bedrock showed mixed results depending on the oscillator period. In general the median response of Method 3 is lower than the UHS at periods of less than 0.3 seconds but compares favorably at higher periods. The agreement at lower periods is better in the 500-year events than in the 2500-yr events. As described in the description of Method 3, scaling factor is based on weighting factors applied to the original records. The scaling factor is then applied to unweighted (original) records and thus the median response will not necessarily match the UHS. At low periods, the weighing factors are dominated by ground motions with magnitudes around M = 4.5 to 6.0, and distances below 50 km. These records have high ground motion amplitudes. As a result, the scaling factor in this bin is very low. Since it is given high weighting it has the effect of reducing the scaling factor. Therefore, after it is applied overall to the unweighted ground motions, the median response is below the UHS. The difference of the median response was within 18% of the UHS on average.

The standard deviation of Method 3 is consistently higher than that of the UHS for all periods and return periods. The difference of the standard deviation was within 43% of the UHS standard deviation on average. The agreement is best over the period range of 0.1 to 0.3 seconds. The agreement was similar in the 500-year and 2,500 year

events. The high variability is likely attributed to the use of records having a wide range of magnitude and site-to-source distances.

The median response spectrum of Method 4 (Kottke and Rathje, 2008) obtained at bedrock matched very well the design spectra for periods greater than 0.1 s as shown in Figures 3.8a through 3.11a and Figure 3.12. This median acceleration response was obtained with a *RMSE* and a $\sigma_{\ln}$ *RMSE* below 0.050 and 0.600, respectively. These low values were obtained by limiting the scaling to a period range between 0.1 s and 2.0 s. Below period $T = 0.1$ s, this method showed that the ground motions contain very high frequency incapable of being scaled to the design spectrum. Additionally, in all cases the PGA obtained by this method was almost twice the PGA of the design spectra.

A first attempt was made to match the records to a wider period range (i.e. starting at $T = 0.01$ s). This first attempt led to higher errors (e.g. $RMSE > 0.2$) and a poor scaling result. Figure 3.13 shows a comparison between the spectral match obtained using both the wide (T [0.01 – 2.0s]) and the narrow (T [0.1 – 2.0]) period range. This mismatch at low periods is attributed to the fact that these ground motions contains a different spectral shape compared to the design spectrum. The UHS from the USGS does not provide information about the spectral shape for periods between zero and $T = 0.1$ s. However, it is common practice to estimate these values with linear interpolation. Areas in which ground motions do not contain high frequency, this practice might be acceptable. On the other hand, for NEUS this practice is not recommended due to the high frequency content present in the ground motions. Therefore the best practice is to limit the spectral match within a period range with spectral shape compatibility.

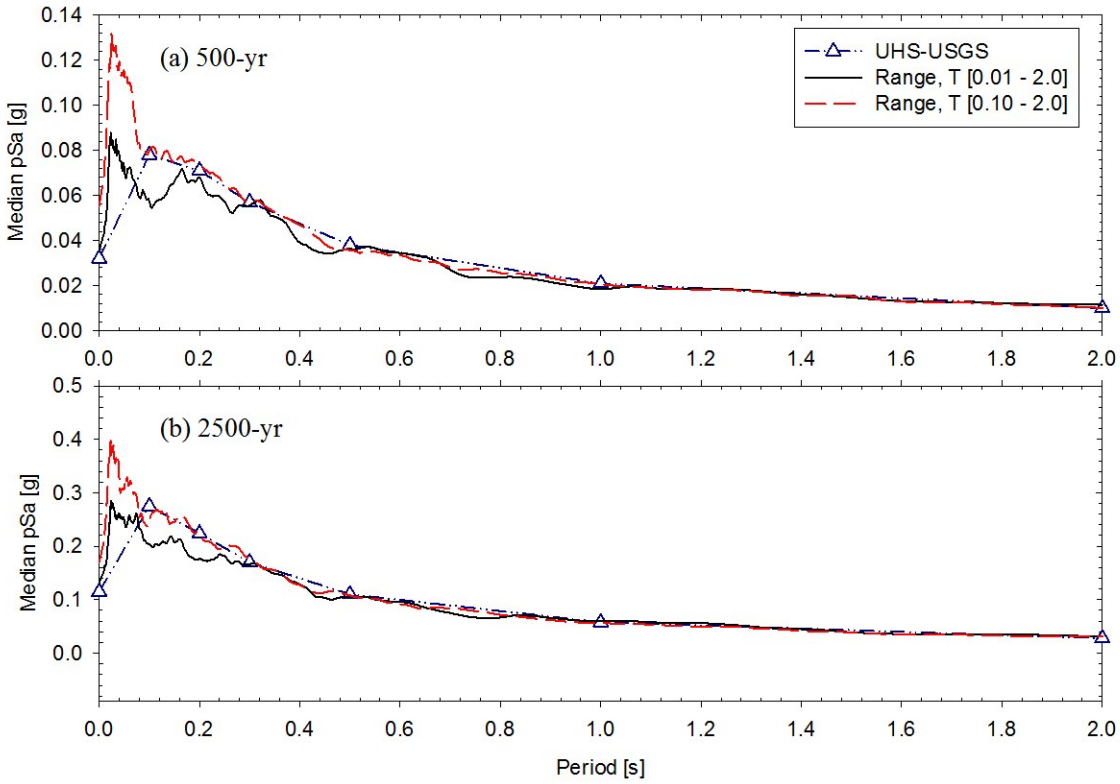

Figure 3.13 - Difference between wide and narrow period ranges for records scaling in Method 4 at the Sakonnet River Bridge at (a) 500-yr and (b) 2500-yr events

Even though Method 4 matches very well the UHS, its variability is consistently lower than the UHS variability. The difference of the standard deviation of Method 4 was within 39% of the UHS standard deviation on average. In this case, the variability of the response is usually lower than the UHS variability because the procedure is designed to minimize the error. The practitioner, however, has the option of selecting a suite of records with a higher variability comparable with that from the UHS.

The median response spectrum of Method 5 (Hines et al., 2011) are sometimes lower and sometimes higher than the UHS as shown in Figures 3.8a, 3.9a, and 3.11a. The difference of the median response of Method 5 was within 28.5% of the UHS on average. The spectral shape obtained by Method 5 is similar to Method 4 including the

high frequency content. Given that this method does not scale the records to match a target spectrum, the median of the response will depend largely on the characteristics of the ground motion records that are selected for the analysis.

The variability of Method 5 is generally lower than the UHS variability. However, the standard deviation was higher than the UHS for the 500-yr event at Sakonnet River bridge (Figure 3.10). The difference of the standard deviation of Method 5 was within 43% of the UHS standard deviation on average. The generally lower variability is likely attributed to the preselection that places upper and lower boundaries on the pSa that is essentially constraining the variability.

Method 6 (spectrally matched synthetic motion) utilized only one synthetic record matched to a site-specific UHS. By design the synthetic motion is developed to match the UHS at all periods. In this case the difference of the median response was within 18% of the UHS on average. Given that only one record is used it is not possible to determine the variability in the response spectrum. Comparing Method 4 and Method 6, both yield similar results, however, Method 4 has a better match overall at $T \geq 0.1$ s while the synthetic motion matches slightly closer the design spectra below this period.

2. The ability of the method to characterize a response spectrum over a period range versus a single period.

Methods 1 2, and 3 perform the scaling at a single oscillator period and it is necessary to repeat the procedure per every period of interest when a period range is desired. Methods 4, 5, and 6 generate a continuous acceleration response over a period range. Method 4

uses a single scaling factor throughout the specified range, while Methods 5 and 6 do not require any scaling.

3. **The ability of the method to account for a range of magnitude and site-to-source distance earthquakes that are consistent with the UHS.**

The majority of the methods presented herein use magnitude and site-to-source distance as a prerequisite to build a ground motion selection database. For this, the modal values obtained from the deaggregation matrices are usually considered. From the selected methods, Method 3 is the only one that uses a different approach. In this case, this method factors in the contribution to hazard of all possible sources. It combines all the magnitudes and distances from the ground motions and applies a weighing factor to favor those with a higher contribution and suppress those that contribute the least. In this case, the modal values of magnitude and source-to-site distance do not matter because all the selected data has been taken into consideration.

4. **Set-up time and run time required to obtain the response spectrum at bedrock.**

The initial setup of each method is similar when it comes to build the database for the preselected ground motion records. Methods 1, 2, and 3 will require much more time to generate an acceleration response than Methods 4, 5, and 6 if a period range is required. Methods 1 and 2 are very similar and thus the time consumption is basically the same.

However, in terms of repetitive procedure for a single run, Method 1 requires 14 different scaling computations while Method 2 only requires obtaining the median value of the suite of records and the single scaling factor. Another disadvantage of Method 1 is

that it has a higher chance of containing a pair of records with a scaling factor greater than 4, causing a substitution of the pair.

Method 3 requires more time for the initial setup because the user needs to build the bins and select the records according to the bins. Also, the contribution to hazard factor of each bin must be determined. There is no computer program available to run these methods, therefore to reduce the required time to obtain the acceleration response at bedrock a numeral analysis program such as Matlab is preferred.

Even though Method 4 utilizes a complex algorithm to select, scale, and determine the suite of records to compute the acceleration response at bedrock, it has the advantage of having a computer program called SigmaSpectra (Kottke and Rathje, 2013). Once the user is familiar with the program, the required time to obtain the response at bedrock is greatly reduced. This program, however, is limited to certain file extensions such as .AT2. For example, if the database format is .ATH, the user must change it to .AT2 before using SigmaSpectra.

Method 5 has the advantage of not requiring any scaling procedure of the selected ground motions. However, the final suite of motions is determined visually and might require some time depending on the number of records available in the preselected database.

Method 6 is generated using a computer program. Similar to Method 4, once the user knows how to use the program, the required time to compute the acceleration response at bedrock should not take much.

5. **How the site response analysis result is affected by the method.**

The site response analysis was performed using Strata (Rathje and Kottke, 2013). To evaluate this criterion, the ratio between the median response at ground surface and the median response at bedrock ($pSa_{surface}/pSa_{bedrock}$) was obtained for each method. Similarly, the ratio between the variability at surface and bedrock ($\sigma_{ln,surface}/\sigma_{ln,bedrock}$) was computed and compared. These results are shown in Figures 3.14 through 3.17. Because Method 6 was obtained with a single ground motion, its variability was not evaluated. The results of this site response analysis are shown in Figure 3.18 for both design events.

Based on these figures, Methods 1, 2, 3, and 4 have a similar median response ratio. Most of the records have a ratio above unity meaning the soil profile amplifies the response. The amplification was highest near the fundamental period of the sites. In most cases, Methods 1 through 4 have a surface/bedrock median response ratio varying from 1 to 5. Method 4 has ratios below unity in the high frequency range as shown in Figures 3.14a through 3.18a. Method 5 has a completely different surface/bedrock median response ratio results compared to the other methods with ratios ranging from 0.7 to 5.

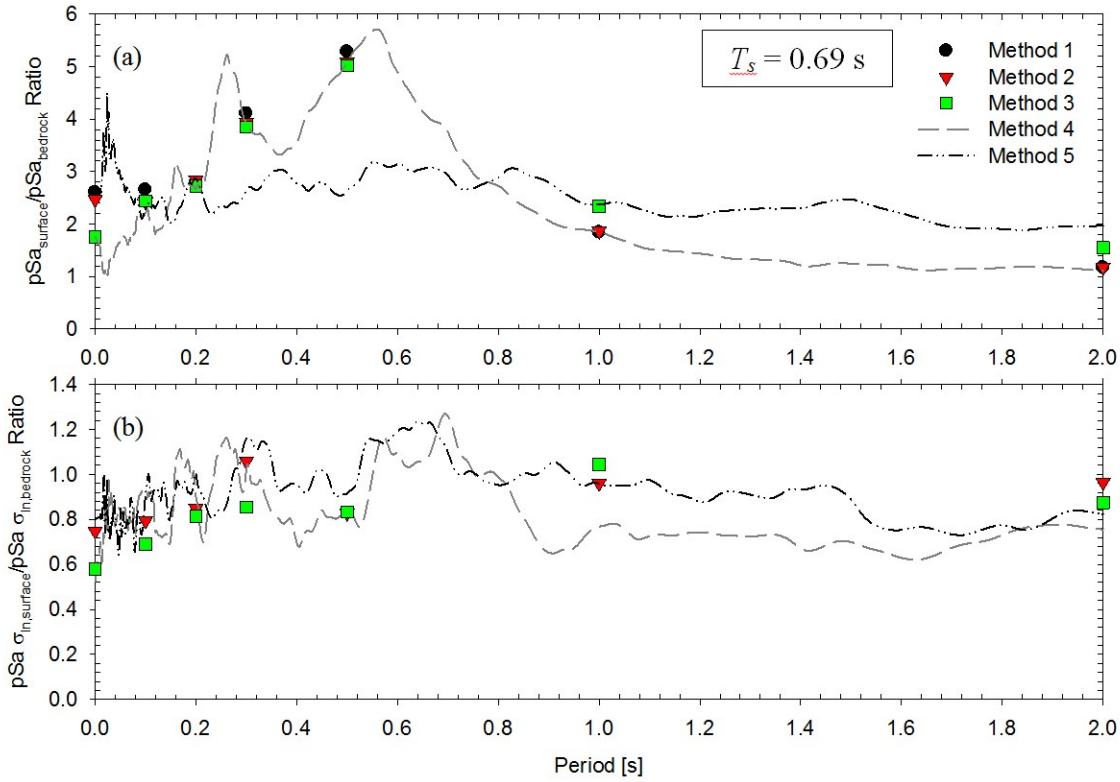

Figure 3.14 - Surface/bedrock ratios of (a) median pSa and (b) St Dev for Washington Bridge, 500-yr event

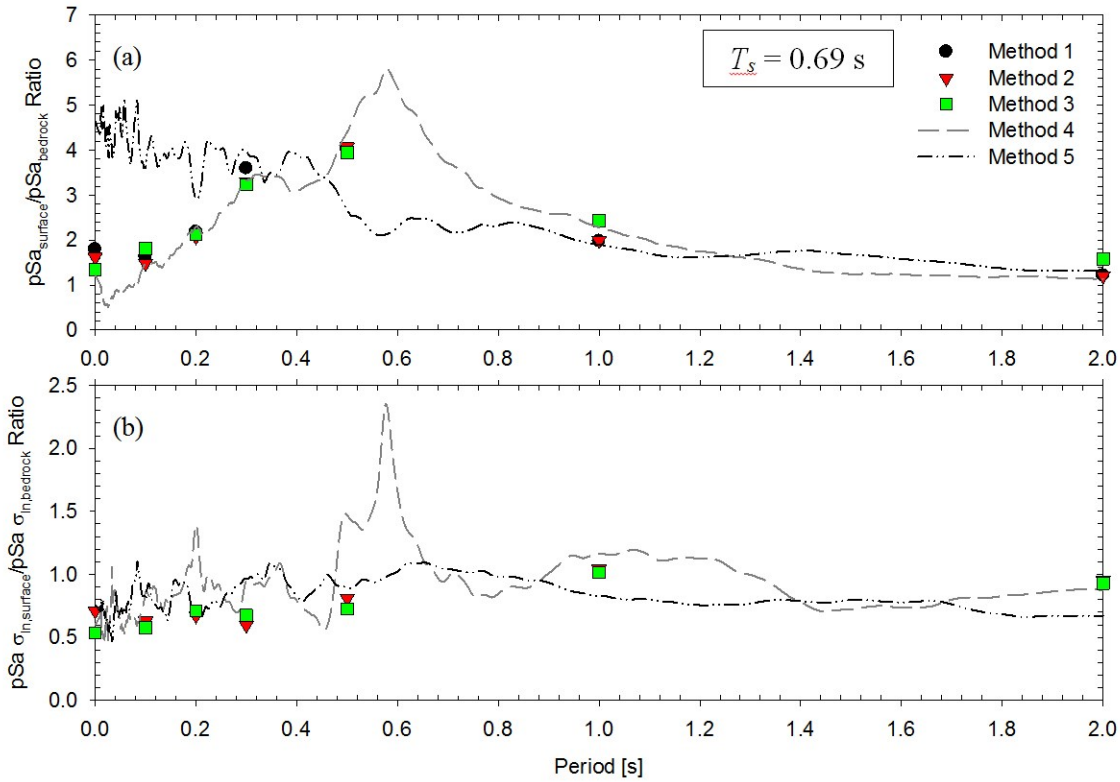

Figure 3.15 - Surface/bedrock ratios of (a) median pSa and (b) St Dev for Washington Bridge, 2500-yr event

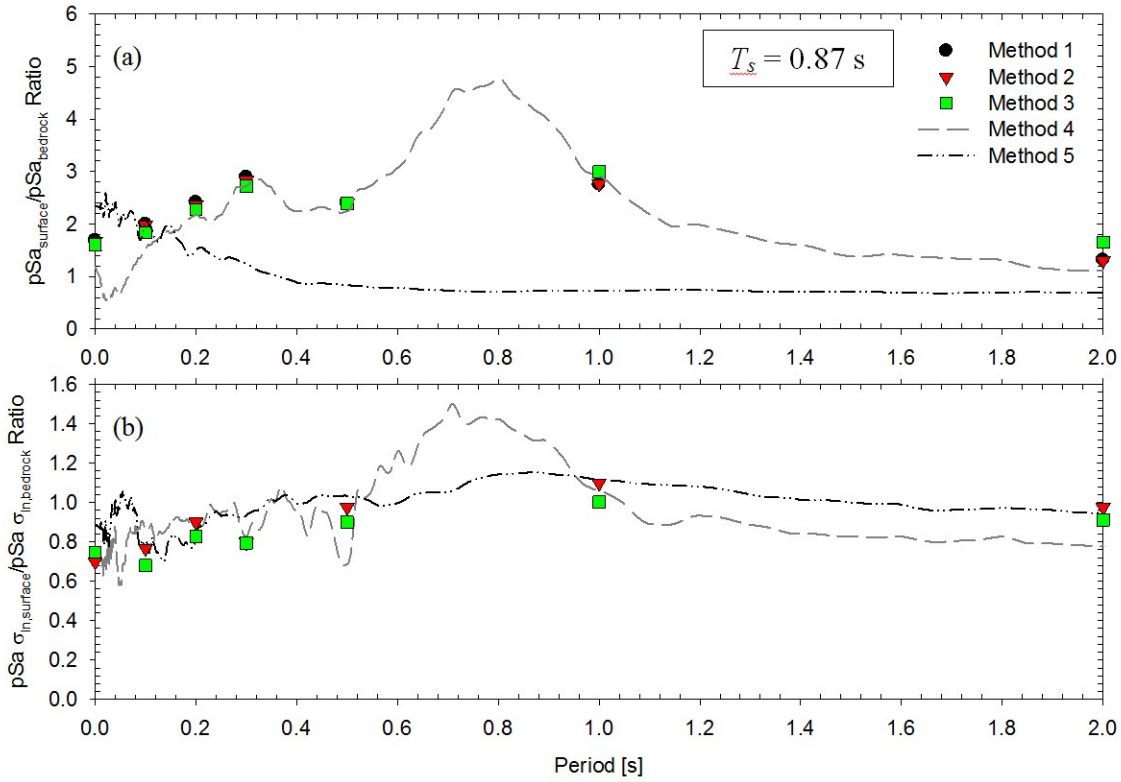

Figure 3.16 - Surface/bedrock ratios of (a) median pSa and (b) St Dev for Sakonnet River Bridge, 500-yr event

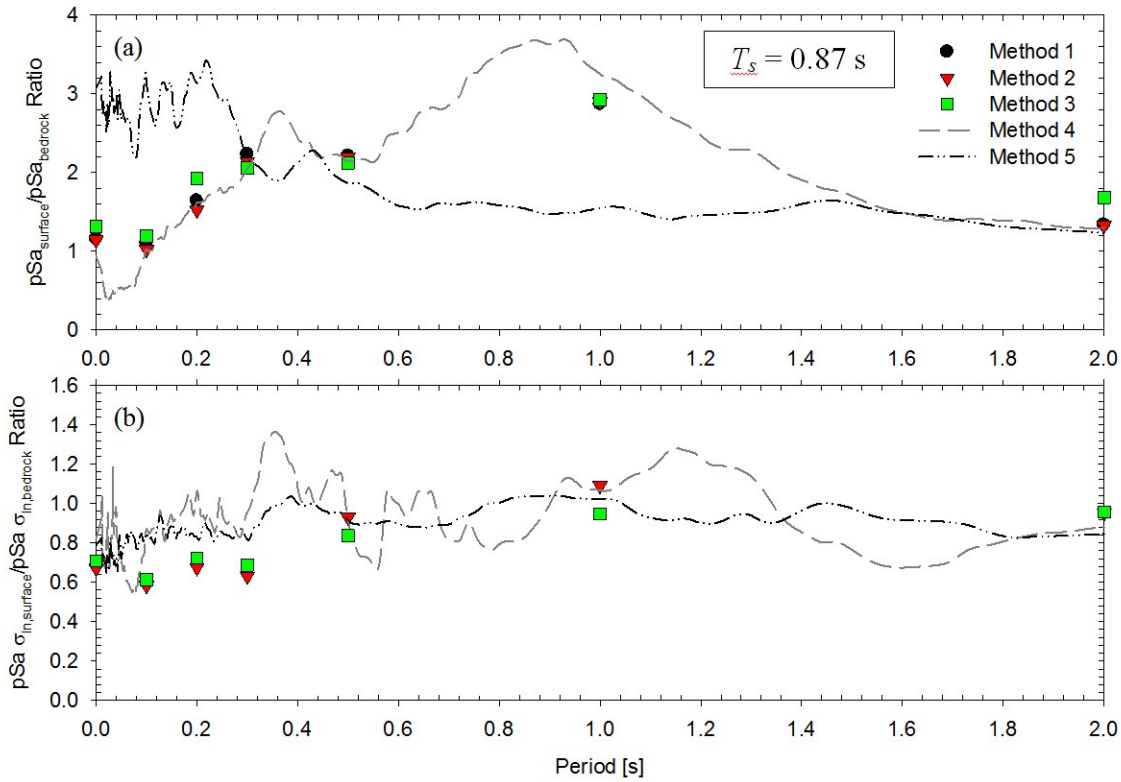

Figure 3.17 - Surface/bedrock ratios of (a) median pSa and (b) St Dev for Sakonnet River Bridge, 2500-yr event

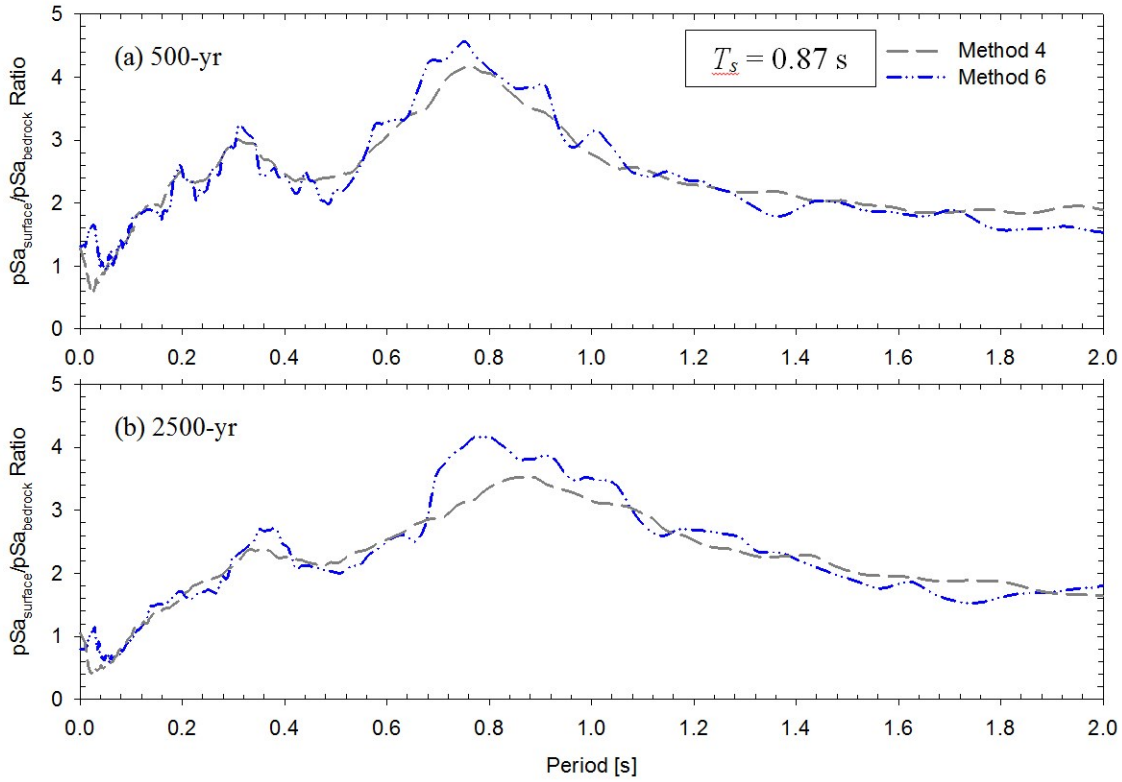

Figure 3.18 - Surface/bedrock pSa ratios for Sakonnet Bridge with SS-UHS for (a) 500 and (b) 2500-yr event

Comments on the UHS

One of the major problems encountered when using methods that match the UHS in a period range (i.e., Methods 4, 5, and 6), is the inability of these to match the spectral responses at low periods. Perhaps, the problem does not rely on the selection/scaling method alone, but with the target spectrum as well. The reason behind this is that the target spectra do not recreate the high frequency content of ground motions from the earthquakes in NEUS.

Both the UHS from the USGS and the site-specific UHS (SS-UHS) are shown in Figure 3.19. The site-specific UHS was generated by a professional seismologist, however no information was provided on how the spectrum was generated. Additionally, an acceleration response with high frequency content is also included. This acceleration

response correspond to an earthquake with a magnitude of $M = 5.4$ and distance $R = 15.4$ km. Both response spectra were anchored to the PGA of the UHS of both return period designs for comparison purposes.

Figure 3.19 clearly depicts this problem with the ground motions in NEUS. This undesired mismatch between the record and the target spectra makes the spectral matching procedure more difficult. The problem stems from the fact that the UHS is defined only at specific periods that are connected linearly. However, this linear approximation is not necessarily correct. This is especially true for periods $T < 0.1$ s. The site-specific UHS, for the most part, contains a wider spectrum in the high frequency; however it also fails to deliver a more realistic spectrum capable of mimicking the high frequency content. For an analysis in which the period range of interest falls in this area the actual spectral response will be underestimated. This could be very critical for rigid structures or buildings constructed in hard soils (i.e., Site Classification B) with low fundamental periods. Because of this unrealistic shape, it is not advisable to generate synthetic ground motions using the UHS from the USGS. The synthetic motion will match the linear approximation between zero and 0.1 s which will result in an underestimation of the true response spectrum. This is highly unconservative and must be avoided. Even the SS-UHS falls short in estimating the spectral shape in this region. In the necessity of scaling records within the low period ($0.0 < T < 0.1$) it is better to use methods capable of tracking the high frequency content such as Method 4 or Method 5. Using these methods (particularly Method 4 scaled at $T \geq 0.1$ s) will most likely produce overestimated response spectra, and therefore overconservative results. In the lack of a

properly defined target spectrum within this period range, this seems to be the appropriate solution.

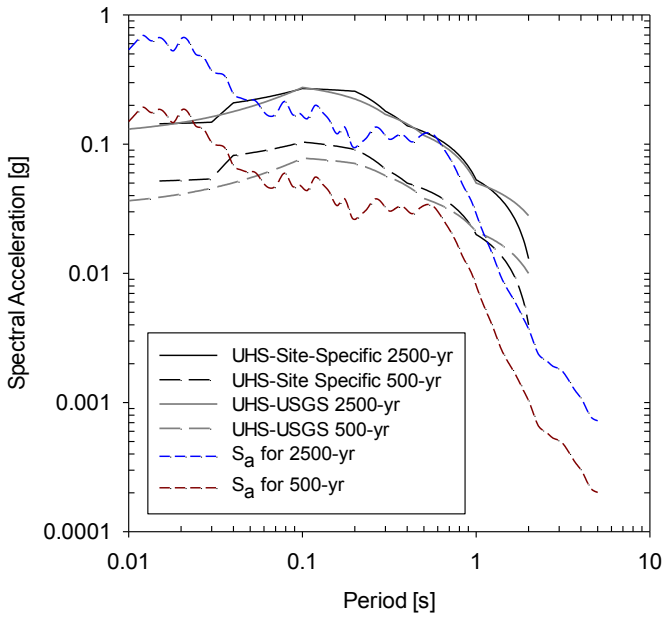

Figure 3.19 - Comparison between design spectra from UHS-USGS and site-specific target spectra by professional seismologist

Conclusions

Site-specific seismic studies in the Northeastern United States (NEUS) is a difficult task in most part because the earthquake sources in this region are not well defined, and because the available database of earthquake with strong motions is very limited. In addition, different site conditions, relative low magnitude earthquakes, high frequency content of ground motions, among other characteristics make the use of ground motions from actives regions (i.e., Western United States) not suitable for the seismic hazard analysis in NEUS.

The objective of this study was to compare and evaluate methods for ground motion selection/scaling in the northeastern United States. A review of the literature

identified sixteen references pertaining to methods for selecting/scaling ground motions. They covered a range of mathematical complexity and some methods included parameters describing the ductility of the structure. Of these methods, six methods were selected for further comparison and evaluation. They were chosen to represent methods that would be easiest to implement and did not require structural parameters.

Five different criteria were defined to critically evaluate and compare the selected methods. The criteria evaluates (1) the ability of the method to produce a median response spectrum at bedrock that matches the UHS and its variability, (2).the ability of the method to characterize a response spectrum over a period range versus a single period, (3) the ability of the method to account for a range of magnitude and site-to-source distance earthquakes that are consistent with the UHS, (4) the Set-up time and run time required to obtain the response spectrum at bedrock, and (5) how the site response analysis result is affected by the method.

Site response analyses were performed at two different sites that were classified as Site Class D and E in accordance with NEHRP. The uniform hazard spectrum (UHS) was used as the target spectrum for comparison as this is the most common approach in most design codes. Response spectra were calculated at the bedrock and ground surface levels for both the 500-year and 2,500-year seismic events. Major conclusions from this study are as follows.

The median response spectrum of Method 1 matches exactly the UHS with zero variability at a specified period. Relative to other methods, the procedure involved to obtain the suite of records requires a considerable amount of time. Based on all the

evaluated criteria, this method is applicable to cases when the median response is desired and the period of the structure is known.

The median response spectrum of Method 2 matches exactly the UHS at a specified period. In addition, the computed standard deviation agrees very well with that of the UHS compared to any of the other methods. The time required to obtain the suite of records is comparable with Method 1. Therefore this method is applicable to cases when both the median and the variability of the response are desired and the period of the structure is known.

The median response spectrum of Method 3 fairly matches the UHS at a specified period and has the highest variability compared to other methods. This is the only method that utilizes a contribution to hazard factor when selecting ground motions. Relative to other methods it requires great amount of time to produce the suite of records with the required scaling factor. Based on all the evaluated criteria, this method is applicable when the hazard contribution from earthquakes with different magnitudes and source-to-site distances are required and the period of the structure is known.

The median response spectrum of Method 4 matches very well the UHS along a defined period range. Its variability is low compared to the UHS variability and other methods because the suite of records is selected based on the lowest variability. However, if a higher variability is required, the practitioner may select a different suite of records that matches closely the UHS variability. Compared to other records, this method is simple and requires little time to obtain a suite of records. Based on all criteria, this method is applicable to any type of analysis. However, in some cases, it might overestimate the response spectrum at lower periods (i.e. $T < 0.1$ s).

The median response spectrum of Method 5 barely matches the UHS and has the lowest variability compared to the UHS variability and any other method along a defined period range. The response spectrum of this method is highly influenced by the user judgment. Relative to other methods, the time required to obtain a suite of motions is average. Compared to other methods, in Method 5 site conditions seem to provide differences in the response characteristics at ground surface. The method is applicable if no alteration of the records is desired as this method does not scale the records.

The response spectrum of Method 6 matches the UHS along a defined period range, but because it is based on a single record, it provides zero variability. The UHS is defined base on the contribution of a multiple ground motions from a database. Therefore, using a single ground motion is not consistent with the UHS approach. Compared to other methods, Method 6 consumes little amount of time. Based on the evaluated criteria, this method is applicable to any analysis. However, the use of a single ground motion is not recommended.

The bedrock ground motion records that represent the NEUS show very high response at periods between 0 and 0.1 seconds. However, the UHS specified by USGS, is linearly interpolated between the known periods of 0 and 0.1 seconds. Generating spectrally matched synthetic records or scaling ground motions suites within this period is highly uncertain and likely unconservative. A more conservative approach is to scale motions to the higher period ranges and allow the response below 0.1 seconds to extent above the UHS.

Acknowledgements

This study was funded by the Rhode Island Department of Transportation (RIDOT) and the Transportation Center at the University of Rhode Island (URITC). Their support is greatly acknowledged. We also want to thanks Dr. Adrián Rodríguez-Marek and Dr. Russell Green for their suggestions and comments, and Dr. Ellen Rathje and Dr. Albert Kottke for helping us using both Strata and SigmaSpectra.

References

AASHTO. (2012). *LRFD Bridge Design Specifications.* Washington, D.C.: 6th Ed. American Association of State Highway and Transportation Officials.

Ambraseys, N. N., Simpson, K. A., & Bommer, J. J. (1996). Prediction of Horizontal Response Spectra in Europe. *Earthquake Engineering and Structural Dynamics, 25*, 371-400.

ASCE. (2000). *Seismic analysis of safety-related nuclear structures and commentary.* ASCE Standard No. 004-98, American Society of Civil Engineers.

ASCE. (2006). *Minimum design loads for buildings and other structures.* ASCE Standard No. 008-05, American Society of Civil Engineers.

ASCE. (2007). *Seismic Rehabilitation of Existing Buildings.* Reston, Virginia: ASCE/SEI 41-06, American Society of Civil Engineers.

Atkinson, G. M., & Boore, D. M. (1995). Ground-Motion Relations for Eastern North America. *Bulletin of the Seismological Society of America, 85*(1), 17-30.

Atkinson, G. M., & Boore, D. M. (2006). Earthquake Ground-Motion Prediction Equations for Eastern North America. *Bulletin of the Seismological Society of America, 96*(6), 2181-2205.

Ay, B. Ö., & Akkar, S. (2012). A procedure on ground motion selection and scaling for nonlinear response of simple structural systems. *Earthquake Engineering and Structural Dynamics, 41*, 1693-1707.

Beyer, K., & Bommer, J. J. (2007). Selection and Scaling of Real Accelerograms for Bi-Directional Loading: A Review of Current Practice and Code Provisions. *Journal of Earthquake Engineering, 11*, 13-45.

Bommer, J. J., & Acevedo, A. B. (2008). The Use of Real Earthquake Accelerograms as Input to Dynamic Analysis. *Journal of Earthquake Engineering, 8*, 43-91.

Boore, D. M. (2005). *SMSIM — Fortran Programs for Simulating Ground Motions from Earthquakes: Version 2.3 — A Revision of OFR 96–80–A.* Department of the Interior, U.S. Geological Survey.

Bradley, B. A. (2012). A ground motion selection algorithm based on the generalized conditional intensity measure approach. *Soil Dynamics and Earthquake Engineering, 40*, 48-61.

Bradshaw, A. S., & Green, R. A. (2011). Estimating CSRs for Evaluating Liquefaction that are Consistent with Building Code Design Spectra. *GeoRisk 2011* (pp. 534-543). ASCE.

Bradshaw, A. S., Green, R. A., & Baxter, C. D. (2007). Evaluation of liquefaction potential at a silt site in Providence, Rhode Island. *Journal of the Boston Society of Civil Engineers Section, 22*(1), 5-18.

Catalán, A., Benavent-Climent, A., & Cahís, X. (2010). Selection and scaling of earthquake records in assessment of structures in low-to-moderate seismicity zones. *Soil Dynamics and Earthquake Engineering, 30*, 40-49.

CEN. (2004). *Eurocode 8: Design of structures for earthquake resistance – Part 1: General rules, seismic actions and rules for buildings.* The European Union Per Regulation 305/2011, Directive 98/34/EC, Directive 2004/18/EC.

Dhakal, R. P., Mander, J. B., & Mashiko, N. (2006). Identification of critical ground motions for seismic performance assessment of structures. *Earthquake Engineering and Structural Dynamics, 35*, 989-1008.

FEMA. (1997). *NEHRP Recommended Provisions for Seismic Regulations for New Buildings and other Structures.* Washington, D.C.: FEMA 302, Building Seismic Safety Council Program on Improved Seismic Safety Provisions.

FEMA. (2000). *Recommended Seismic Design Criteria for New Steel Moment-Frame Buildings.* FEMA 350, Federal Emergency Management Agency, SAC Joint Venture.

FEMA. (2005). *Federal Guidelines for Dam Safety: Earthquake Analyses and Design.* Washington, D.C.: FEMA 65, Interagency Committee on Dam Safety for FEMA.

FEMA. (2009). *Quantification of Building Seismic Performance Factors.* Washington, D.C.: FEMA P-695 Report, prepared by Applied Technology Council for Federal Emergency Management Agency.

Frankel, A., Mueller, C., Barnhard, T., Perkins, D., Leyendecker, E. V., Dickman, N., et al. (1996). *National Seismic-Hazard Maps: Documentation June 1996.* Denver, CO: U.S. Geological Survey, Open-File Report 96-532.

Hancock, J., Watson-Lamprey, J., Abrahamson, N. A., Bommer, J. J., Markatis, A., McCoy, E., et al. (2006). An improved method of matching response spectra of recorded earthquake ground motion using wavelets. *Journal of Earthquake Engineering, 10*(SI 1), 67-89.

Hines, E. M., Baise, L. G., & Swift, S. S. (2011). Ground-Motion Suite Selection for Eastern North America. *Journal of Structural Engineering, 137*(3), 358-366.

ICC. (2006). *International Building Code.* International Code Council.

Ishibashi, I., & Zhang, X. (1993). Unified dynamic shear moduli and damping ratios of sand and clay. *Soils and Foundations, 33*(1), 182-191.

Katsanos, E. I., Sextos, A. G., & Manolis, G. D. (2010). Selection of earthquake ground motion records: A state-of-the-art review from a structural engineering perspective. *Soil Dynamics and Earthquake Engineering, 30*, 157-169.

Kayhan, A. H., Korkmaz, K. A., & Irfanoglu, A. (2011). Selecting and scaling real ground motion records using harmony search algorithm. *Soil Dynamics and Earthquake Engineering, 31*, 941-953.

Kottke, A. R., & Rathje, E. M. (2008). A Semi-Automated Procedure for Selecting and Scaling Recorded Earthquake Motions for Dynamic Analysis. *Earthquake Spectra, 24*(4), 911-932.

Kottke, A., & Rathje, E. M. (2013). SigmaSpectra. Retrieved from https://nees.org/resources/sigmaspectra.

McGuire, R. K., Silva, W. J., & Costantino, C. (2001). *Technical Basis for Revision of Regulatory Guidance on Design Ground Motions: Hazard - and Risk - consistent Ground Motion Spectra Guidelines.* US Nuclear Regulatory Commission, Washington, DC.

Naeim, F., Alimoradi, A., & Pezeshk, S. (2004). Selection and Scaling of Ground Motion Time Histories for Structural Design Using Genetic Algorithms. *Earthquake Spectra, 20*(2), 413-426.

NIST. (2011). *Selecting and Scaling Earthquake Ground Motions for Performing Response-History Analyses.* NIST GCR 11-917-15, NEHRP Consultants Joint Venture A partnership of the Applied Technology Council and the Consortium of Universities for Research in Earthquake Engineering.

Park, Y. J., & Ang, A. (1985). Mechanistic seismic damage model for reinforced concrete. *Journal of Structural Engineering, 111*(4), 722-739.

Rathje, E. M., & Kottke, A. (2013). Strata. Retrieved from https://nees.org/resources/strata.

Rodríguez-Marek, A. (2013). Personal communication.

Silva, W. J., & Lee, K. (1987). WES RASCAL code for Synthesizing Earthquake Ground Motions. *State-of-the-Art for Assessing Earthquake Hazards in the United States, Report 24*.

Somerville, P., Collins, N., Abrahamson, N., Graves, R., & Saikia, C. (2001). *Ground motions attenuation relations for the Central and Eastern United States.* Final Report to the U.S. Geological Survey, Contract No. 99HQGR0098.

Toro, G. R., Abrahamson, N. A., & Scheiner, J. F. (1997). Model of Strong Ground Motions from Earthquakes in Central and Eastern North America: Best Estimates and Uncertainties. *Seismological Research Letters, 68*(1), 41-57.

Vanmarcke, E. H., Cornell, C. A., Gasparini, D. A., & Hou, S.-n. (1976). SIMQKE-I: Simulation of Earthquake Ground Motions.

Wang, G. (2011). A ground motion selection and modification method capturing response spectrum characteristics and variability of scenario earthquakes. *Soil Dynamics and Earthquake Engineering, 31*, 611-625.

Watson-Lamprey, J., & Abrahamson, N. (2006). Selection of ground motion time series and limits on scaling. *Soil Dynamics and Earthquake Engineering, 26*, 477-482.

Zhai, C.-H., & Xie, L.-L. (2007). A new approach of selecting real input ground motions for seismic design: The most unfavourable real seismic design ground motions. *Earthquake Engineering and Structural Dynamics, 36*, 1009-1027.

APPENDIX A

Link between small and large strain behavior of cohesive soils

Introduction

The objective of this appendix is to document additional laboratory data in support of manuscript 1 (Chapter 1). Specifically, additional laboratory tests were performed on reconstituted samples of high plasticity clay from the Gulf of Mexico and high quality samples of sensitive Presumpscot clay from Gulf of Maine. This data is intended to be combined with other work done at URI (Baffer, 2013; Sharma et al., 2011) for publication in the ASCE Journal of Geotechnical and Geoenvironmental Engineering. The test results presented in this section were obtained after publication of manuscript 1, and are an extension of this work.

Experimental Program

Tested soils

Samples tested included reconstituted Gulf of Mexico clay and undisturbed sensitive clay from Maine called Presumpscot clay. Samples of Gulf of Mexico clay were reconstituted from a slurry prepared at the Marine Geomechanics Laboratory at URI with a preconsolidation stress σ'_c = 68 kPa. At the end of consolidation, the soil cake was covered with cheese cloth, waxed, and stored in a controlled-temperature room to avoid loss of moisture.

For the Presumpscot sensitive clay, one block sample and two Shelby tubes were obtained from a site in Falmouth, Maine. These samples were provided by Professor Melissa Landon Maynard from the University of Maine. The samples were obtained at

depths of 4.3 m (block), 6.7 m (Shelby), and 11 m (Shelby). Presumpscot clay is found in the coastal and inland region of Maine and its formation is attributed to the flocculation of clay particles in salty marine waters beneath glaciers (Langlais, 2011). Similarly to the Gulf of Mexico clay, the Presumpscot clay was covered and stored properly to avoid loss in moisture. Properties of these tested soils are summarized in Table A.1.

Table A.1 - Soil properties of cohesive soils

Soil Properties	**Gulf of Mexico**	**Presumpscot Clay**
State	Reconstituted	Undisturbed
Number of tests	5	4
[1]Specific gravity, G_s	2.71	2.72
[1]Liquid Limit, LL [%]	93	56
[1]Plasticity Index, PI [%]	57	32
$S_u/\sigma'_v\|_{OCR=1}$ [kPa]	0.28	0.22
Preconsolidation Stress, σ'_c [kPa]	68	140 – 156
Bulk density, ρ_b [g/cm^3]	1.65	1.73 – 1.80
Water content, w_c [%]	58	45 – 50
Void ratio, e_0	1.59	1.2 – 1.34

[1]*(Gulf of Mexico clay data obtained from Brausse, 2001)*

Grain size distributions of both soils are shown in Figure A.1. The data for the Gulf of Mexico clay was obtained from Brausse (2001) and the data from the Presumpscot clay was obtained from hydrometer tests according to ASTM D 422 (ASTM, 2002). To determine the preconsolidation stress of the Presumpscot clay, three

1-D consolidation tests were carried out. Figure A.2 shows the 1-D consolidation test results obtained from these tests and Table A.2 summarize the consolidation parameters. The preconsolidation stress ranges between 135 and 156 kPa. Sample quality of the Presumpscot clay was assessed using the proposed method by Lunne et al. (1997) and Landon et al. (2007). The first approach measures the volume change ($\Delta e/e_0$) of the sample when it is recompressed to the estimated in-situ stresses; a low ratio means a better sample quality. The second approach consists in measuring the shear wave velocity in the laboratory and compared it to the shear wave velocity measured in situ ($v_{s,lab}/v_{s,SCPTU}$); the closer to unity, the better the sample quality The results are shown in Table A.3.

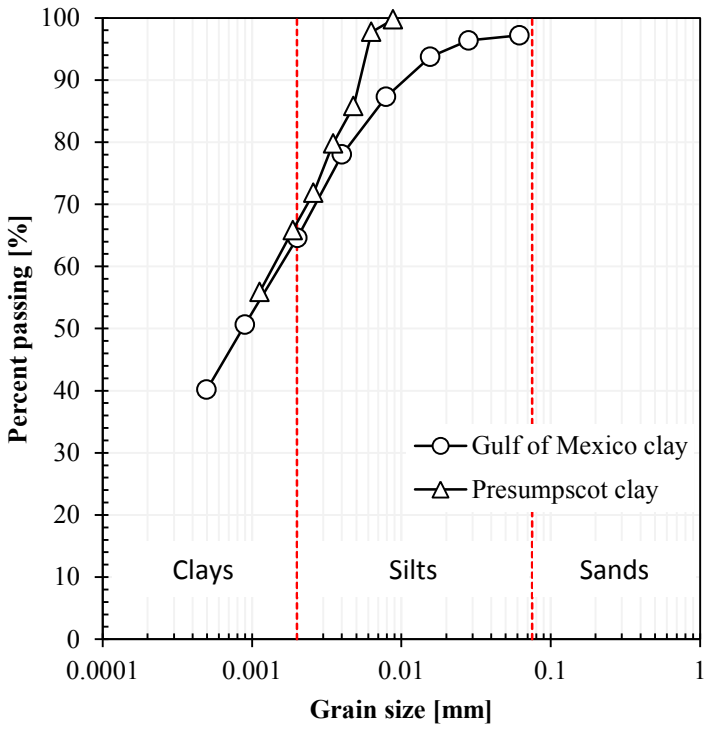

Figure A.1 - Grain size distribution of tested soils

Sample preparation for the soil cake and the block sample consisted of carving a sub-section of the soil and trimming it to a final diameter of 7 cm and a height of 14 cm. The typical procedure is shown in Figure A.3. For the Shelby tubes samples, the clay tends to adhere to the tube walls, and it must be debonded from the Shelby tube before extraction of the sample. Debonding consists of detaching the soil from the walls of the Shelby tube using a thin wire around the soil/tube contact.

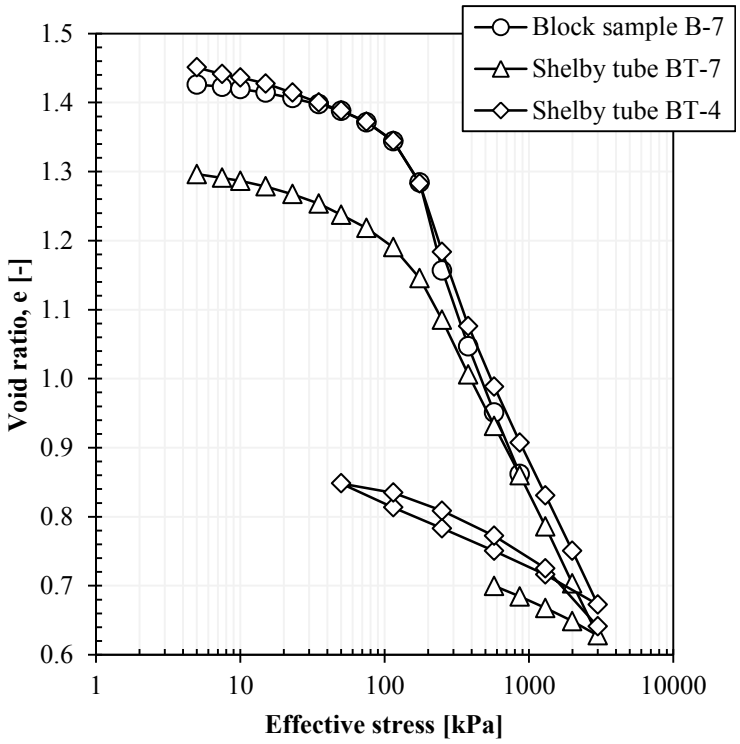

Figure A.2 – 1-D consolidation tests of Presumpscot clay for estimating the preconsolidation stress

Table A.2 - Soil consolidation properties

Sample ID	Dry density, ρ_d [g/cc]	Depth [m]	In-situ stress [kPa]	Preconsolidation Stress, σ'_p [kPa]	Compression Index, c_c	Swell Index, c_s
Block B-7	1.11	4.3	30	156	0.704	0.039
Shelby B-4	1.10	6.7	42	145	0.488	0.055
Shelby B-7	1.18	11	70	135	0.418	0.044

Table A.3 - Sample quality assessment as proposed by Lunne et al. (1997) and Landon et al. (2007)

Sample ID	Depth [m]	OCR	Lab v_s*	In situ $v_{s,SCPTU}$†	$\frac{v_s}{v_{s,SCPTU}}$	$\Delta e/e_0$	Sample Quality††
Block B-7	4.3	5	104	120	0.87	0.026	Very Good to Excellent
Shelby B-4	6.7	3	95	141	0.68	0.057	Fair to Good
Shelby B-7	11	2	127	178	0.71	0.071	Poor

**End of consolidation, using bender elements*
†Langlais (2011)
††Lunne et al. (1997) and Landon et al. (2007), Sample quality based on $\Delta e/e_0$ and $v_{s,lab}/v_{s,SCPTU}$

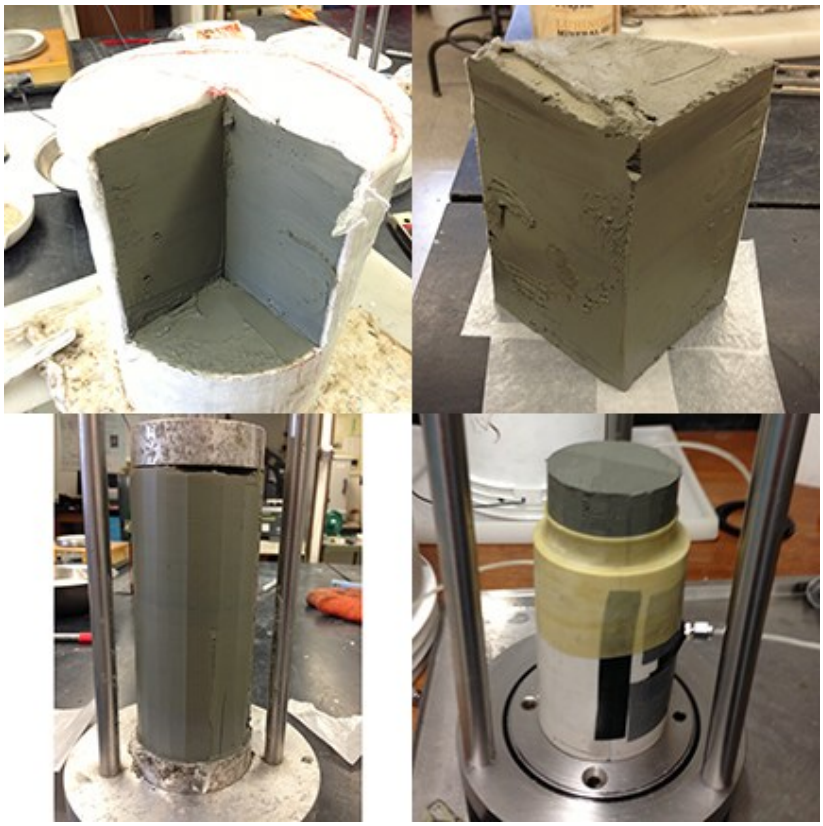

Figure A.3 - Sample carving/trimming procedure of block sample.

Testing Procedure

The test equipment and procedure is the same used in manuscript 1 (Chapter 1) and it will not be repeated here. However, only bender elements were used to measure shear wave velocity with a shear wave frequency of 3 kHz. Samples of Gulf of Mexico clay were isotropically consolidated to 400 kPa, and sheared at OCR = 1, 2, 4, 8, and 16. Samples

of Presumpscot clay were consolidated to in-situ stresses (see Table A.2). The soil testing matrix used for these soils is shown in Table A.4. The identification number of the samples corresponds to the OCR and effective confining stresses at the shear phase. For example, Sample 04-100, had an OCR = 4 and was sheared at σ'_{conf} = 100 kPa.

Table A.4 - Soil testing matrix used in this study

Soil Material	Test Type	Stresses [kPa]	OCR
Gulf of Mexico clay	CID	25, 50, 100, 200, 400	1, 2, 4, 8, 16
Presumpscot clay	CID	30, 42, 70	2, 3, 5

Results

Gulf of Mexico Clay

Results from the Gulf of Mexico clay are summarized in Figure A.4 and Table A.5. Figure A.4a depicts the results of the deviator stress and it shows that specimens sheared under higher OCR (i.e., OCR = 4, 8, 16) have a clear peak in the deviator stress. These same specimens showed a peak in the small strain shear modulus as depicted in Figure A.4b. These peaks, however, did not occur necessarily before the full mobilization of the shear strength of the specimen as it was observed in previous studies for dilatant soils (i.e., Sharma et al, 2011). Such is the case of Sample 16-025 where the maximum small strain shear modulus occurred at ε_a = 5.9 % while the peak deviator stress (failure) occurred at ε_a = 5.2 %. Although Sample 04-100 showed a peak in G_0, this peak is lower than the initial value of G_0 (see Figure A.4b). Different from other tested materials, in the beginning of the shear phase, the small strain shear modulus decreases. Also, with the

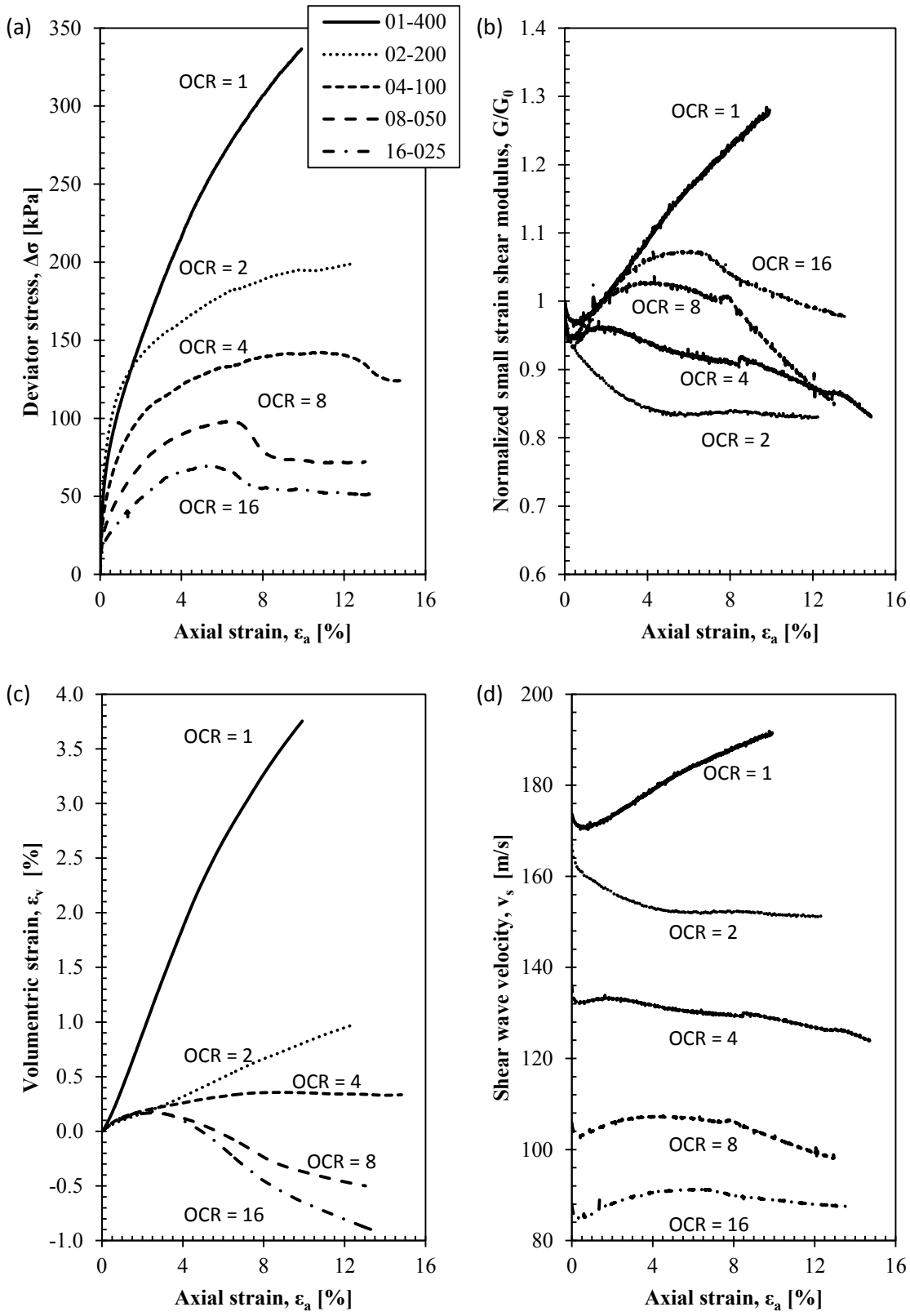

Figure A.4 – Results of Gulf of Mexico clay for (a) Effective vertical stress, (b) G/G_0, (c) volumetric strain, and (d) Shear wave velocity versus axial strain

exception of Sample 02-200, there seems to be a trend in which the curves coincide in the initial increasing slope of G_0 and then they deviate as the shearing continues. Figure A.5 shows a close up of the initial shear phase focusing on these behaviors. Comparing both Figure A.4b and A.4c, there is a relationship between the dilation of the sample and the peak observed in G_0. Samples with OCR = 8 and 16, are the only samples that experienced dilation (volumetric strain going from positive to negative) and a clear peak in the small strain shear modulus. Because Sample 01-400 test was stopped before a clear peak in the deviator stress (or a constant value) and showed high volumetric contraction, it was not considered to determine the G_0/σ'_{1f} relationship.

Table A.5 - Summary of tests results for Gulf of Mexico clay

Test No.	OCR	σ'_3 [kPa]	ρ_b[1] [g/cc]	e_0[1]	v_{s0}[1] [m/s]	G_0[1] [MPa]	σ'_{1f} [MPa]	G_0/σ'_{1f}
1	1	400	1.86	1.65	174	56	0.737	76
2	2	200	1.88	1.53	167	52	0.399	131
3	4	100	1.83	1.61	136	34	0.242	140
4	8	50	1.83	1.55	106	20	0.148	139
5	16	25	1.80	1.59	88	14	0.094	148

[1]*Measured at the end of consolidation (σ'_{3con}).*

By making a direct comparison between the initial small strain shear modulus (G_0) and the effective vertical stress at failure (σ'_{1f}) as shown in Figure A.6, the reconstituted high plasticity clay from the Gulf of Mexico has a G_0/σ'_{1f} = 134 with a correlation of $R^2 = 0.995$.

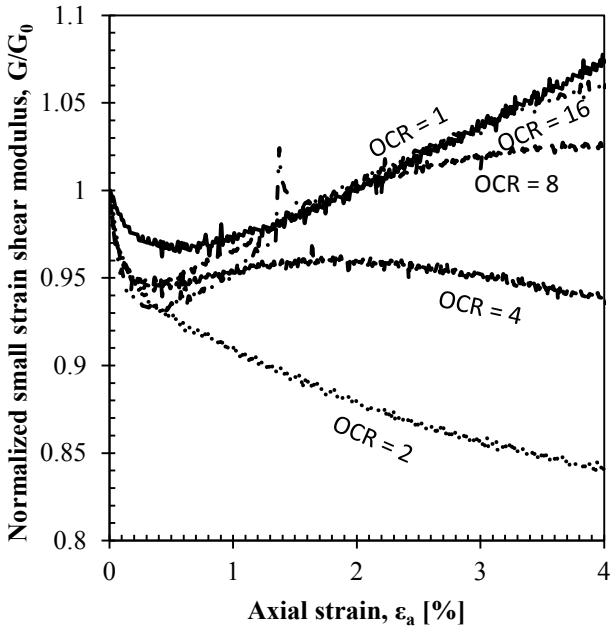

Figure A.5 - Close up of Figure A.4b at initial axial strain

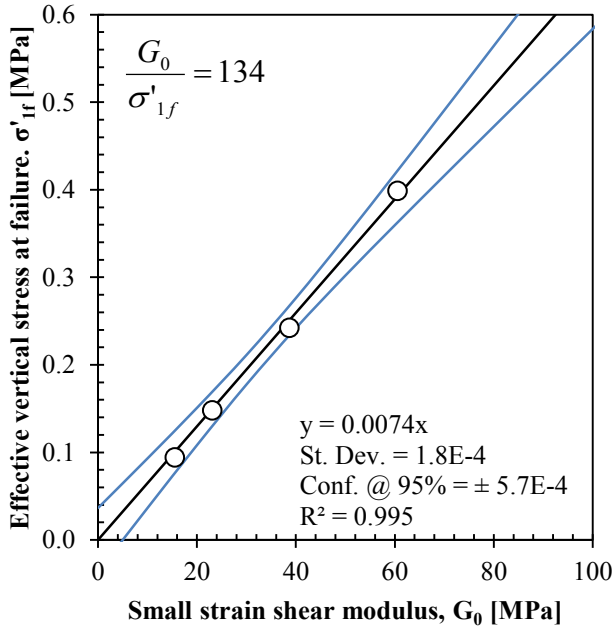

Figure A.6 – G_0/σ'_{1f} relationship for Gulf of Mexico clay

Presumpscot Clay

Results obtained for the Presumpscot clay are shown in Figure A.7 and summarized in Table A.6. Based on the stress-strain curves in Figure A.7a, two tests showed a defined peak typical of a dilative behavior while the other two had strain-hardening behavior typical in contractive conditions. The dilative samples also have clear peaks in the small strain shear modulus as shown in Figure A.7b. Nevertheless, in all cases, the maximum small strain shear modulus occurs before the full mobilization of the shear strength which is consistent with findings from previous research. A close up of the initial part of the normalized small strain shear modulus behavior is shown in Figure A.8. A closer look at this region shows a similar behavior from the reconstituted clay, that is, a decrease in the initial small strain shear modulus followed by an increment. This behavior is more evident in low quality samples. Based on the volumetric strain (Figure A.7c) none of the specimens are dilative. However those samples with clear peaks showed a sudden change in the slope of the volumetric strain. This figure also shows that volumetric contraction decreases with an increase in the OCR. It is important to note how the sample quality affects the results of the tests. The difference in the stress-strain curve, small strain shear modulus, and volumetric strain, suggests that samples from the block sample are of significantly higher quality than those obtained in Shelby tubes. This difference in sample quality is in good agreement with the quality assessment from Lunne et al (1997) and Landon et al. (2007).

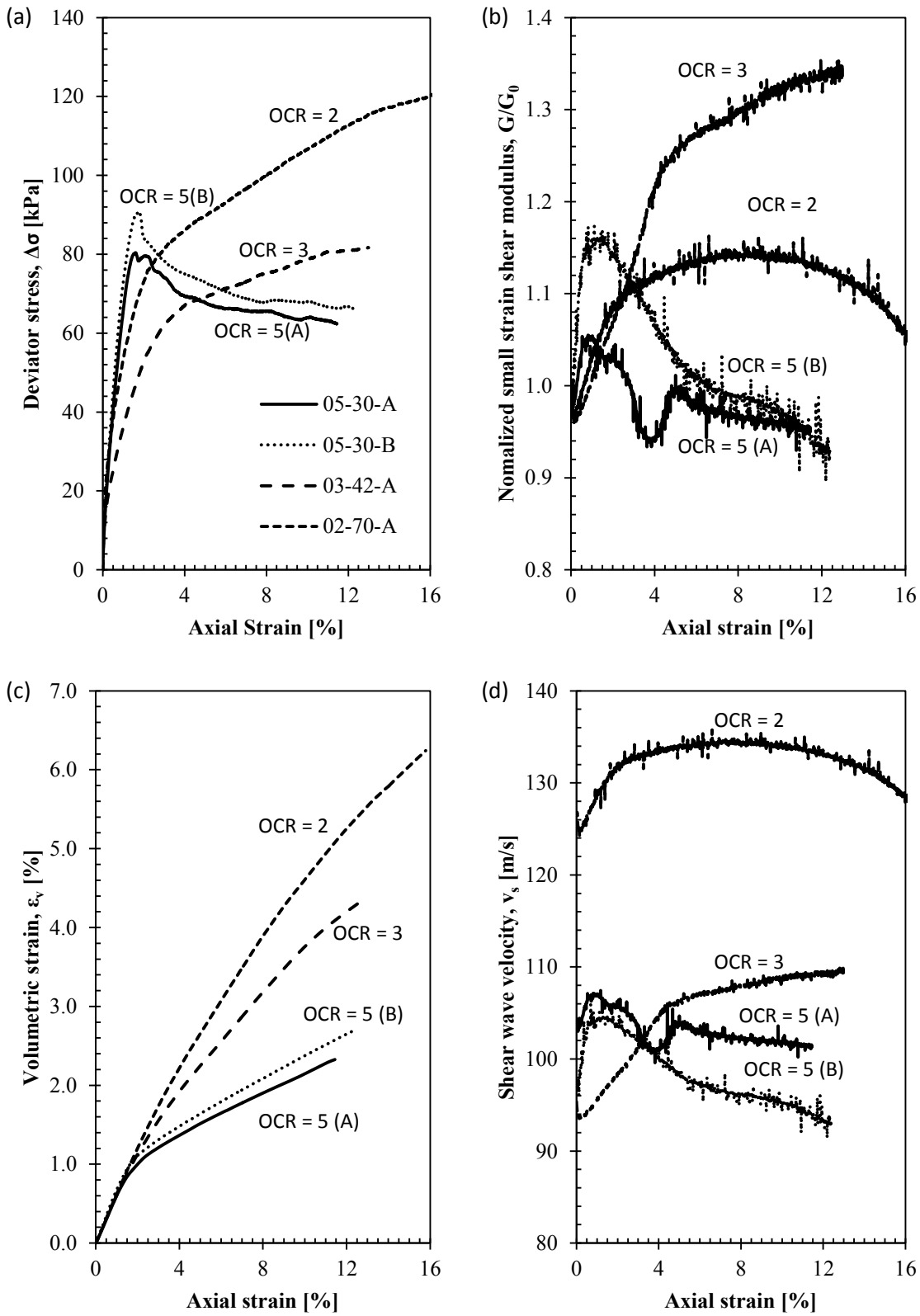

Figure A.7 - Results of Presumpscot clay for (a) Effective vertical stress, (b) G/G_0, (c) volumetric strain, and (d) Shear wave velocity versus axial strain

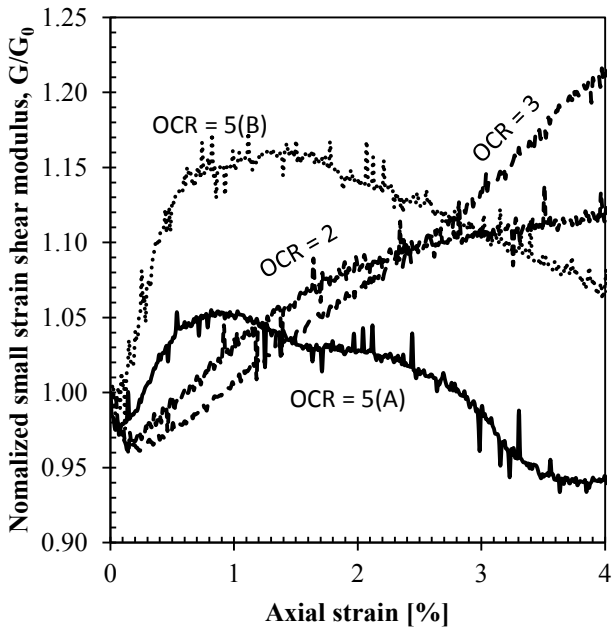

Figure A.8 - Close up of Figure A.7b at initial axial strain

Figure A.9 shows the relationship obtained for the Presumpscot clay with a G_0/σ'_{1f} = 146 and a correlation $R^2 = 0.84$. Considering that most of the data points fall close to each other, stating this relationship based on a single data outside the cluster might not be appropriate. However, compared with the result obtained from the Gulf of Mexico clay, the difference between the two materials is less than 10%.

Table A.6 - Summary of tests results for Presumpscot clay

Test No.	OCR	σ'_3 [kPa]	ρ_b[1] [g/cc]	e_0[1]	v_{s0}[1] [m/s]	G_0[1] [MPa]	σ'_{1f} [MPa]	G_0/σ'_{1f}
1	5	30	1.74	1.34	104	19	0.110	172
2	5	30	1.74	1.33	97	16	0.121	136
3	2	70	1.76	1.27	127	28	0.192	147
4	3	42	1.75	1.30	95	16	0.124	129

[1] *Measured at the end of consolidation (σ'_{3con}).*

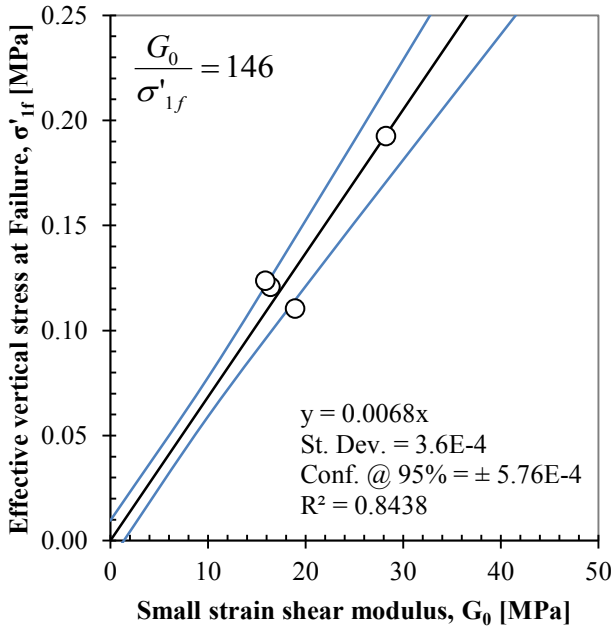

Figure A.9 - G_0/σ'_{1f} relationship for Presumpscot clay

Conclusions

This appendix is an extension of the work presented in Chapter 1. The relationship between the small strain shear modulus (G_0) and the effective stress at failure (σ'_{1f}) was evaluated for two marine clays. The two tested soils consisted of (1) reconstituted samples of high plasticity clay from the Gulf of Mexico and (2) high quality samples of Presumpscot clay from Gulf of Maine. Isotropic consolidated-drained triaxial tests were performed with shear wave velocity measurements using bender elements. The results show that the relationship between the small strain shear modulus (G_0) and the effective stress at failure (σ'_{1f}), $G_0/\sigma'_{1f} = 140 \pm 6$ for both materials.

Acknowledgements

The samples of Presumpscot clay were provided by Melissa Landon Maynard, Dr. of the University of Maine. This assistance is greatly appreciated.

References

ASTM D422 (2002). Standard Test Methods for Particle-Size Analysis of Soils. West Conshohocken, PA 19428-2959, US

Baffer, B.A. (2013). Relationship between small strain shear modulus and undrained shear strength in direct simple shear. *MS Thesis*. University of Rhode Island

Brausse, M. (2001). Underconsolidation and Apparent Overconsolidation in Marine Sediments: a Study of Stress States in the Northwestern Gulf of Mexico. *MS Thesis*. University of Rhode Island

Landon, M. M., DeGroot, D. J., & Sheahan, T. C. (2007) Nondestructive sample quality assessment of a soft clay using shear wave velocity. *Journal of Geotechnical and Geoenvironmental Engineering*, Vol. 133, No. 4, pp. 424-432.

Langlais, N.D. (2011) Site characterization using the seismic piezocone in Presumpscot clay and development of piezocone correlations to engineering parameters. *MS Thesis*. University of Maine

Lunne, T., Berre, T., & Strandvik, S. (1997). Sample disturbance effects in soft low plastic Norwegian clay. *Proc., Recent Developments in Soil and Pavement Mechanics*, Rio De Janiero, pp. 81–102.

Sharma, R., Baxter, C.D.P., & Jander, M. (2011) Relationship between shear wave velocity and stresses at failure for weakly cemented sand during triaxial compression. *Soils and Foundations*, Vol. 51, No. 4, 2011, pp. 761-771.

APPENDIX B

Link between small and large strain behavior of calcareous sands

Introduction

The objective of this appendix is to document additional laboratory data in support of manuscript of Chapter 1. Specifically, additional laboratory tests were performed on samples of calcareous sands from Cabo Rojo, Puerto Rico (Figure B.1) to determine the relationship between the small strain shear modulus (G_0) and the effective vertical stress at failure (σ'_{1f}). Calcareous sands are characterized by having high carbonate content, high porosity, high specific gravity, but low densities (Sandoval, 2008). These factors make calcareous sands prone to crushing during loading. These sands are formed by skeletal remains of marine organisms and their particles differ in nature and shape, and can be found cemented or uncemented (Cataño, 2006). Some studies on the calcareous sands from Cabo Rojo, PR were performed by Cataño (2006) and Sandoval (2008). Cataño (2006) studied the stress-strain behavior of uncemented calcareous sands and compared it with silica sand. The experimental program consisted of several tests including direct shear tests, isotropically consolidated undrained triaxial tests, and resonant column tests. Results showed that the calcareous sand was more ductile, more crushable, more contractive, and less stiff than the silica sand, but with higher effective friction angles (Cataño, 2006). Sandoval (2008) studied the liquefaction resistance of the calcareous sands from Cabo Rojo, Puerto Rico. For this, more than 30 undrained cyclic triaxial tests were performed on reconstituted samples. The results were compared to Ottawa #20-30 sand. The results showed that calcareous sands have higher liquefaction resistance than Ottawa #20-30 sand when tested under similar initial conditions.

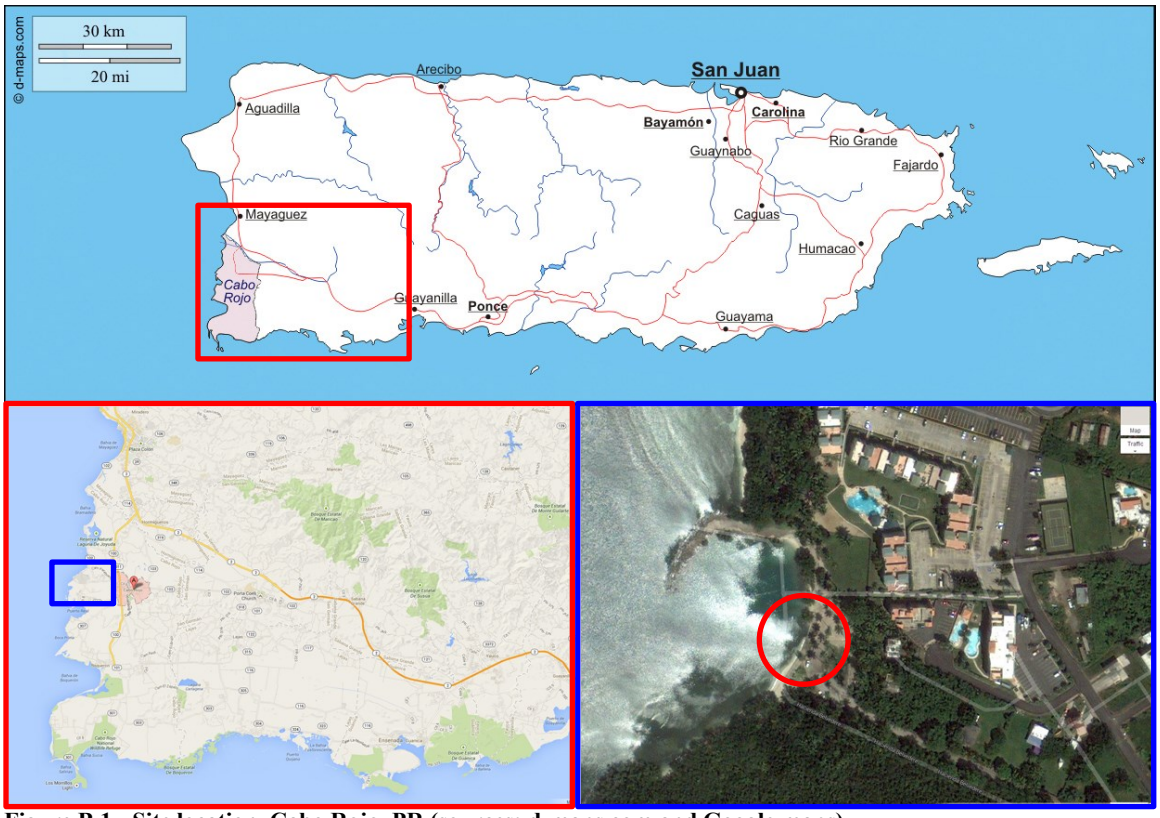

Figure B.1 - Site location, Cabo Rojo, PR (sources: d-maps.com and Google maps)

Experimental Program

Tested Soil

Several in-situ tests were performed including Standard Penetration Test (SPT), Seismic Cone Penetration Test with water pore pressure measurement (sCPTu), Flat dilatometer (DMT) and shear wave velocity measurements (Morales, personal communication, 2013). In addition, sampled material was collected in various 5-galon buckets and shipped to the Marine Geomechanics laboratory at URI. Laboratory tests included determination of determination of e_{max}, e_{min}, specific gravity, carbonate content, and grain size analysis. Material properties of the calcareous sand are summarized in Table B.1 and the grain size distribution is shown in Figure B.2.

Table B.1 - Calcareous sand properties (from Morales, personal communication, 2013)

Material	Carbonate Content $CaCO_3$	Specific Gravity, G_s	e_{max}	e_{min}	D_{10} [mm]	Fines Content
Calcareous sand	> 95 %	2.87	1.75	1.34	0.225	0 %

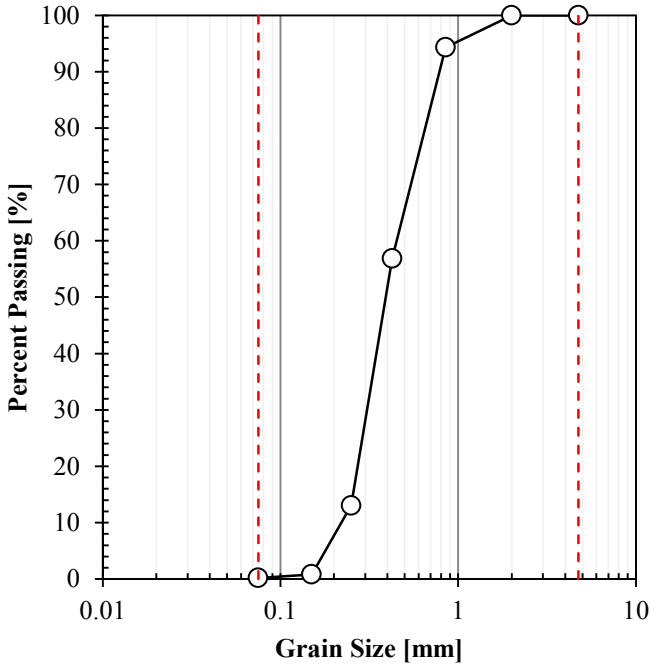

Figure B.2 – Grain size distribution of the calcareous sand

Testing Procedure

Sample preparation and testing procedures are the same conducted for the quartz sand in Chapter 1, and therefore are not discussed herein. The testing matrix is shown in Table B.2.

Table B.2 - Soil testing matrix used for calcareous sand

Soil Material	Test Type	Relative Density, D_R [%]	Confining Stress, σ'_c [kPa]
Calcareous sand	CID	30, 70, 95	50, 100, 200

Results

Figure B.3 shows typical results for the stress-strain and volume-strain relationships of the calcareous sands for different confining stresses. A total of eight tests were conducted to establish the G_0/σ'_{1f} relationship. Figures B.2a and B.2b show a clear failure peak for most of the tested samples. Only the sample with D_R = 30 % sheared at a confining stress of 100 kPa has a smoother failure behavior although the peak can be identified. The volumetric strain shows that most of the samples failed with a dilative behavior. A closer look between the volumetric strain and the small strain shear modulus show that the peak of the former occurs before the maximum small strain shear modulus. Similarly, the peak of the small strain shear modulus occurred before the maximum deviation stress. The peak of the small strain shear modulus occurring before the maximum deviator stress is consistent with the findings obtained in Chapter 1 for both quartz sands and non-plastic silts. However, in the findings from Chapter 1, the peak in the volumetric strain did not occur necessarily before the maximum small strain shear modulus, as occurred with the calcareous sand.

Figure B.4 shows the G_0/σ'_{1f} relationship for the calcareous sand. Based on this results, G_0/σ'_{1f} = 128 for the calcareous sand. In this case, half of the points fall within the 95% confidence lines.

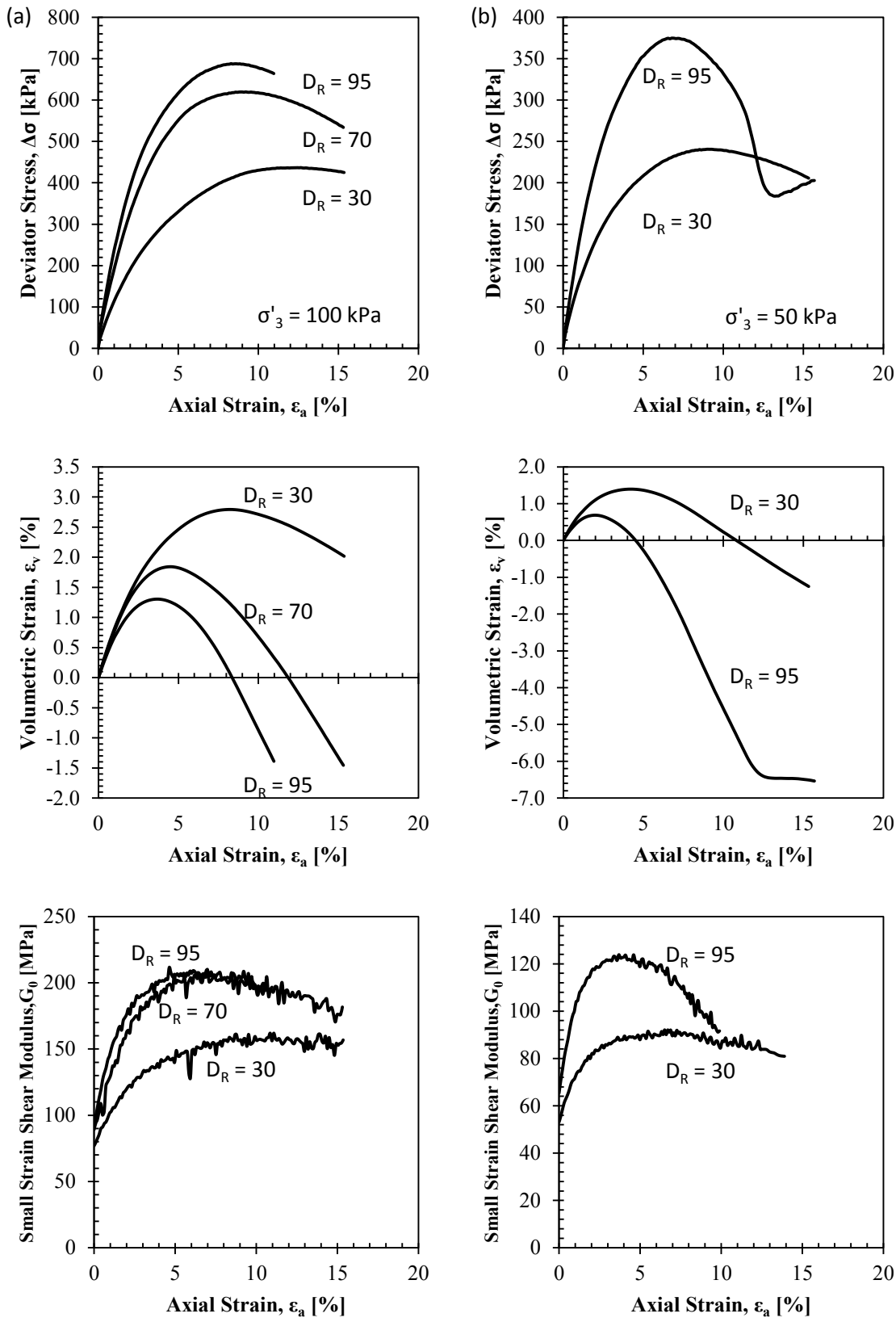

Figure B.3 - Typical results of CID triaxial tests for calcareous sand. (a) σ'_3 = 100 kPa, (b) σ'_3 = 50 kPa

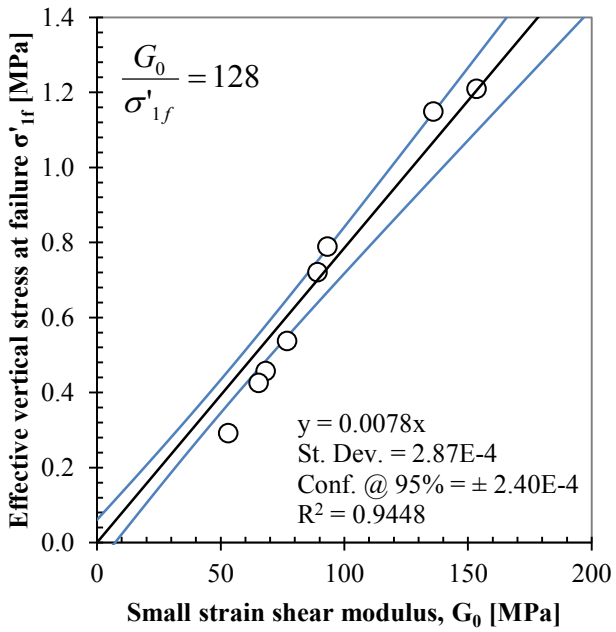

Figure B.4 - G_0/σ'_{1f} ratio for calcareous sand

Conclusions

This appendix presents data as an extension of the work conducted for Chapter 1. In this case, calcareous sands were tested to obtain the G_0/σ'_{1f} relationship. A total of eight samples were tested to obtain this relationship. The relative density was varied between D_R = 30 to 95 %. Based on this results, the relationship between the small strain shear modulus and the effective stress at failure, G_0/σ'_{1f} = 128. This material obtained the lowest value for the G_0/σ'_{1f} relationship compared with the Gulf of Mexico, Presumpscot clay, quartz sand, non-plastic silt, and weakly cemented sand.

References

Cataño, J. (2006). Stress strain behavior and dynamic properties of Cabo Rojo calcareous sands. *MS Thesis,* University of Puerto Rico at Mayagüez

Morales, A. C. (2013). *Personal communication.*

Sandoval, E. (2008). Resistencia a licuación de las arenas calcáreas de Cabo Rojo. *MS Thesis*, University of Puerto Rico at Mayagüez

APPENDIX C

Summary of Results from Chapter 1 and Appendices A and B for all Tested Soils

Table C.1 - Summary of G_0/σ'_{1f} relationship for tested soils

Soil	No. Tests	Stress range [kPa]	Bulk density†, ρ_b [g/cc]	Void ratio††, e_0	$\frac{G_0}{\sigma'_{1f}}$
Non-plastic silt	14	50 – 200	1.57 – 1.74	0.57 – 0.74	219
Cemented sand	22	100 – 300	1.67 – 2.13	0.26 – 0.60	188
Quartz sand	15	50 – 200	1.58 – 1.74	0.52 – 0.68	180
Sensitive clay	4	30 – 70	1.73 – 1.80	1.27 – 1.34	146
High plasticity clay	5	25 – 400	1.63 – 1.66	1.52 – 1.65	134
Calcareous sand	8	50 – 200	1.09 – 1.23	1.32 – 1.62	128

† *Sample preparation*
†† *End of consolidation*

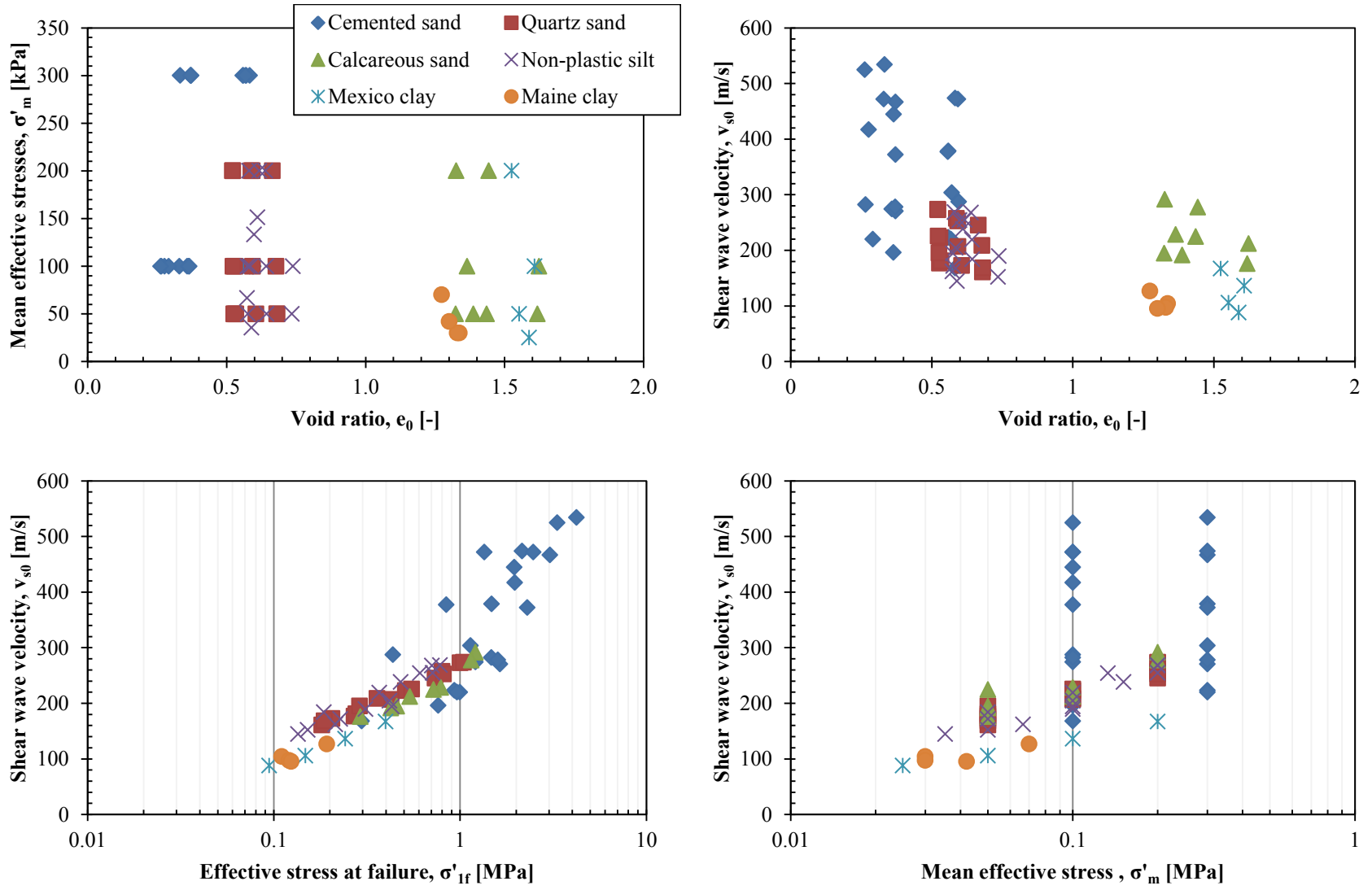

Figure C.1 - Summary of all tested soils comparing shear wave velocity, void ratio and effective stresses

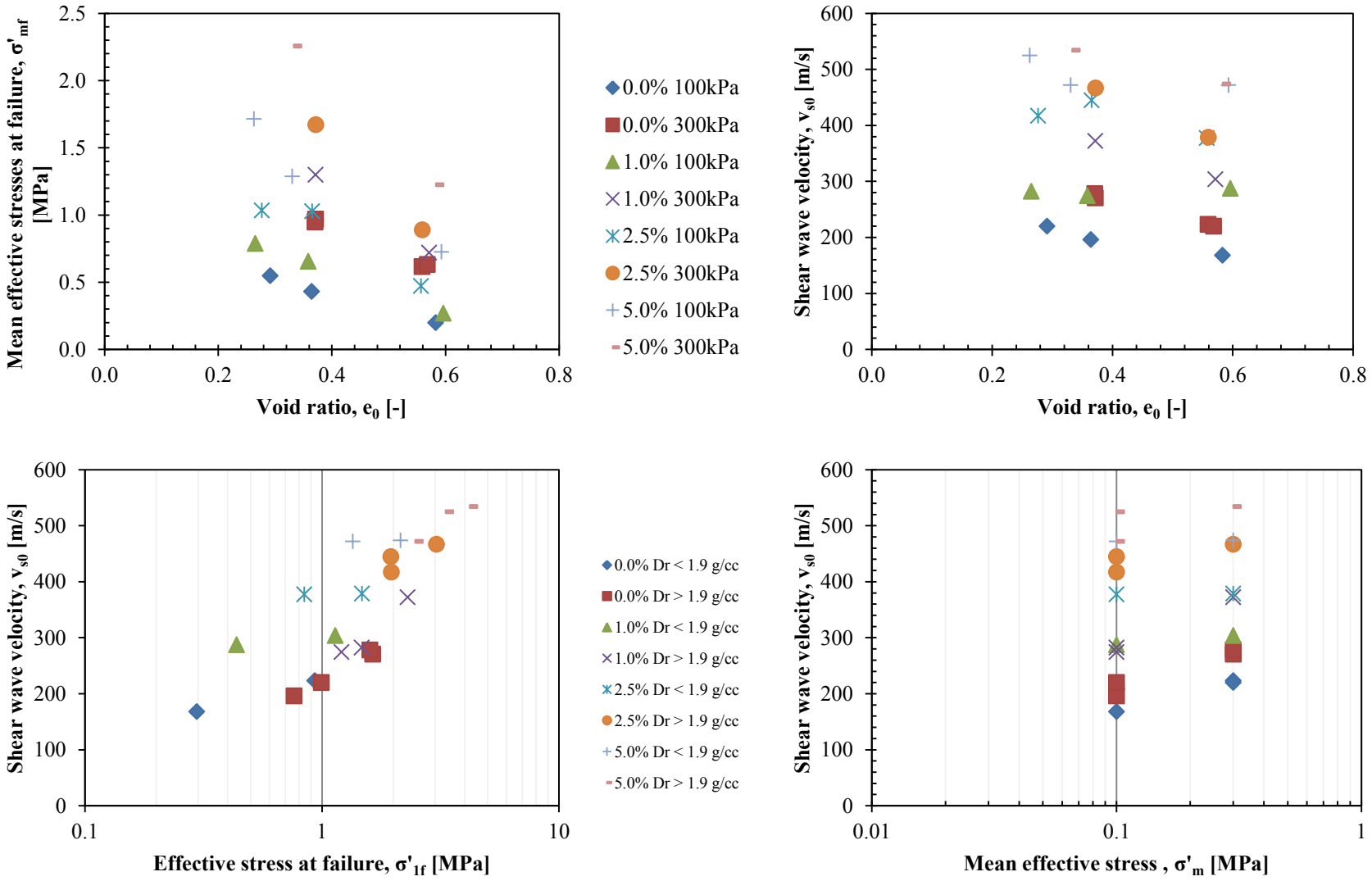

Figure C.2 - Summary of cemented sands comparing shear wave velocity, void ratio and effective stresses

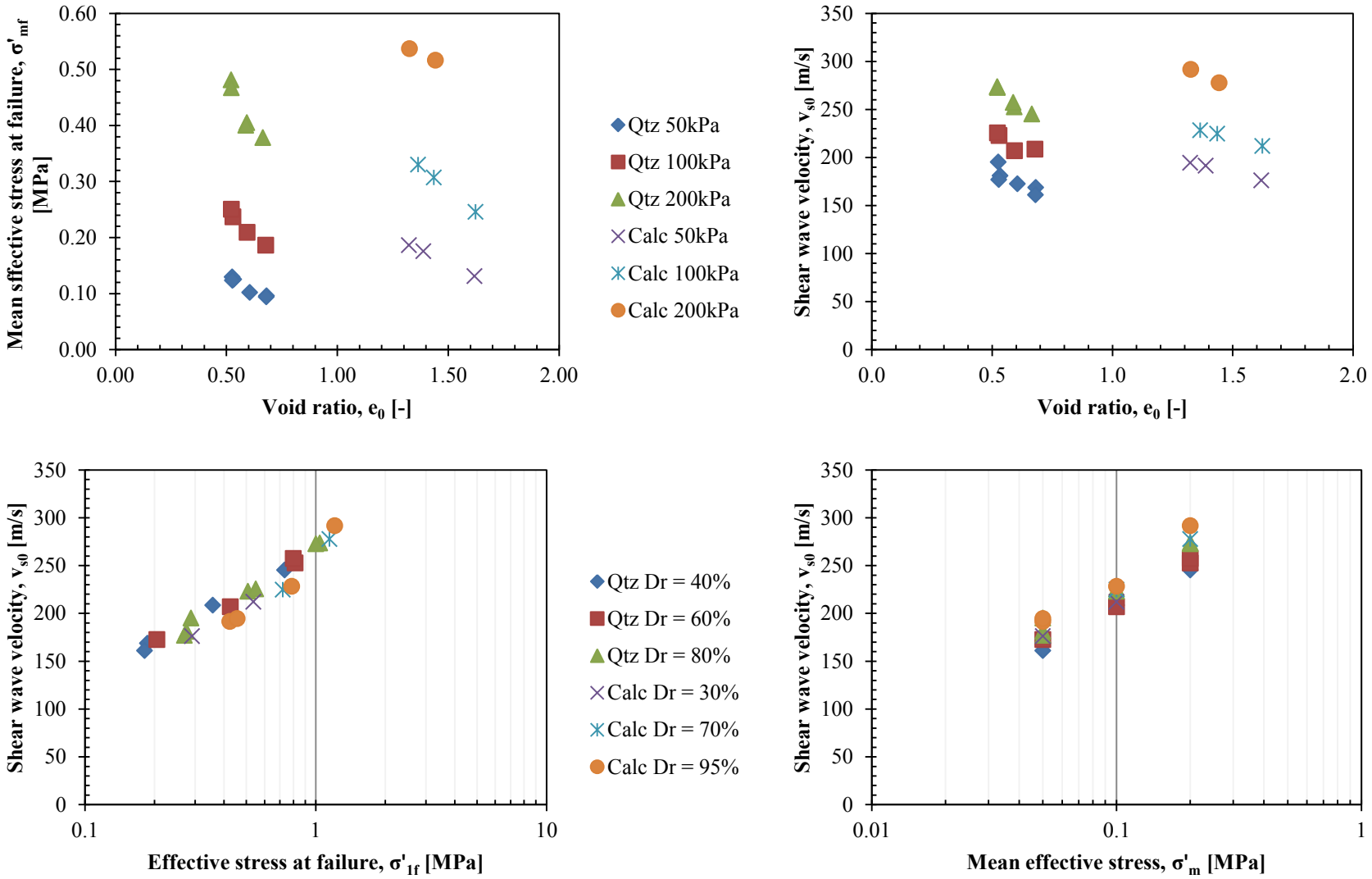

Figure C.3 - Summary of quartz and calcareous sands comparing shear wave velocity, void ratio and effective stresses

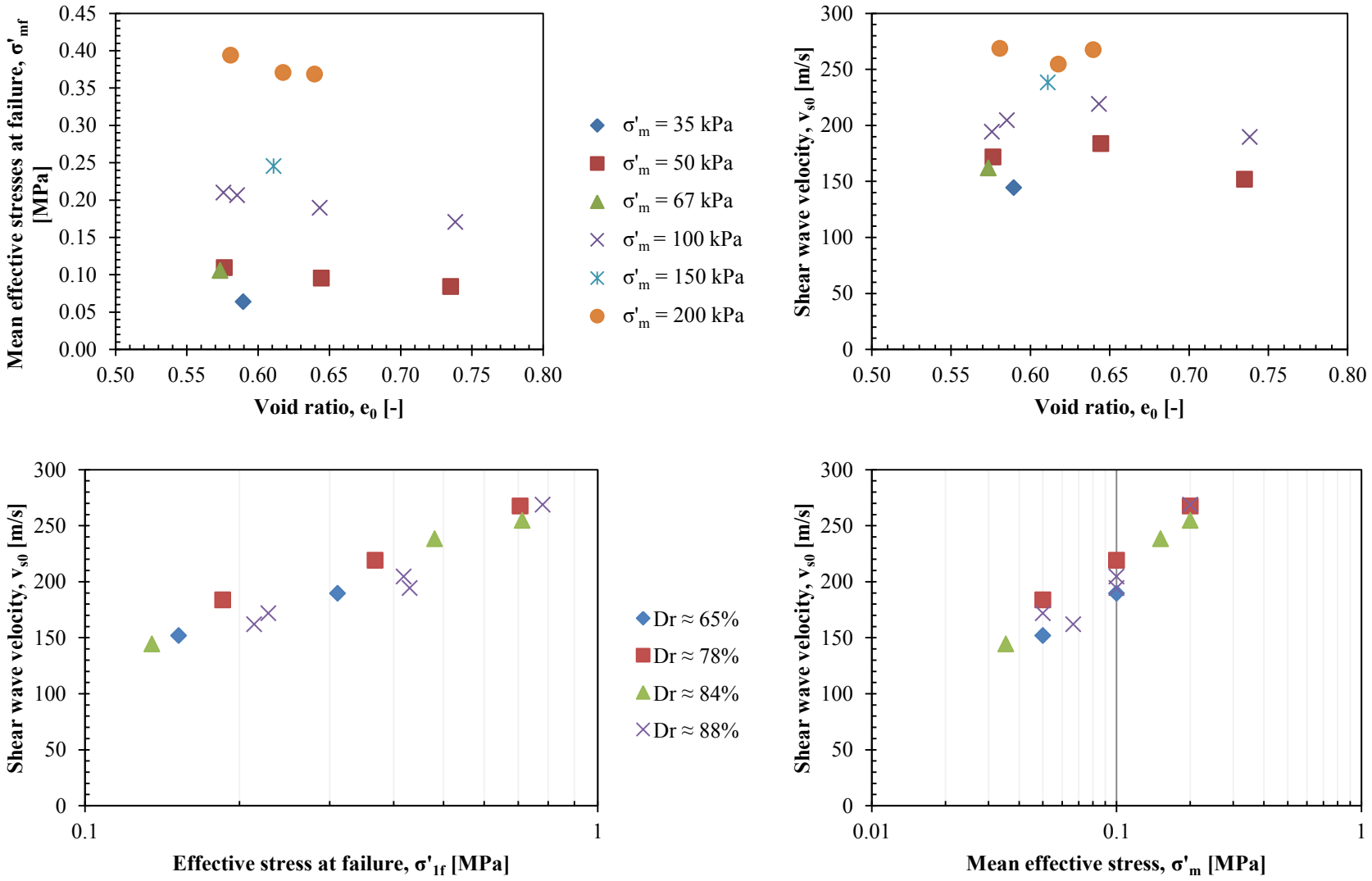

Figure C.4 - Summary of non-plastic silts comparing shear wave velocity, void ratio and effective stresses

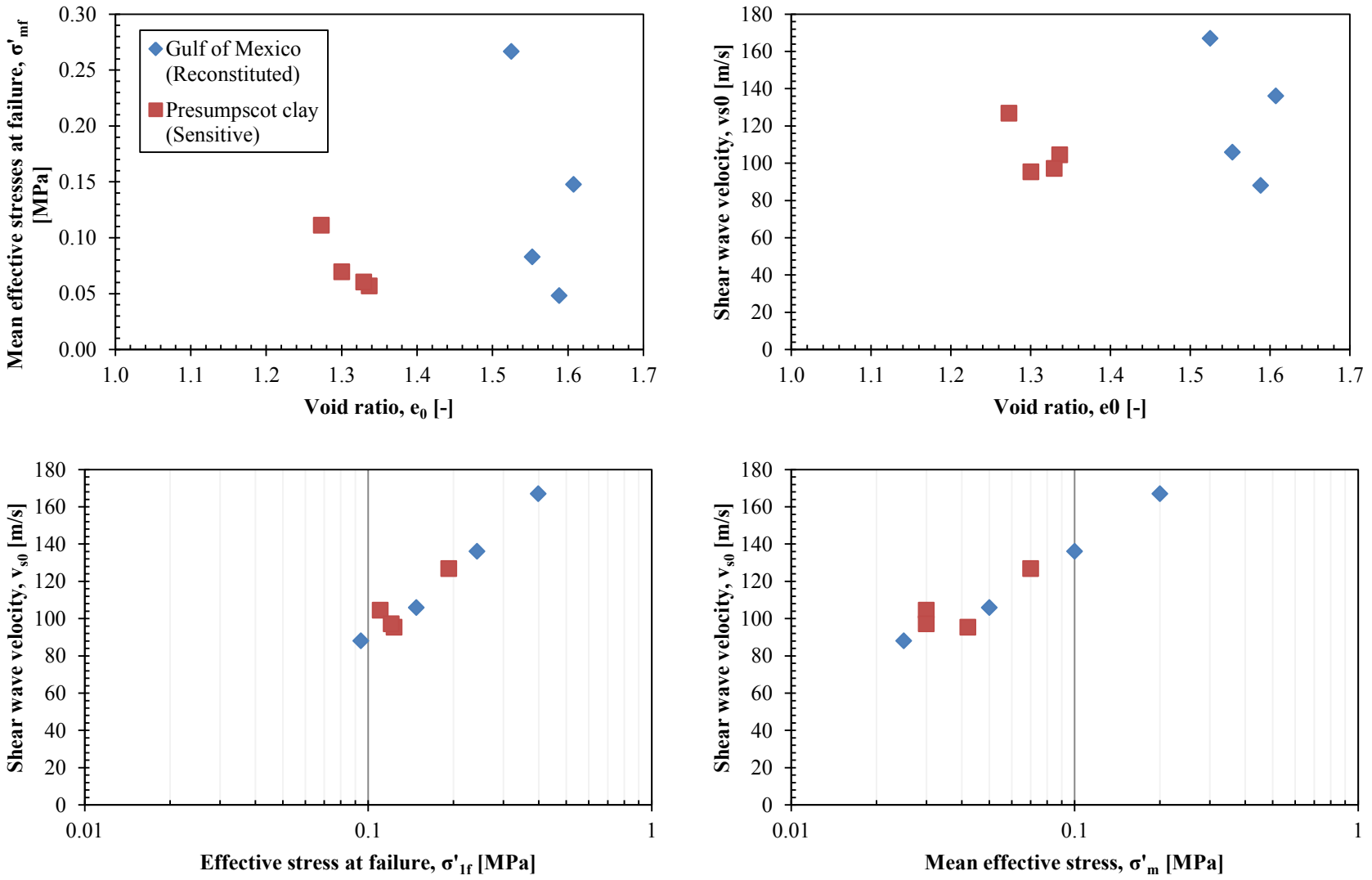

Figure C.5 - Summary of reconstituted (Gulf of Mexico) and sensitive (Presumpscot) clays comparing shear wave velocity, void ratio and effective stresses

APPENDIX D

Estimating Shear Strength Parameters for Non-Plastic Silts and Calcareous Sands from Shear Wave Velocity

Introduction

The objective of this appendix is to present preliminary work to establish a relationship between small and large strain parameters of soils for estimating shear strength properties. Specifically, this appendix focuses on correlating the shear wave velocity (v_s) with the effective stress friction angle (ϕ') of cohesionless soils. The v_s-ϕ' relationship is derived from isotropic consolidated drained triaxial laboratory tests on non-plastic silts and calcareous sands with shear wave velocity measurements using bender elements. This correlation is then compared with published equations developed for cone penetration tests (CPT) to estimate the effective stress friction angle.

Shear wave velocity is being used increasingly in geotechnical practice to characterize soils (Hardin & Richart, 1963; Robertson et al., 1995; Fam & Santamarina, 1996; Andrus & Stokoe, 2000; Cha & Cho, 2007; Landon et al., 2007; Baxter et al., 2008). Shear wave velocity is dependent of many parameters including soil structure, stress history, degree of saturation, grain characteristics, and many others, but is primarily affected by the void ratio (e) and the effective confining stresses (σ') acting on the soil (Richart et al, 1970). The internal friction angle is also dependent of void ratio and, to a minor degree, the effective confining stresses. Therefore developing a relationship between the shear wave velocity and the friction angle could be of practical value. The

benefit of such a relationship will help in determining the in-situ shear strength of soil where sampling could be difficult.

Experimental Program

Tested soils

For this study, two different soils were tested: non-plastic silt obtained from three different sites in Providence, RI and calcareous sand obtained from Cabo Rojo, PR. At both sites, seismic cone penetration tests with pore pressure measurements (SCPTu) were conducted. The grain size distribution of the soils is presented in Figure D.1. Material properties and soil testing matrix are listed in Table D.1.

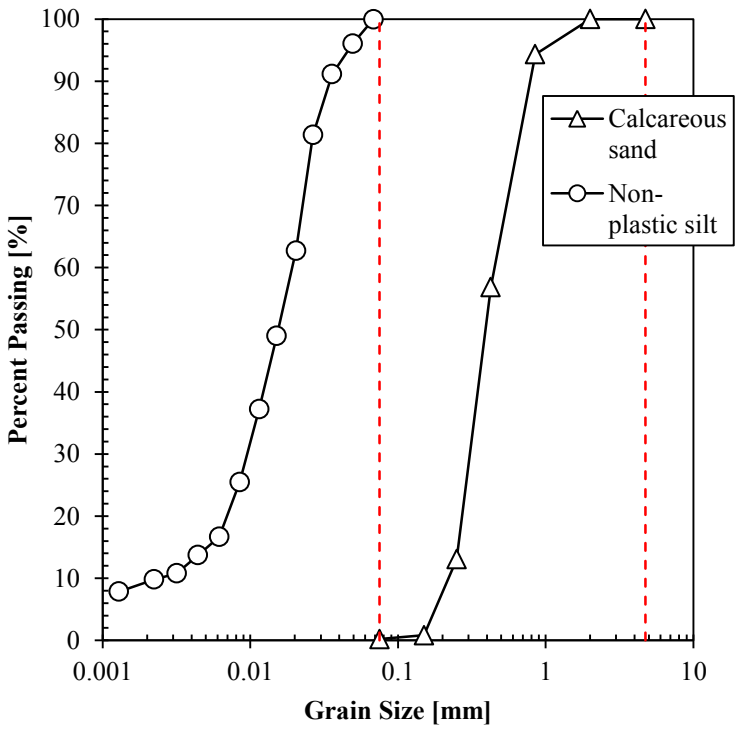

Figure D.1 - Grain size distribution for non-plastic silt and calcareous sand

Table D.1 - Material properties and testing matrix of soils tested in this study

Material Type	Specific Gravity, G_s	e_{max}	e_{min}	Relative Density, D_R [%]	Effective Confining Stress [kPa]
Calcareous sand	2.87	1.75	1.34	30, 70, 95	50, 100, 200
Non-plastic silt	2.75	1.17	0.488	80, 60	50, 100, 200

Laboratory Testing Procedure

Isotropically consolidated drained triaxial tests were performed on non-plastic silt and calcareous sand with shear wave velocity measurements using bender elements. The test equipment and procedure are the same implemented in Chapter 1 and it will not be repeated here. Laboratory test data from non-plastic silt are the same from Chapter 1. Calcareous sand sample preparation is the same used for the quartz sand in Chapter 1.

V_s-ϕ' Relationship

The shear wave velocity is mainly affected by stress state conditions (σ') and void ratio (e) of the soil. To remove the effects of stress, shear wave velocity is typically normalized for overburden stress using a power law relationship with the atmospheric pressure as a reference pressure (Eq. D.1).

$$v_{s1} = v_s * \left(\frac{P_a}{\sigma'_m} \right)^n \tag{D.1}$$

where v_{s1} = normalized shear wave velocity for overburden stress, P_a = atmospheric pressure (≈100 kPa), σ'_m = mean effective stress, and n = power law factor. Under isotropic conditions $\sigma'_m = \sigma'_v$. Because laboratory tests are isotropically consolidated and stresses in situ are anisotropic, Eq. D.1 needs to be modified as Eq. D.2 to account for the difference in lateral stress conditions using the lateral earth pressure coefficient, K_0, as:

$$v_{s1} = v_s * K_0^{n/2} * \left(\frac{P_a}{\sigma'_m} \right)^n \tag{D.2}$$

where K_0 = lateral earth coefficient at rest condition and can be obtained as:

$$K_0 = 1 - \sin\phi' \text{ (Jaky, 1944)} \tag{D.3}$$

The stress dependency of the friction angle is also evaluated and determined graphically, and can also be expressed by a similar power law relationship as:

$$\phi'_1 = \phi' * \left(\frac{P_a}{\sigma'_m} \right)^m \tag{D.4}$$

where ϕ'_1 = normalized friction angle due overburden stress, and m = power law coefficient.

The relationships derived from equations D.2 and D.4 were compared with two CPT correlations from the literature (i.e., Kulhawy and Mayne, 1990; Sandven, 2003). To estimate friction angle from CPT, Kulhawy and Mayne (1990) presented the following equation:

$$\phi' = \tan^{-1}\left[0.1 + 0.381 \log\left(\frac{q_c}{\sigma_{vo}'} \right) \right] \tag{D.5}$$

where q_c= measured cone tip resistance and σ'_{v0} = initial vertical effective stress. In this case q_c is not corrected for unequal area effects (Bradshaw et al., 2012). The equation developed by Sandven (2003) is based on bearing capacity theory, and incorporates a pore pressure parameter (B_q) defined as:

$$B_q = \frac{u_2 - u_0}{q_t - \sigma_{v0}} \tag{D.6}$$

where q_t = cone tip resistance corrected for unequal area effects, σ_{v0} = initial total vertical stress, u_2 = pore pressure measured at the cone shoulder, and u_0 = hydrostatic pressure. Another parameter is the cone resistance number and is defined by the following equation:

$$N_m = \frac{q_t - \sigma_{v0}}{\sigma_{v0}' + a} \tag{D.7}$$

where a = attraction ($=c'\tan\phi'$). A third parameter β describes the extent of plastified zones around the cone (Sandven 2003). All these parameters are used to obtain the tan ϕ' using the Figure D.2.

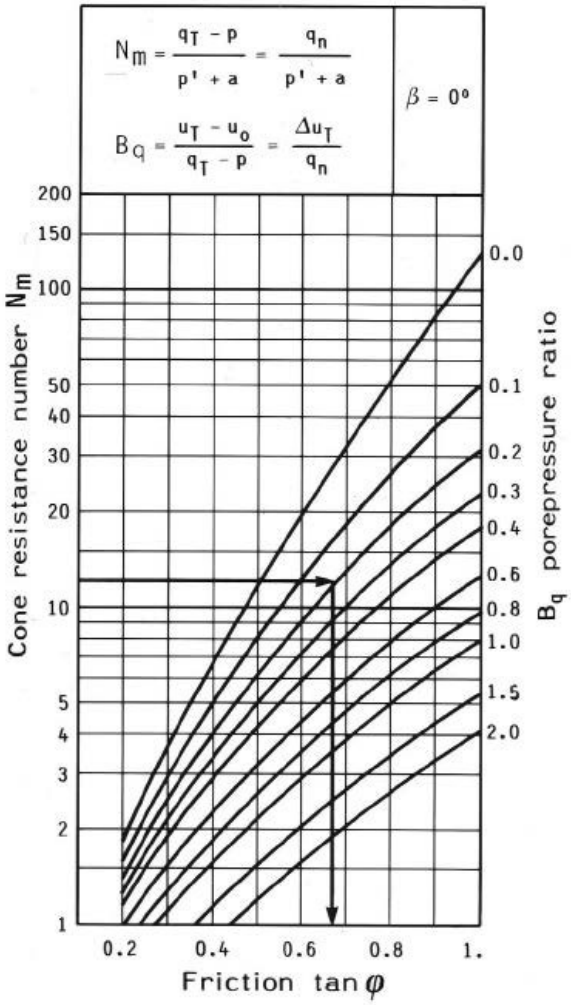

Figure D.2 - Chart used to estimate effective stress friction angle from CPT data in this study (Sandven 2003)

Results

Non-Plastic Silt

Samples were prepared using the modified moist tamping by the normalized energy approach (Taylor, 2011) at an initial degree of saturation of 55% (Figure D.3).

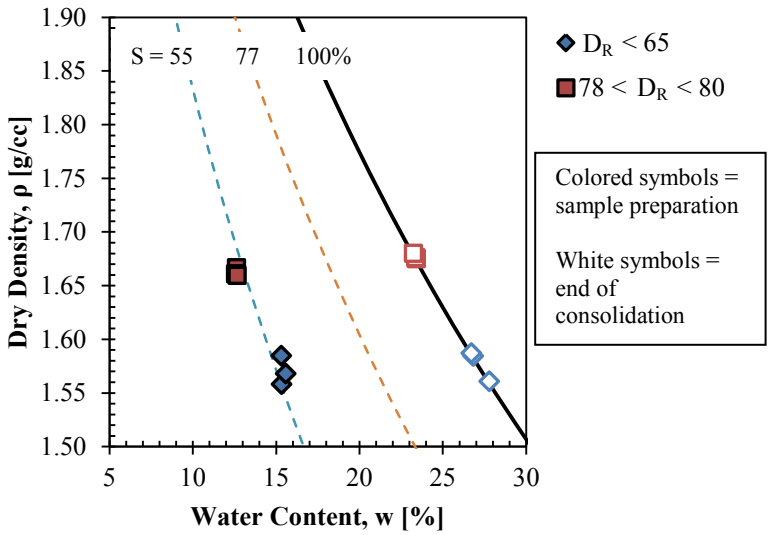

Figure D.3 - Saturation ratio of tested specimens at sample preparation and at the end of consolidation for non-plastic silt

Figure D.4 shows the relationship between shear wave velocity and the mean effective stress and the normalized shear wave velocity. The shear wave velocity was measured during consolidation and shear phases. The shear wave velocity used for the relationship is the v_s at the end of consolidation, and the normalized shear wave velocity was obtained from Eq. D.2. For the non-plastic silt from Providence, RI, Bradshaw et al (2012) used a power law factor of $n = 0.25$. Based on Figure D.4, $n = 0.27$.

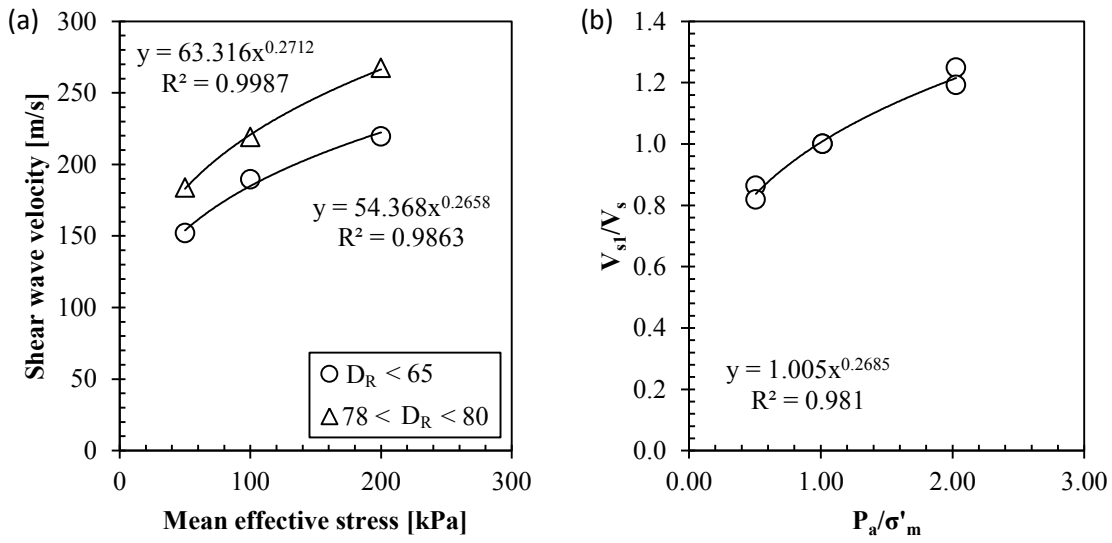

Figure D.4 - (a) Shear wave velocity versus mean effective stress and (b) normalized shear wave velocity for non-plastic silt

Figure D.5 shows the stress dependency of the effective friction angle (ϕ'). The friction angle was obtained from the CID triaxial tests using the maximum deviator stress as failure criterion. Based on Figure D.5, the stress dependency of the friction angle is negligible at least in this stress range, and for these densities. Therefore, it was concluded that no correction for overburden stresses is required for the friction angle.

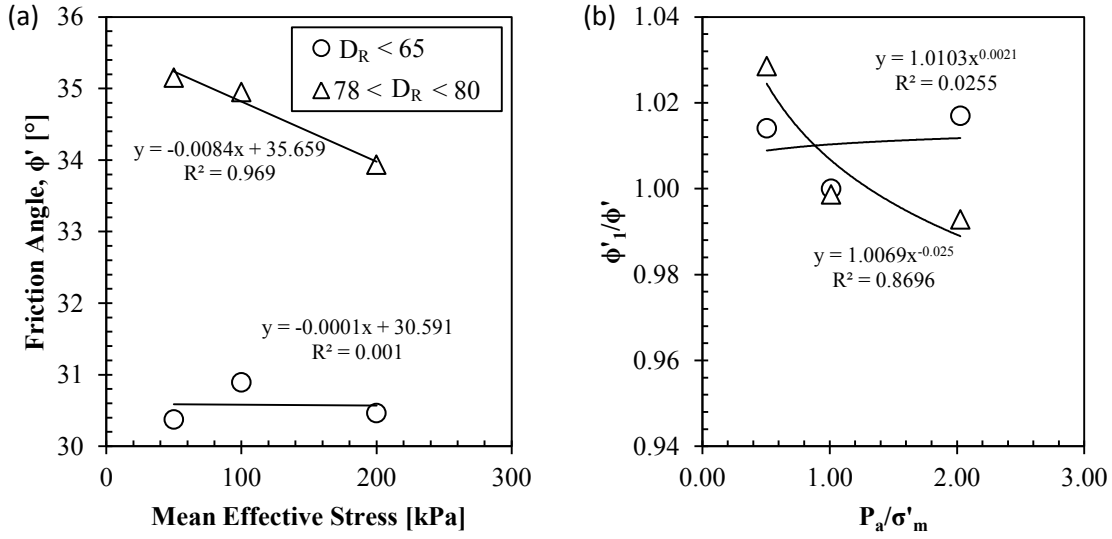

Figure D.5 - Stress dependency of friction angle for non-plastic silt

Once the stress dependency is removed from both parameters (ϕ' is negligible), the relationship between v_s and ϕ' and void ratio can be evaluated. Figure D.6a and D.6b shows the void ratio dependency of the normalized shear wave and the friction angle, respectively. In accordance with the findings of Hardin and Richart (1963) for different sands, the relationship between shear wave velocity and void ratio is linear. The relationship between the friction angle and void ratio is also linear within this range. As the void ratio increases, the soil becomes looser and therefore, both the shear weave velocity and the friction angle decreases. By combining the normalized shear wave velocity (v_{s1}) and the effective stress friction angle (ϕ') from the triaxial tests, the following linear correlation can be established. The v_{s1}-ϕ' relationship is shown in Figure D.7. This relationship it has been established for a very narrow band of stresses (50 kPa to 200 kPa) and densities conditions ($65 \leq D_R \leq 80$) for the same soil fabric.

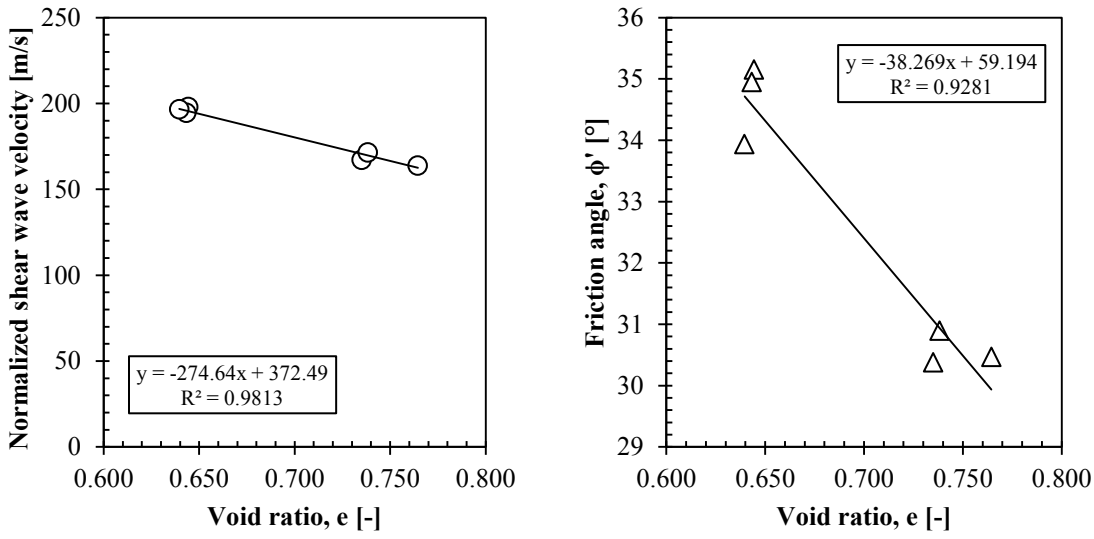

Figure D.6 - Effects of void ratio in (a) normalized shear wave velocity and (b) friction angle for non-plastic silt

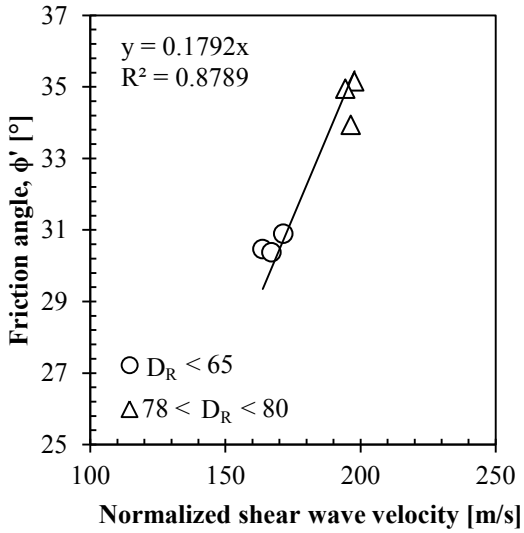

Figure D.7- v_{s1}-ϕ' relationship for non-plastic silt

Based on Figure D.7, the v_{s1}-ϕ' relationship has a linear trend with a slope equal to 0.179. However, the relationship is based in only two clusters of data points from a narrow region. Additional analyses are required to validate this relationship.

Figure D.8 shows effective stress friction angle (ϕ') estimates from four different CPT explorations using the correlations proposed by Kulhawy and Mayne (1990) and Sandven (2003). The results from these correlations are compared with the developed relationship from this report. Shear wave velocity was obtained in-situ along with the CPT explorations. Additional details of the site can be found in Bradshaw et al. (2012). The normalized shear wave velocity (v_{s1}) from in-situ measurements was calculated using Eq. D.1. The results from Figure 8 show that the relationship proposed in this report is able to match the other correlations in some sections, but not along the whole depth. The best approximation is seen in Figures D.8a and D.8b up to 17 m depth. After this depth the results are mirrored at about $\phi' = 35$. Figures D.8c and 8d did not show good agreement with the published correlations.

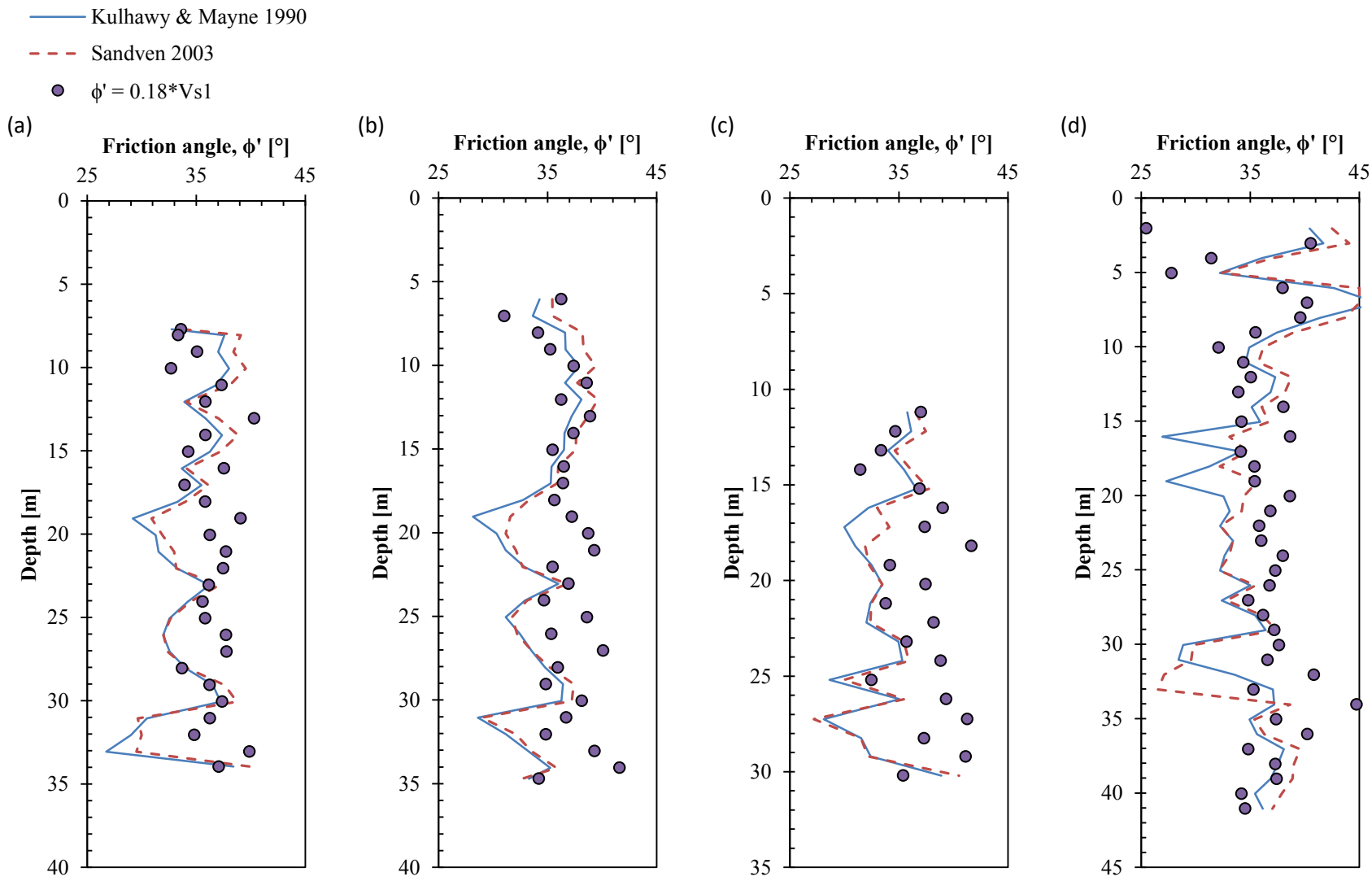

Figure D.8 - Comparison of v_{s1}-ϕ' relationship with published correlations between q_c-ϕ' for the non-plastic silt

Calcareous Sand

Figure D.9 shows the stress dependency of the shear wave velocity for the calcareous sand. Normalizing the shear wave velocity results in the power law factor, $n = 0.29$ with a correlation $R^2 = 0.99$. The stress dependency of the friction angle is shown in Figure D.10. This figure shows some stress dependency for the friction angle, however, the power law factor is very small ($m = 0.09$) and therefore is also neglected for the analysis.

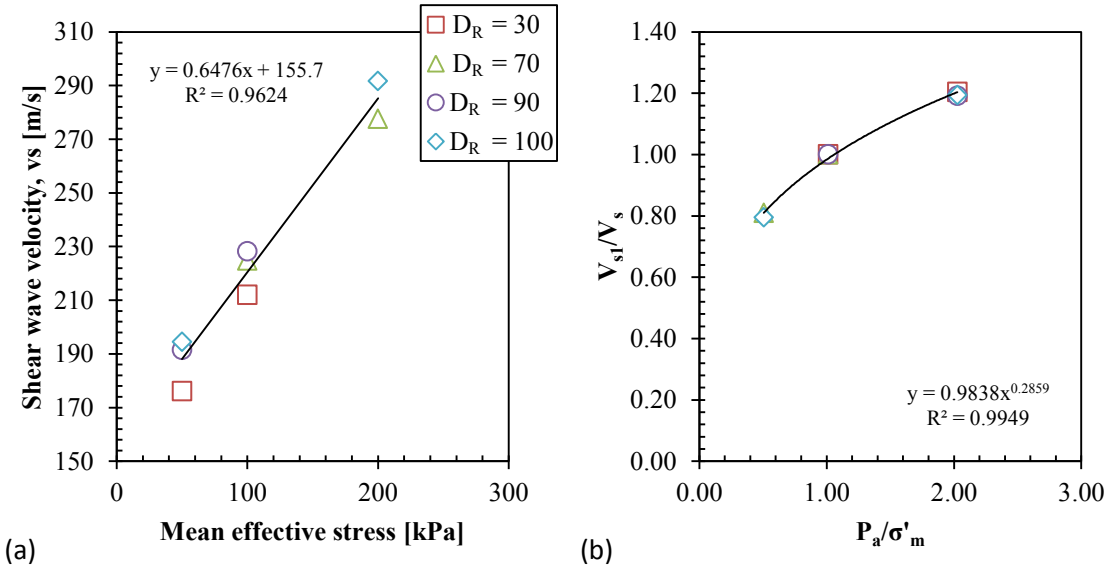

Figure D.9 - (a) Shear wave velocity versus mean effective stress and (b) normalized shear wave velocity for calcareous sand

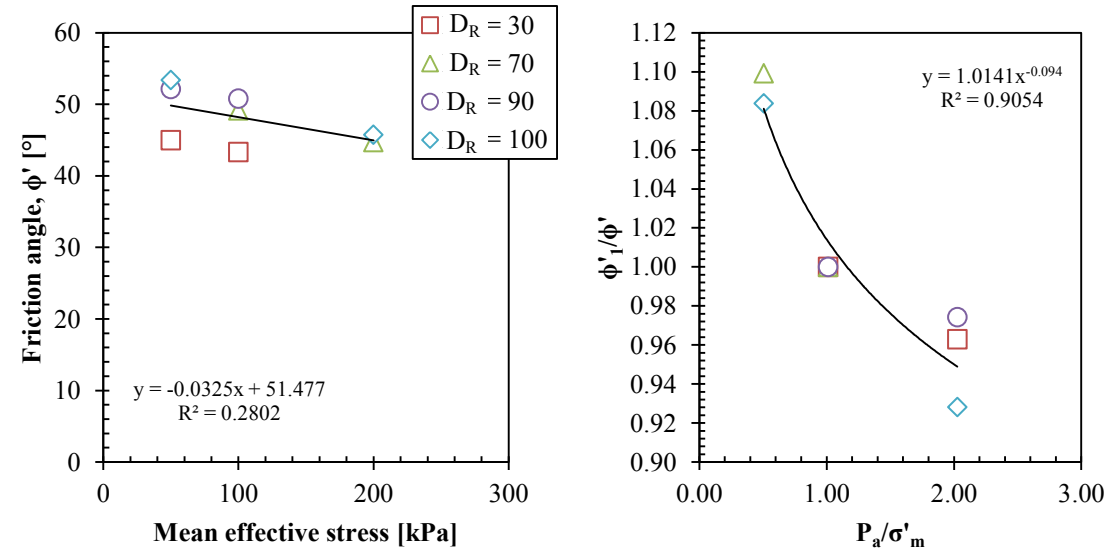

Figure D.10 - Stress dependency of friction angle for calcareous sand

After removing the stress dependency of the shear wave velocity the dependency on void ratio is evaluated as shown in Figures D.11a and D.11b. Figure D.11a shows similar results to those observed in the non-plastic silt (i.e. a linear relationship between shear wave velocity and void ratio). However, the data did not collapse as well into a single line. In fact, the correlation R^2 obtained from this figures is poor ($R^2 = 0.48$). This contrasts greatly with the normalization procedure in Figure D.9b where the correlation is close to unity. Similarly, the friction angle also shows a linear relationship with the void ratio. However, stress dependency seems to have some effects on the denser samples as demonstrated in Figure D.11b.

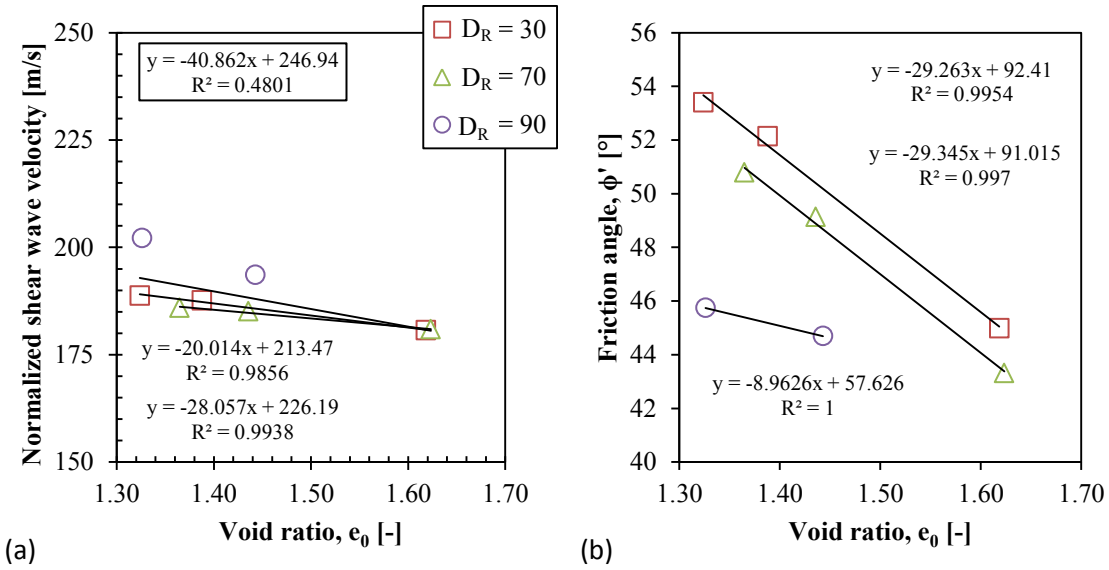

Figure D.11 - Effects of void ratio in (a) normalized shear wave velocity and (b) friction angle for calcareous sand

The v_{s1}-ϕ'relationship for the calcareous sand is shown in Figure D.12. Unfortunately these results are inconclusive. First, the figure shows what it seem to be two possible relationships. Second, the two linear regressions contain an intercept $b \neq 0$, which has no physical meaning. For example, the regression obtained from y_1 suggests

that at $v_{s1} = 0$, $\phi' = -168$. Third, forcing the regression through zero makes the correlation R^2 worse, but with a slope equal to 0.25.

Despite the poor results obtained for the calcareous sand, the two relationships listed below were compared with the correlations from the CPT data.

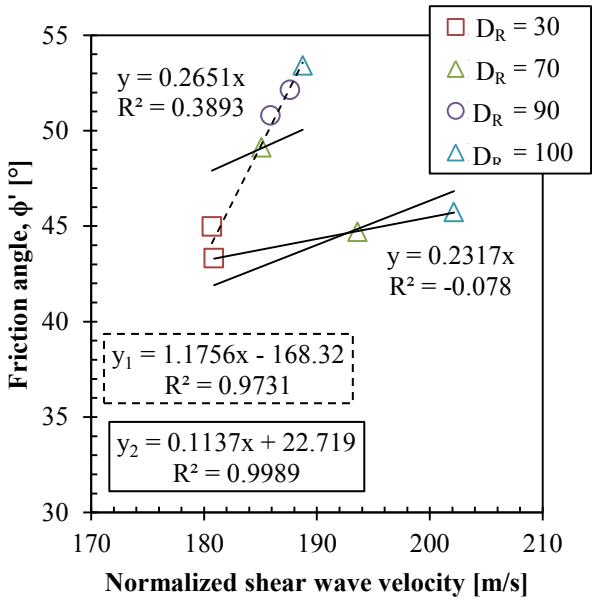

Figure D.12 - v_{s1}-ϕ' relationship for calcareous sand

$$\phi = 0.119 * v_{s1} + 22 \tag{D.8}$$

$$\phi = 0.25 * v_{s1} \tag{D.9}$$

Figure D.13 shows the shear wave velocity profile and the comparison of v_{s1}-ϕ' relationship with published correlations from CPT for the calcareous sand. The shear wave velocity profile was included to compare it the friction angle profile. Because the established relationship is defined in a narrow range of shear wave velocity, the maximum value of the friction angle is defined at v_{s1} = 200 m/s. Therefore ϕ'_{max} = 46 and 50 for Eqs D.8 and D.9, respectively. By limiting the maximum values of friction angle relationship seems to provide reasonable results, at least in the first profile.

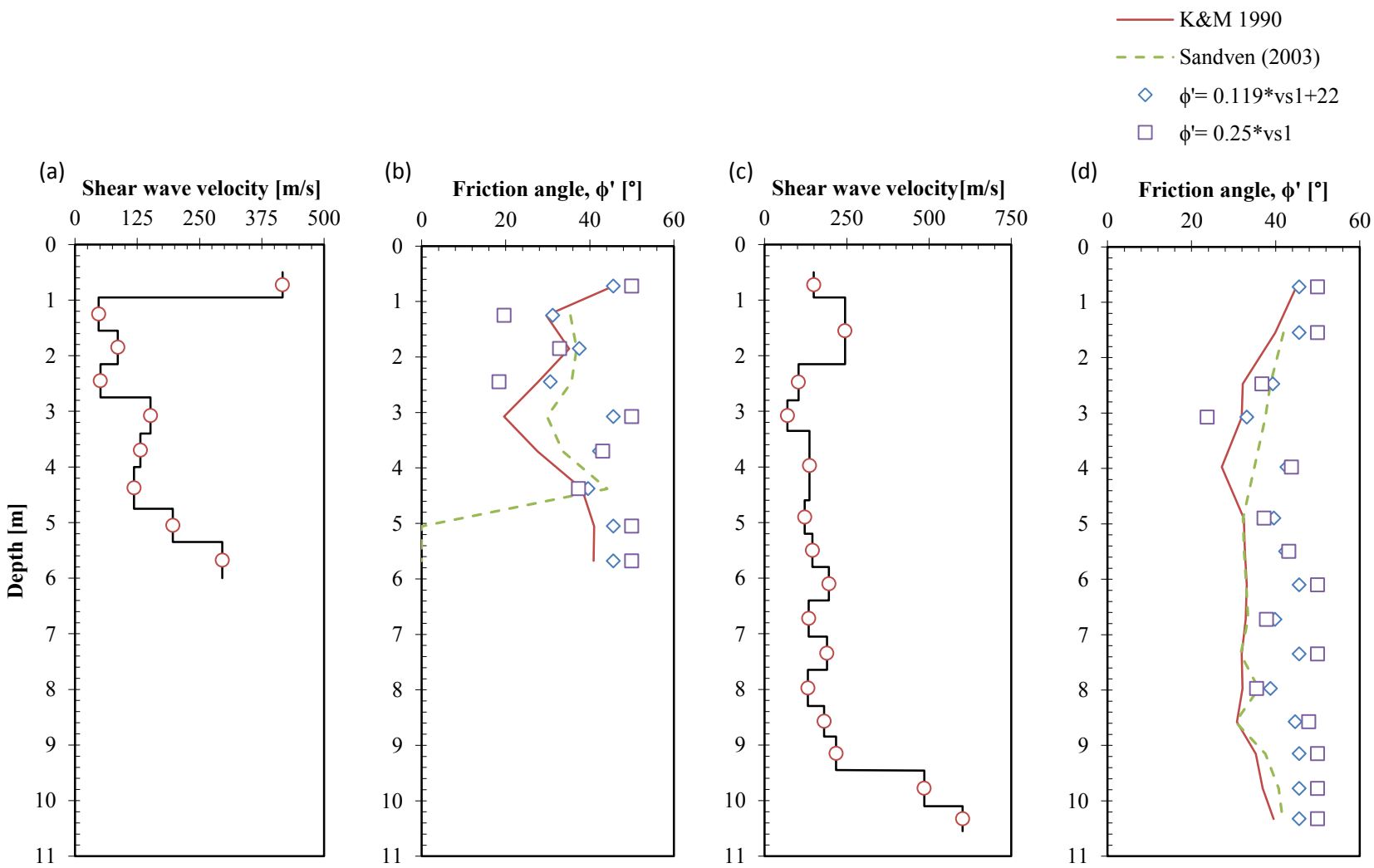

Figure D.13 - (a, c) Shear wave velocity profile and (b, d) comparison of v_{s1}-ϕ' relationship with published correlations between q_c-ϕ' for the calcareous sand (Morales, 2013)

The inconsistencies obtained with the v_{s1}-ϕ' relationship when compared with the two CPT correlations, suggest that the relationship as is defined is not reliable. Therefore further analysis is required to establish a better estimation of the friction angle from shear wave velocity measurements.

Conclusions

An attempt to estimate shear strength properties from shear wave velocity measurements was presented. Two different sites with two different cohesionless soils were selected for the analysis. The in the first site is located in Providence, RI and the soil profile consisted of non-plastic silt. For this site, four CPT explorations were performed with shear wave velocity measurements. The second site is located in Cabo Rojo, PR and the soil profile characterized by very loose calcareous sands. In this site, two CPT explorations were carried out with shear wave velocity measurements.

The stress dependency of the shear wave velocity and the friction angle was considered to develop the relationship. It was found the friction angle is insensitive for the stress range tested. It is believe that soil fabric plays an important role for the development of such correlation.

The v_{s1}-ϕ' relationship established in the laboratory showed mixed results with both the non-plastic silt and the calcareous sands when compared with published correlations to estimate friction angle from CPT. The relationship as defined is not suitable and further work is required to establish an acceptable approach to determine shear strength parameters from shear wave velocity measurements.

References

Andrus, R. D., & Stokoe, K. H., II. (2000). Liquefaction resistance of soils from shear-wave velocity. *Journal of Geotechnical and Geoenvironmental Engineering,* 126(11), 1015-1025.

Baxter C. D. P., Bradshaw, A. S., Green, R. A, & Wang, J-H. (2008). Correlation between Cyclic Resistance and Shear-Wave Velocity for Providence Silts. *Journal of Geotechnical and Geoenvironmental Engineering*, 134(1), 37-46.

Bradshaw, A. S., Morales-Velez, A. C., & Baxter, C. D. (2012). Evaluation of Existing CPT Correlations in Silt. *Geotechnical Engineering Journal of the SEAGS & AGSSEA*, 43(4), 10.

Cha, M. & Cho, G-C. (2007). Shear Strength Estimation of Sandy Soils Using Shear Wave Velocity. Geotechnical Testing Journal, 30(6), pp. 12.

Fam, M A. & Santamarina, J. C. (1996). Study of clay-cement slurries with mechanical and electromagnetic waves. *Journal of Geotechnical Engineering,* 122(5), 365-373.

Hardin, B. O., & Richart, F. E. (1963). Elastic Wave Velocities in Granular Soils. *Journal of the Soil Mechanics and Foundations Division,* 89(SM 1), 33-65.

Jacky, J. (1944). The coefficient of earth pressure at rest. In Hungarian A nyugalmi nyomas tenyezoje." *J. Soc. Hung. Eng. Arch. (Magyar Mernok es Epitesz-Egylet Kozlonye)*, 355–358.

Kulhawy, F. H., & Mayne, P. W. (1990). Manual on estimating soil properties for foundation design. *Electric Power Research Institute*.

Landon, M. M., DeGroot, D. J., & Sheahan, T. C. (2007). Nondestructive sample quality assessment of a soft clay using shear wave velocity. *Journal of Geotechnical and Geoenvironmental Engineering*, 133(4), 424-432.

Morales, A. C. (2013). *Personal communication.*

Richart, F. E., Hall, J. R., & Woods, R. D. (1970). *Vibrations of soils and foundations*, Prentice-Hall, Englewood Cliffs, N.J.

Robertson, P. K., Sasitharan, S., Cunning, J. C. & Sego, D. C. (1995). Shear-wave velocity to evaluate in-situ state of Ottawa sand. *Journal of Geotechnical Engineering*, 121(3), 262-273.

Sandven, R. (2003). Geotechnical properties of a natural silt deposit obtained from field and laboratory tests. *(B. Tan et al. (eds.), Ed.) Characterization and Engineering Properties of Natural Soils*, 1237-1276.

Taylor, O. D. (2011). Use of Energy-Based Liquefaction Approach to Predict Deformation in Silts due to Pile Driving. *PhD Dissertation*. The University of Rhode Island.